SILICIDE FORMATION AND THE INTERACTION OF METALS WITH POLYCRYSTALLINE Si

Thesis by

Johnson Olufemi Olowolafe

In Partial Fulfillment of the Requirements for the Degree of Doctor of Philosophy

California Institute of Technology

Pasadena, California 91125

(Submitted January 14, 1977)

To my wife and our parents.

ACKNOWLEDGEMENTS

It gives me great pleasure to express my profound appreciation to Dr. James W. Mayer for his assistance, encouragement, incessant advice and guidance throughout the course of this work. His ability for leadership and tolerance, are unparalleled. To him I owe a lot.

I would like to thank Dr. M-A. Nicolet for his interest in my work and for the many helpful suggestions. I also wish to thank Drs. J.O. McCaldin, James Mercereau and William Goddard, III, for their advice and useful discussions at one stage or another in the course of this work.

Part of the work reported here was performed with Drs. S.S. Lau, R. Pretorius and Kunio Nakamura. I was really privileged to have worked with them. My sincere thanks to them. For allowing me access to Jet Propulsion Laboratory equipments, I thank R. Shima.

For help and guidance in using the 3 MeV accelerator, I am very grateful to Dr. C.A. Barnes and the members of the Kellogg Laboratory staff. For giving me access to the x-ray diffraction facilities, I am indebted to Dr. Pol Duwez and Dr. Thad Vreeland, Jr. I also thank Dr. Mototaka Kamoshida of Nippon Electric Co., Ltd., Japan, for supplying the polycrystalline Si used in part of this work. Dr. D.S. Burnett is gratefully acknowledged for the use of his beta-counting equipment.

My special appreciation goes to all members of

the faculty of Applied Physics Department, especially Dr. T.C. McGill, whose advice and understanding have been of immense help to me particularly at the beginning of my program. Thanks to Messrs. R. Gorris and J. Mallory for outstanding technical work and to Mrs. Paula Samazan, Karen Current, Linda Dozsa and Patricia Neill who have helped me at one time or another during my stay at Caltech. Special thanks are extended to the Mayer family, particularly Mrs. Betty Mayer, who did all their best to make me feel at home throughout the course of my program. For her skillful handling of a difficult typing job, I thank Carol M. Norris.

I am very grateful to my sponsors, the African-American Institute, New York, who brought me to this country and provided financial support for the entire program. The Institute Scholarship and Research financial assistance of Air Force Cambridge Research Laboratories (D.E. Davies) and Gulf Oil Foundation (A. Lewis, Jr.) are deeply appreciated.

Last, but not the least, I thank my wife, Sola, and daughter, little Yinka, for their patience and understanding of what it takes to be a member of the academic world.

ABSTRACT

The main factors affecting solid-phase Si-metal interactions are reported in this work. The influence of the orientation of the Si substrates and the presence of impurities in metal films and at the Si-metal interface on the formation of nickel and chromium silicides have been demonstrated. We have observed that the formation and kinetic rate of growth of nickel silicides is strongly dependent on the orientation and crystallinity of the Si substrates; a fact which, up to date, has never been seriously investigated in silicide formation. Impurity contaminations in the Cr film and at the Si-Cr interface are the most dominant influencing factors in the formation and kinetic rate of growth of $CrSi_2$. The potentiality and use of silicides as a diffusion barrier in metallization on silicon devices were also investigated.

Two phases, Ni_2Si and NiSi, form simultaneously in two distinct sublayers in the reaction of Ni with amorphous Si, while only the former phase was observed on other substrates. On <111> oriented Si substrates the growth rate is about 2 to 3 times less than that on <100> or polycrystalline Si. Transmission electron micrographs establish that silicide layers grown on different substrates have different microcrystalline structures. The concept of grain-boundary diffusion is speculated to be an important factor in silicide formation.

The composition and kinetic rate of $CrSi_2$ formation are not influenced by the underlying Si substrate. While the orientation of the Si substrate does not affect the formation of $CrSi_2$, the purity of the Cr film and the state of Si-Cr interface become the predominant factors in the reaction process. With an interposed layer of Pd_2Si between the Cr film and the Si substrate, $CrSi_2$ starts to form at a much lower temperature (400°C) relative to the Si-Cr system. However, the growth rate of $CrSi_2$ is observed to be independent of the thickness of the Pd_2Si layer. For both Si-Cr and Si-Pd_2Si-Cr samples, the growth rate is linear with time with an activation energy of 1.7 ± 0.1 eV.

A tracer technique using radioactive ^{31}Si ($T_{1/2}$ = 2.26 h) was used to study the formation of $CrSi_2$ on Pd_2Si. It is established from this experiment that the growth of $CrSi_2$ takes place partly by transport of Si directly from the Si substrate and partly by breaking Pd_2Si bonds, making free Si atoms available for the growth process.

The role of $CrSi_2$ in Pd-Al metallization on Si was studied. It is established that a thin $CrSi_2$ layer can be used as a diffusion barrier to prevent Al from interacting with Pd_2Si in the Pd-Al metallization on Si.

As a generalization of what has been observed for polycrystalline-Si-Al interaction, the reactions

between polycrystalline Si (poly Si) and other metals were studied. The metals investigated include Ni, Cr, Pd, Ag and Au. For Ni, Cr and Pd, annealing results in silicide formation, at temperatures similar to those observed on single crystal Si substrates. For Al, Ag and Au, which form simple eutectics with Si annealing results in erosion of the poly Si layer and growth of Si crystallites in the metal films.

Backscattering spectrometry with 2.0 and 2.3 MeV ^{4}He ions was the main analytical tool used in all our investigations. Other experimental techniques include the Read camera glancing angle x-ray diffraction, scanning electron, optical and transmission electron microscopy. Details of these analytical techniques are given in Chapter II.

Part of this thesis has been previously published under the following titles:

"Iron Silicide Thin Film Formation at Low Temperatures," Thin Solid Films 25, 415 (1975), S.S. Lau, J.S.Y. Feng, J.O. Olowolafe and M-A. Nicolet.

"Interaction of Metal Layers with Polycrystalline Si," J. Appl. Phys. 47, 1278 (1976), K. Nakamura, J.O. Olowolafe, S.S. Lau, M-A. Nicolet and J.W. Mayer.

"Influence of the Si Substrates on the Formation of Ni Silicides," Thin Solid Films 38, 143 (1976). J.O. Olowolafe, M-A. Nicolet and J.W. Mayer.

"Formation Kinetics of $CrSi_2$ Films on Si Substrates with

and Without Interposed Pd_2Si Layer," J. Appl. Phys. 47, 5182 (1976), J.O. Olowolafe, M-A. Nicolet and J.W. Mayer.

"Chromium Thin Films as a Barrier to the Interaction of Pd_2Si with Al," Solid-State Electron. (in press), J.O. Olowolafe, M-A. Nicolet and J.W. Mayer.

"Analysis of Semiconductor Structures by Nuclear and Electrical Techniques," (Section D), Air Force Cambridge Research Laboratories Scientific Report No. 2 (1975).

"Radioactive Silicon Tracer Studies of the Formation of $CrSi_2$ on Pd_2Si and PtSi," (to be published), R. Pretorius, J.O. Olowolafe and J.W. Mayer.

TABLE OF CONTENTS

CHAPTER I. Introduction

A. General

Deposited layers of metals are widely used for metallization in integrated circuits and related devices.[1] It is common practice to deposit two or more layers of metals 0.1 to 1 μm thick on the surface of integrated circuit structures. The evaporated metals are heat-treated to form intermetallic layers, known as silicides, which give the desired properties either as ohmic contacts or as Schottky barriers. The processing temperature is usually chosen between 400 and 500°C to form the silicides and, hence, good electrical contact between the metals and Si.

Increasing applications of silicides in silicon technology and the advancing performance of the technology increase the need to understand the process of formation of a silicide. A well-controlled growth of a silicide layer becomes more important when the number of circuits per unit area on a silicon chip becomes larger.

A multilayer system is not uncommon in metallization schemes in ICs.[1] Typical among them is the Pd-Cr-Al ternary system on Si reported in this work.

Recent studies have focused attention on the characteristics of the silicide formation process, and on the properties of the resultant compounds. It is known that near-noble metals Ni, Pd and Pt form silicides at

temperatures as low as 200°C, which is only about 0.3 to 0.4 of the eutectic temperature of the binary systems. The growth is parabolic in time, in contrast to $CrSi_2$, VSi_2 and $MoSi_2$ which increase linearly in time at constant temperatures.

Numerous intermetallic and silicide phases have been identified for metal systems commonly used in thin film applications.[2-17] Phase diagrams are shown in Fig. 1 for Ni, Pd and Cr silicide which are reprinted from Hansen.[18] This figure illustrates that Ni, Pd and Cr like many other metals, have numerous silicide phases.[18,19] The phases identified in these diagrams represent equilibrium conditions, however. Generally, the compounds shown were produced by slowly cooling a liquid phase mixture of the metal and silicon. In contrast, the silicides formed from thin film couples heated to temperature below 600°C must depend on solid state transport for mixing of the metal and silicon. This is a nonequilibrium process, dominated entirely by kinetics. Equilibrium diagrams provide excellent clues to possible compounds that may develop when a thin film couple reacts at low temperatures; however, these diagrams are not sufficient to describe which phases will result from the kinetic processes which occur when these thin films are heated. One phase may dominate because it is more efficient in transporting the material needed to continue the mixing process.[20] Alternatively, a phase may be absent because it does not

Figure 1. Metal-Si phase diagrams of (a) Ni, (b) Pd, and (c) Cr silicides. These figures are taken from "Constitution of Binary Alloys," by Max Hansen.

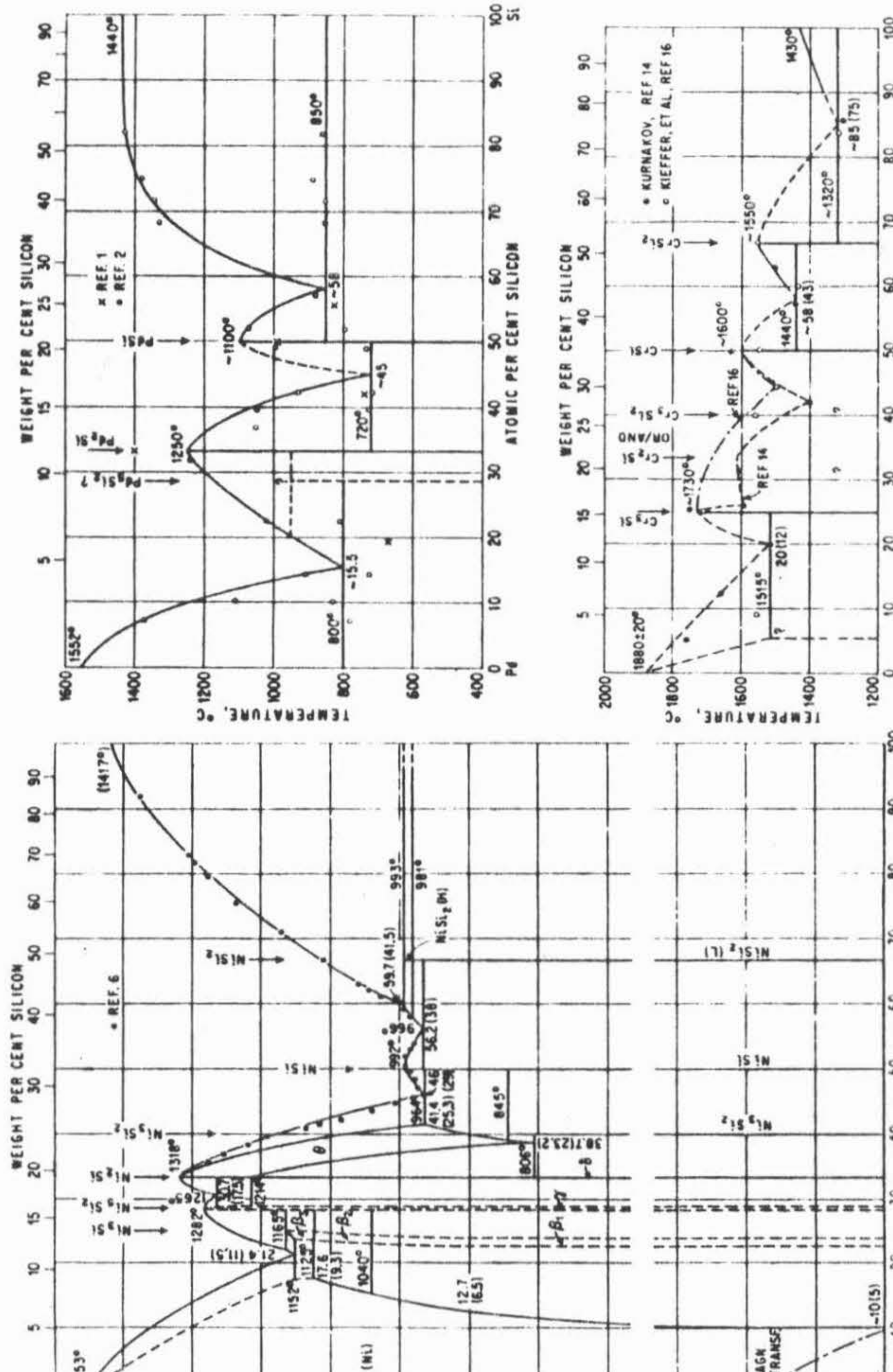
WEIGHT PER CENT SILICON
ATOMIC PER CENT SILICON
TEMPERATURE, °C
• KURNAKOV, REF 14
○ KIEFFER, ET AL, REF 16
× REF. 1
• REF. 2
• REF. 6

nucleate at the low temperatures involved. In general, only one phase is present at a given temperature and time. Kidson had earlier pointed out that if the rate constants of diffusion in a given phase are small the phase layer may be too thin to be detected.[21] Finally, phases which form in the kinetic mode may not have a direct equilibrium counterpart. Nonequilibrium phases have also been identified in the study of amorphous materials.[22]

Table 1 gives a summary of silicides that have been identified by He ion backscattering spectrometry.[17] The number of phases indicated in the phase diagrams, the structures, the temperature at which they were observed, the kinetics and the melting temperatures are indicated.

In the studies of Si-metal interactions reported so far, not much attention has been given to factors that could be very influential in the formation and kinetic rate of growth of silicides. It is therefore the main objective of my studies to investigate the influence of factors like orientation of Si substrates, impurity (oxygen, etc.) contamination of metal films, the condition of the metal-Si interface and presence of an interposed silicide layer given a ternary system on the formation and growth rate of silicides. Some factors are more effective in influencing one silicide growth than in others, while in some systems a number of these factors might be competing simultaneously.

In particular, we have studied the influence of

Table 1. Silicides, their structures, kinetic rate of formation and related temperatures. Column two gives the most metal rich, the most Si rich and an intermediate silicide phase as given in the phase diagrams. Most of the data is from J.W. Mayer and K.N. Tu, J. Vac. Sci. Technol. 11, 86 (1974).

TABLE 1

Metal+	Phases	Structure	Backscattering Phase	Backscattering T_{obs} °C	Backscattering Kinetics	T_{melt} °C	T_{obs} °K / T_{melt} °K	Ref.
Ti (3)	Ti_5Si_3	hexagonal				2120		
	TiSi	orthohombic				1700		
	$TiSi_2$	" (C49)	$TiSi_2$	600	$t^{\frac{1}{2}}$	1540	~0.5	11
Zr (7)	Zr_2Si	tetragonal				2110		
	ZrSi	ortho				2095		
	$ZrSi_2$	" (C49)	$ZrSi_2$	700		1520	~0.5	23
Hf (5)	Hf_2Si	tetra				2430		
	HfSi	ortho or hexa (FeB)	HfSi	550	$t^{\frac{1}{2}}$	2200	~0.3	
	$HfSi_2$	ortho (C49)	$HfSi_2$	750		1900	~0.5	12
V (3)	V_3Si	cubic (β-W)				2070		
	V_5Si_3	tetra (D8m)				2150		
	VSi_2	hexa (C40)	VSi_2	600	$t, t^{\frac{1}{2}}$	1750	~0.5	14,24
Nb (4)	Nb_4Si	hexa						
	Nb_3Si	cubic (Cu_3Au)						
	$NbSi_2$	hexa (C40)	$NbSi_2$				~0.5	25
Ta (3)	Ta_2Si	tetra (Al_2Cu)				2460		
	$TaSi_2$	hexa (C40)				2200		
Cr (5)	Cr_3Si	cubic (β-W)				1730		
	CrSi	cubic (FeSi)				1600		
	$CrSi_2$	hexa (C40)	$CrSi_2$	450	t	1550	~0.4	11*
Mo (3)	Mo_3Si	cubic (β-W)				2120		
	$MoSi_2$	tetra (C11b)	$MoSi_2$	1200	t	2050	~0.6	11
W (2)	W_3Si_2	tetra				2350		
	WSi_2	tetra (C11)	WSi_2	650	$t^{\frac{1}{2}}$	2165	~0.35	26
Ni (6)	Ni_3Si	cubic (Cu_2Au)				1165		
	Ni_2Si	ortho ($PbCl_2$)	Ni_2Si	200	$t^{\frac{1}{2}}$	1318	~0.31	15*
	NiSi	ortho (MnP)	NiSi	600		992	~0.7	
	$NiSi_2$	cubic (CaF_2)	$NiSi_2$	800		993	~0.85	23
Pd (3)	Pd_3Si	ortho (Fe_3C)				960		
	Pd_2Si	hexa (Fe_2P)	Pd_2Si	200	$t^{\frac{1}{2}}$	1330	~0.35	11,27*
	PdSi	ortho (MnP)	PdSi	735		1090	~0.75	4,28
Pt (5)	Pt_3Si	mono				870		
	Pt_2Si	hexa (Fe_2P)	Pt_2Si	200	$t^{\frac{1}{2}}$	1100	~0.4	
		tetra (Al_2Cu)						
	PtSi	ortho (MnP)	PtSi	200	$t^{\frac{1}{2}}$	1229	~0.35	29,8
Fe (4)	Fe_3Si							
	FeSi	cubic (CrSi)	FeSi	450	$t^{\frac{1}{2}}$	1410	~0.44	30
	$FeSi_2$	cubic	$FeSi_2$	550				

+The number in parentheses indicated the number of phases found in bulk samples.

*Also, present work.

the factors affecting the formation and growth rate of silicides in the interaction of thin films of Ni and Cr with Si. These two metals are representative of two categories of the silicide-forming transition metals in the periodic table. Ni, which is a near-noble metal, forms the phase Ni_2Si at a temperature as low as 200°C[15] with growth rate of Ni_2Si proportional to $(time)^{1/2}$. On the other hand, Cr, which is a refractory metal, forms the phase $CrSi_2$ at a relatively high temperture of 450°C and the rate of $CrSi_2$ formation proceeds linearly with time.[11] It has been reported that Ni is the diffusing species in Ni_2Si formation while Si is in $CrSi_2$ formation.[31,32]

The formation and growth rate of nickel silicides on <100>, <111>, amorphous (evaporated) and poly Si substrates are studied in detail. Transmission electron microscopy analysis was done on the Ni_2Si layers to show, for the first time in studies of silicide formation, how grain-boundary diffusion plays a dominant role in the kinetic rate of growth of silicides. So far, the substrate orientation was believed to have only minor influence on silicide formation.[30,33] We present results which show that the state of the substrate can significantly affect the formation process and the resultant phases of silicides observed.

The kinetic rate of growth of $CrSi_2$ on single crystal Si on different orientations and on Pd_2Si grown

on <100> Si substrates is also presented. We have shown that the influences of impurities, probably oxygen, uniformly distributed in the film and the states of Si-metal interface are more dominant than the orientation of the underlying Si substrates in the formation and growth of $CrSi_2$. The effects of an interposed Pd_2Si layer between the Si substrate and the thin Cr layer on the composition, structure and growth rate of $CrSi_2$ is also presented.

The Pd-Si system and Pd_2Si have been well studied.[2-11,13,34] Data on the rate of formation and structural properties of Pd_2Si have been reported. The electrical properties (barrier heights, contact resistance, etc.) of this silicide have been measured.[3-5] However, the interaction of Cr with Si is less well known.[11] There have been no detailed reports on the kinetics of growth of $CrSi_2$. Reports on the growth rate, activation energy, and structures of $CrSi_2$ are almost nonexistent. The nonavailability of detailed information on $CrSi_2$ and the use of Cr for metallization in semiconductor industry are other motivating factors in our studies of the interaction of Cr with Si.

To understand the concept of formation of $CrSi_2$ on Pd_2Si we investigated the transport mechanism of silicon in the process of $CrSi_2$ formation. Three possible mechanisms can be postulated: silicon can diffuse through Pd_2Si to react with Cr to form $CrSi_2$; in this case, the

Pd_2Si layer only acts as a medium for Si transport. Second, the Pd_2Si bonds can be broken to provide free Si for $CrSi_2$ growth at the Pd_2Si-Cr interface while new Pd_2Si bonds are formed at the Si-Pd_2Si interface. Third, these two processes might be going on simultaneously.

In this investigation, we have used an approach similar to that which Pretorius et al.[35] used in the investigation of the transport mechanism of Si during solid phase epitaxial growth of Si in the Si(crystal)/Pd_2Si/Si(amorphous) system. The approach can be briefly described as follows. Radioactive ^{31}Si is formed from the reaction $^{30}Si(n,\gamma)^{31}Si$ by irradiating a chip of Si in a nuclear reactor. This radioactive Si is evaporated on Pd on single crystal Si before Cr was evaporated on top. The thickness of the radioactive Si is such that it will be completely consumed in the process of Pd_2Si formation. By etching off the $CrSi_2$ layer and counting the activity, using a Geiger counter, we can determine the sources of Si in the process of $CrSi_2$ formation.

The importance of silicides as a diffusion barrier in metallization has not been investigated in detail. Heat treatments of Al or Au on Si substrates at temperatures used in integrated circuit (IC) metallization is known to have resulted in the migration of Si into the overlying Al or Au layers.[36-39] When the metal film is in contact with the Si substrate at selected places only, as is typically the case in IC's, this dis-

solution occurs nonuniformly. Heavy localized erosion of the Si substrate results. Bower has used a Ti layer between Si and Al to defer this pitting.[40] He, indeed, showed that a $TiAl_3$ compound formed during the post-metallization heat-treatment. In a similar way, Nakamura et al. have deferred the recrystallization of polycrystalline Si (poly Si) in contact with an Al film by placing buffer layers of V or Ti between the poly Si and the Al film.[41] In a similar fashion, we have investigated the use of silicides as a diffusion barrier in a metallization scheme. In particular, the role of $CrSi_2$ in a multilayer Si-Pd-Cr-Al metallization is reported.

It has been observed that not all metals form compound phases in the process of solid-phase reactions with silicon.[18,19] For metals which form simple eutectics with silicon, heat treatments at temperatures below the eutectic results in the dissolution and recrystallization or regrowth of silicon in the metal matrix.[37,42-44] Well known of these metals are the noble metals, Au, Ag and Cu, and Al. Ottaviani et al. reported that amorphous silicon in contact with silver films and amorphous germanium in contact with aluminum films form crystalline precipitates when heated to temperatures well below the eutectic.[44] It is believed that the driving force for the growth is provided by the higher-energy state of the amorphous material compared with that of the crystalline material. The solid metal

layer provides the solvent and transport medium. Nakamura et al. have demonstrated that the interaction of Al layers with polycrystalline silicon at temperatures between 400 and 560°C results in the dissolution and recrystallization of poly Si in the metal film.[45] The poly Si substrates were grown by chemical vapor deposition at 640°C.

Polycrystalline silicon is currently being investigated as a passivation layer on planar devices.[46,47] The prospects for the use of poly Si for solar cell technology are also very bright. A thermally grown silicon-dioxide has been widely used for the surface passivation of silicon devices and integrated circuits.[48] Also, a semi-insulating polycrystalline film can be used as a replacement of the thick SiO_2 layer in MOS-ICs.[46-47]

In most applications, however, poly Si is used to prevent intermixing by sacrificial dissolution between the deposited Al film and the underlying Si substrate in devices. In these applications, metal layers, typically Al, are deposited on the poly Si and heat treated to provide electrical contacts.[48,49] It is only desirable that the poly Si layers maintain structural integrity.

To investigate the uniqueness of the poly Si/Al phenomenon, we have extended the studies to metals which form simple eutectics with Si (Au and Ag) and to metals which form silicides (Ni, Pd and Cr).

Backscattering with MeV ^4He ions, Read camera glancing angle x-ray diffraction, scanning electron

microscopy (SEM), and transmission electron microscopy (TEM) are the main tools used in all our investigations. Detailed description of these analytical techniques are given in subsequent sections and chapters.

B. Basic Concepts in Backscattering

Ion backscattering has received increasing attention as a diagnostic technique for the microanalysis of silicon structures.[35,50-52] It is a well-established tool in experimental nuclear physics. It has recently become a very powerful technique for surface and thin film anlaysis.[11,13-15,52-55] In this chapter, the essential concepts and basic formulas will be given. The experimental setup will be given in Chapter II.

There are three basic concepts in backscattering and each gives an analytical capability: kinematic factor (mass analysis), differential scattering cross section (quantitative analysis) and energy loss (depth analysis).

1. Kinematic Factor and Differential Scattering Cross Section

When a projectile of mass m with energy E_o collides with a stationary target atom with mass M, there is momentum transfer from the projectile to the target atom. Assuming there is no nuclear reaction, the energies

of the scattered projectile and the recoil particle can be calculated from the laws of conservation of energy and momentum. The kinematic factor, K, is defined as the ratio of the projectile energies after (E_1) and before (E_0) collision. This factor depends on the scattering angle θ in the lab system and the masses involved in the collision process. The kinematic recoil factor is expressed as

$$K(M,m,\theta) \equiv K_M = \frac{E_1}{E_0} = \left(\frac{m\cos\theta + \sqrt{(M^2-m^2\sin^2\theta)}}{m + M}\right)^2 \qquad (1)$$

The subscript M is used because m and θ are predetermined in a given experiment.

The scattering process due to Coulomb interaction is a classical problem.[56] The differential scattering cross section given in laboratory coordinates can be written as:

$$\sigma = \left(\frac{Z_1 Z_2 e^2}{2E_0 \sin^2\theta}\right)^2 \frac{\{\cos\theta + [1-(\frac{m}{M}\sin\theta)^2]^{\frac{1}{2}}\}^2}{[1-(\frac{m}{M}\sin\theta)^2]^{\frac{1}{2}}} \qquad (2)$$

Recoil correction is included in this equation. Z_1 and Z_2 are the atomic numbers of the projectile and target atom, respectively, E_0 is the energy of the projectile before scattering and θ is the laboratory scattering angle.

The average differential scattering cross section, $\bar{\sigma}$, taken over a finite solid angle, Ω, spanned by the detector, is defined as

$$\bar{\sigma} = \frac{1}{\Omega} \int \sigma \, d\Omega \qquad (3)$$

2. Energy Loss - Depth Analysis

When a projectile penetrates a target, it loses its energy throughout its trajectory to the electrons of the target atoms by ionization and by excitation, and it also loses energy by nuclear collisions. During its outward path (i.e., backscattering) it also loses energy to the target atoms until the particle emerges from the target. The energy loss for both inward and outward paths provide information on how deep the projectile has penetrated.

The energy loss of the projectile per unit length expressed as dE/dx ($eV/\mathring{A}$ or eV/cm) depends on the energy of the particle and also on the projectile and the target. The stopping cross section, ε, is related to dE/dx as

$$\varepsilon = \frac{1}{N} \frac{dE}{dx} \left(\frac{eV - cm^2}{atom}\right) \qquad (4)$$

where N is the atomic density ($atoms/cm^3$).

Assuming the incident energy of the projectile on an elemental target of mass M is E_0, the scattered particles have energy $K_M E_0$ when scattered from the surface atoms. K_M is the kinematic recoil factor of the target. The backscattering geometry, notation and

schematic spectrum is given in Fig. 2. The projectile loses energy to the target on its inward path when the particle is scattered at a depth t, the energy at the depth just before the scattering is E and it can be related to E_0 as

$$E = E_0 - \int_0^{\frac{t}{\cos\theta_1}} \frac{dE}{dx}\, dx \qquad (5)$$

where θ_1 is the incident angle with respect to normal.

After scattering at depth t, the particle will lose its energy on its outward direction and it will have energy E_1 when emerging from the target.

$$E_1 = K_M E - \int_0^{\frac{t}{\cos\theta_2}} \frac{dE}{dx}\, dx \qquad (6)$$

The energy difference, ΔE, between the particles scattered from atoms on the surface and that scattered from atoms at a given depth t is defined from Fig. 2 as

$$\Delta E = K_M E_0 - E_1 \qquad (7)$$

and with Eq. 5 substituted in 6, Eq. 7 becomes

Figure 2. Backscattering geometry, notation and schematic energy spectrum.

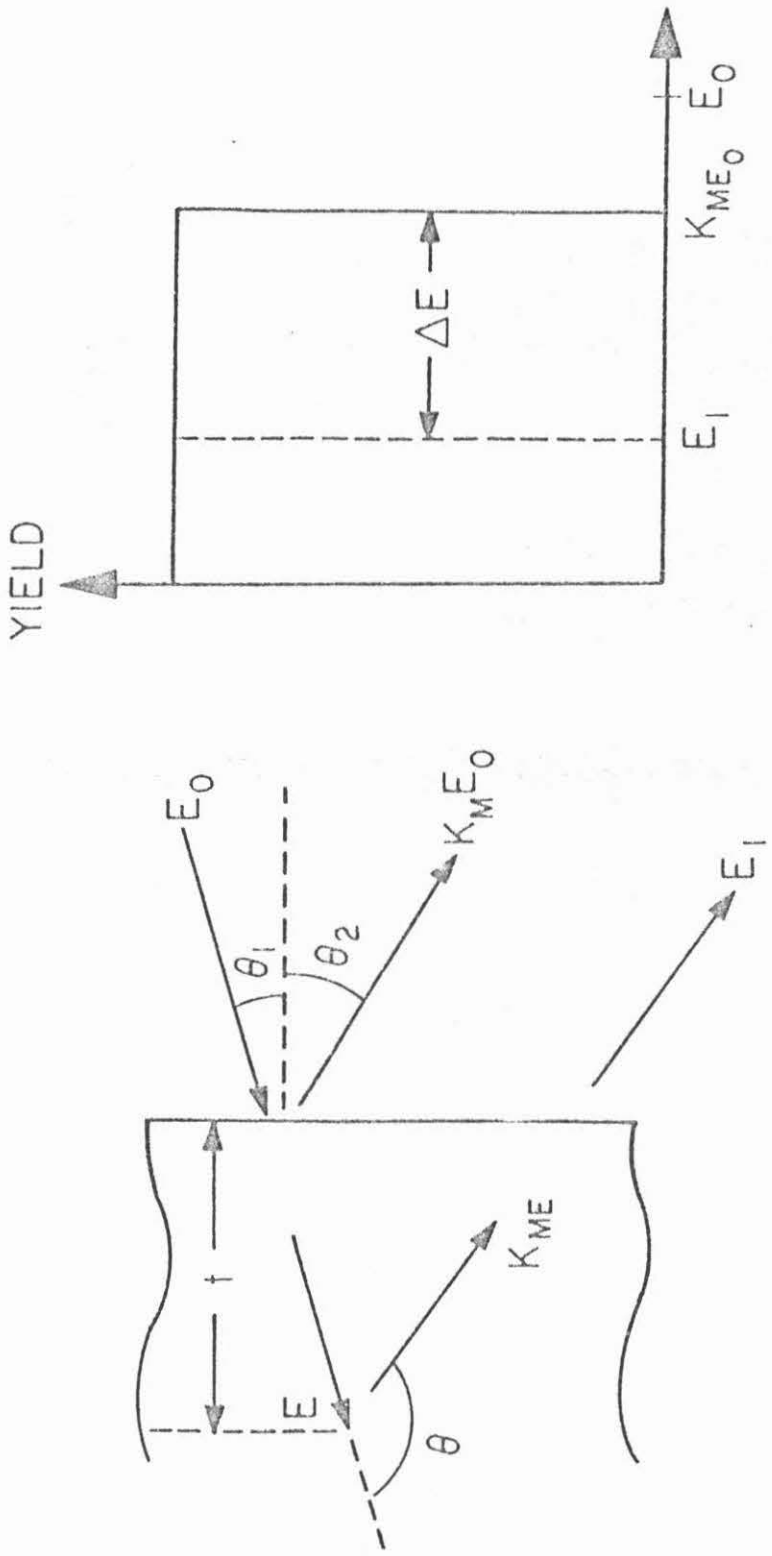
YIELD
E_0
K_{ME_0} E_0
ΔE
E_1
E_0
θ_1
θ_2
$K_M E_0$
E_1
t
E
K_{ME}
θ

$$\Delta E = K_M \int_0^{\frac{t}{\cos\theta_1}} \frac{dE}{dx}\, dx + \int_0^{\frac{t}{\cos\theta_2}} \frac{dE}{dx}\, dx \qquad (8)$$

For small energy loss, dE/dx is a slowly varying function of energy and ΔE the energy loss can be simplified as

$$\Delta E = [S]t \qquad (9)$$

The symbol [S] is called the backscattering energy loss factor and it changes slowly as a function of E and t.

For a very thin film, one can assume tnat dE/dx of the projectile in thin film does not change and can be evaluated at the energy E_0 for its incoming path and $K_M E_0$ for its outgoing path. Equation 8 then simplifies to

$$\Delta E = \left(\frac{K_M}{\cos\theta_1} \left.\frac{dE}{dx}\right|_{E_0} + \frac{1}{\cos\theta_2} \left.\frac{dE}{dx}\right|_{K_M E_0}\right) t \qquad (10)$$

From Eqs. 9 and 10, we obtain [S] as

$$[S] = \frac{K_M}{\cos\theta_1} \left.\frac{dE}{dx}\right|_{E_0} + \frac{1}{\cos\theta_2} \left.\frac{dE}{dx}\right|_{K_M E_0} \qquad (11)$$

For experiments performed such that the incident beam is normal to the target, $\theta_1 = 0$ and $\theta_2 = \pi - 0$, so

$$[S] = K_M \left.\frac{dE}{dx}\right|_{E_0} + \frac{1}{|\cos\theta|} \left.\frac{dE}{dx}\right|_{K_M E_0} \qquad (12)$$

A parallel set of equations for ε instead of dE/dx can be derived to give the backscattering stopping cross section factor in the unit of eV-cm^2. The stopping cross section factor is

$$[\varepsilon] = K\varepsilon(E_0) + \frac{1}{|\cos\theta|}\,\varepsilon(K_M E_0) \equiv \left(\frac{1}{N}\right)\,[S] \qquad (13)$$

Figure 3a gives the shape of a typical dE/dx or ε versus energy curve. E_0 is the incident energy of the projectile. When the projectile penetrates the target at a distance, t, its energy decreases to E. The values of energy loss dE/dx, along the incident and outgoing path as given in Eq. 8 are accentuated with two heavy bars on the dE/dx curve in Fig. 3a. The assumption made in deriving Eqs. 8 to 13 becomes accurate for a very thin target (as $E_0 \sim E$) as is shown in a plot of ΔE versus Δx in Fig. 3b.

The height H_M of the backscattering spectrum given in counts per channel is determined by the number of scattering events in an incremental target thickness Δx. This thickness is related to the channel width δE by $\delta E = [S]\Delta x$, where δE is fixed by the gain of the electronic system and is typically 2-5 keV. Thus

$$H_M(\text{counts/channel}) = Q\Omega\sigma N\Delta x \qquad (14a)$$

or

$$H_M = Q\Omega\sigma N\,\frac{\delta E}{[S]} \qquad (14b)$$

by substituting for Δx. In these equations Q is the integrated charge (typically Q = 20 μC = 20 nA for 15 minutes),

Figure 3. (a) Schematic diagram of dE/dx versus E and regions used for backscattering analysis (Chu, "New Uses of Ion Accelerators, Chapter 2, Ed. J.F. Ziegler). (b) Energy to depth scale relations for 2 MeV $^{4}He^{+}$ backscattering from Si (Chu, "New Uses of Ion Accelerators," Chapter 2, Ed. J.F. Ziegler).

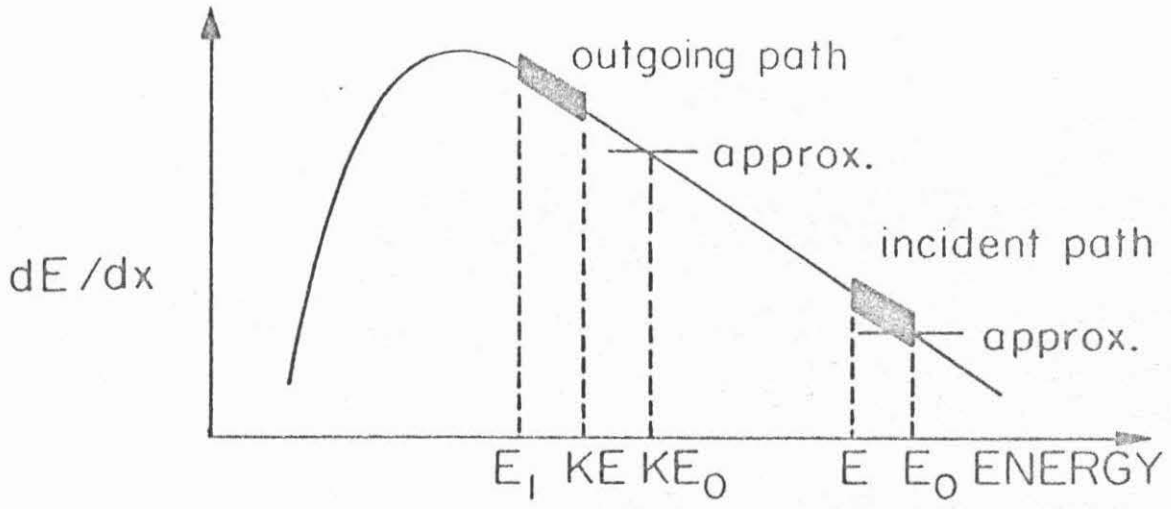
outgoing path
approx.
incident path
approx.
dE/dx
E1 KE KE0
E E0 ENERGY

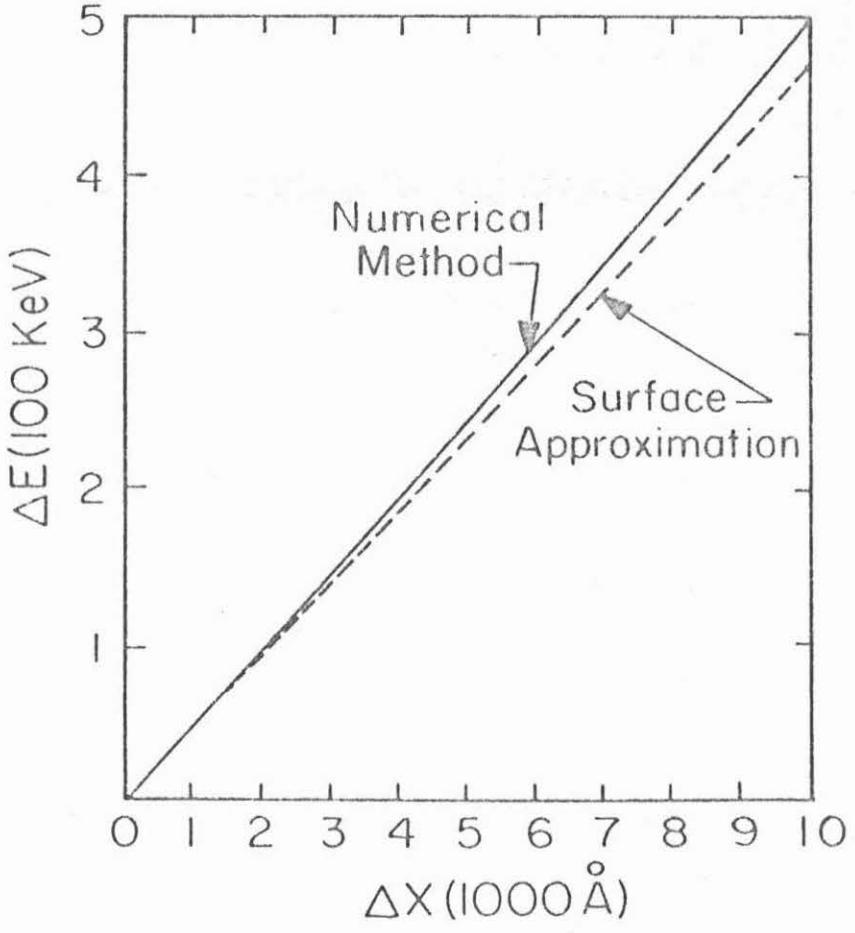
5
4
3
2
1
ΔE(100 KeV)
Numerical Method
Surface Approximation
0 1 2 3 4 5 6 7 8 9 10
ΔX(1000 Å)

Ω is the solid angle (about 4 msterad = 25 mm^2 detector at 8 cm), N is the atomic density (atoms/volume), σ and [S] are as defined before.

3. Compound Analysis by Backscattering

For an integrated charge, Q, of ^4He ions and a detector solid angle, Ω, the total area, A in counts under a peak in a backscattering spectrum is given by

$$A = Q\Omega\sigma Nt \tag{15}$$

where N is the number of atoms per unit volume and t is the thickness of the target, σ is the differential scattering cross section.

Figure 4 gives a schematic representation of an energy spectrum for 2 MeV ^4He ions backscattered from a compound, designated as M_xSi_y in the interaction of a compound forming metal (M) with Si. The letters x and y are integers which define the stoichiometry of the compound layers (alternative, x and y may be fractions such that x + y = 1). The shaded areas give the signal in the compound layer. These areas are defined as in Eq. 15 with Q, Ω and t the same for both signals. The composition ratio of metal to Si atoms per unit volume is therefore given in Eq. 15 to be

$$\frac{N_M}{N_{Si}} = \frac{A_M/\sigma_M}{A_{Si}/\sigma_{Si}} \tag{16}$$

Figure 4. Schematic representation of an energy spectrum for 2 MeV ^{4}He ions backscattered from a typical M_xSi_y on a Si substrate. The composition ratio of the compound layer can be obtained by comparing the shaded area of metal (M) with that of Si or by comparing the plateau height of M with that of Si. The numbers 1 and 2 refer to the Si-M_xSi_y and M_xSi_y-M interfaces respectively, while 3 refers to the surface of M.

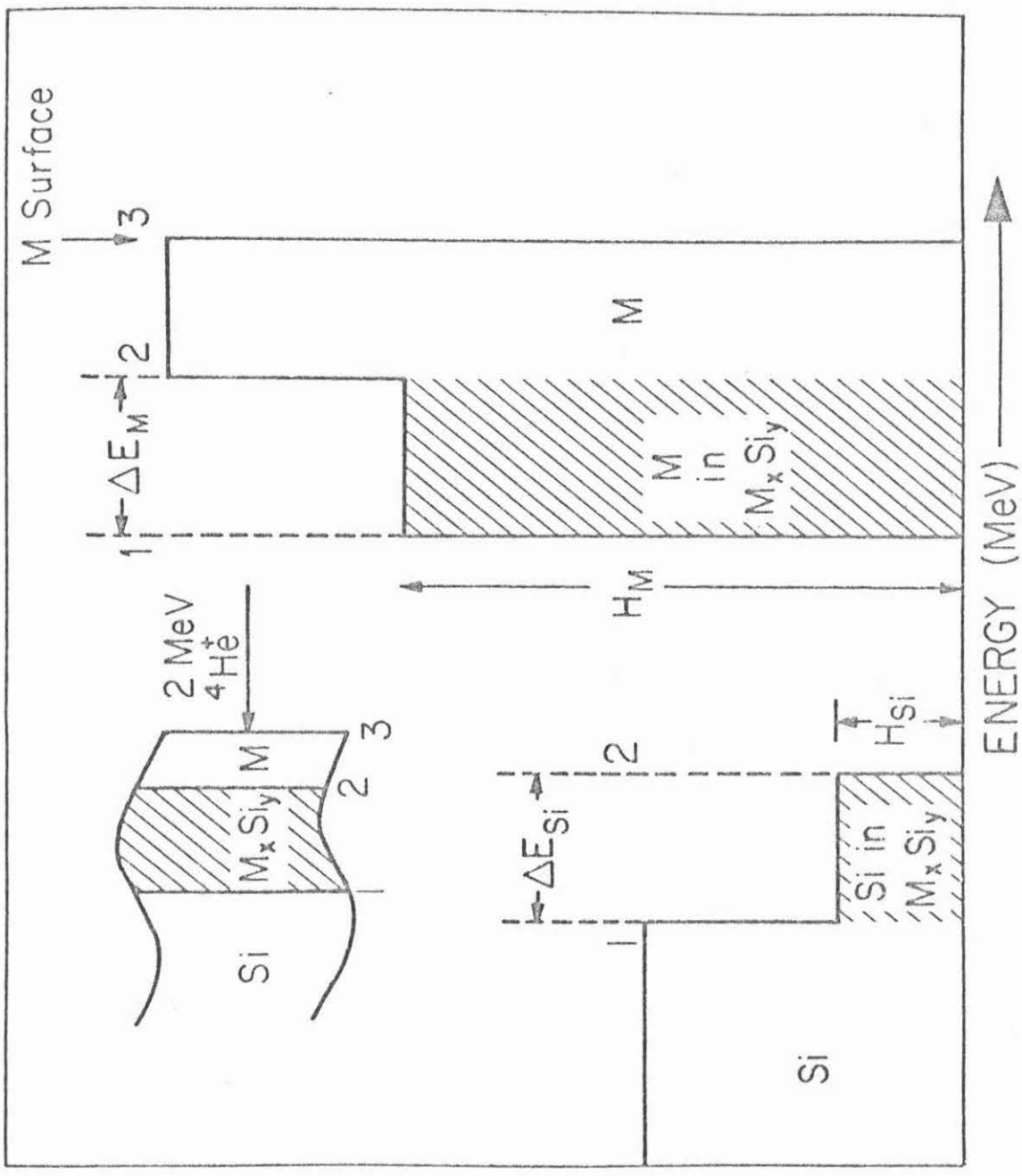
M Surface
3
2
1
ΔE_M
M
M in M_xSi_y
H_M
2 MeV $^4He^+$
M
M_xSi_y
Si
2
3
ΔE_{Si}
2
H_{Si}
Si in M_xSi_y
Si
ENERGY (MeV)
BACKSCATTERING YIELD (COUNTS)

Using Eq. 14, the plateaus heights for the metal, M, and Si are given by

$$H_M \propto N_M \sigma_M / [S]_M^{M_xSi_y} \tag{17}$$

and

$$H_{Si} \propto N_{Si} \sigma_{Si} / [S]_{Si}^{M_xSi_y} \tag{18}$$

where N_M, N_{Si} are the atomic densities of the metal and Si in the compound layer: σ_M and σ_{Si} are the differential scattering cross sections; $[S]_M^{M_xSi_y}$ and $[S]_{Si}^{M_xSi_y}$ are the energy loss factors for the metal and Si respectively in the compound layer. Values of $[S]_M^{M_xSi_y}$ and $[S]_{Si}^{M_xSi_y}$ can be obtained from Eq. 12. These values are calculated for nickel, palladium, chromium and Si in the silicide layers and are given in Table 2. By substituting Eqs. 17 and 18 into Eq. 16 using Table 2, we obtain the metal to Si composition ratio as

$$\frac{N_M}{N_{Si}} = \frac{\sigma_{Si}}{\sigma_M} \frac{H_M \Delta E_M}{H_{Si} \Delta E_{Si}} \tag{19}$$

The composition of dielectric layers has been determined in a similar fashion by using Eqs. 16 or 19.[50]

TABLE 2.

$[S]^{Si}_{Si}$	$[S]^{Ni_2Si}_{Si}$	$[S]^{Ni_2Si}_{Ni}$	$[S]^{Ni}_{Ni}$	σ_{Ni}/σ_{Si}
46.1	101	107	118.6	4.13
	$[S]^{Pd_2Si}_{Si}$	$[S]^{Pd_2Si}_{Pd}$	$[S]^{Pd}_{Pd}$	σ_{Pd}/σ_{Si}
	102	109	120	11.2
	$[S]^{CrSi_2}_{Si}$	$[S]^{CrSi_2}_{Cr}$	$[S]^{Cr}_{Cr}$	σ_{Cr}/σ_{Si}
	85.57	95.04	110.5	3.02

Calculated values of the backscattering energy loss parameters [S] (eV/Å) used in the compositional and kinetic analysis of nickel, palladium and chromium silicides in this work. Values of σ_M/σ_{Si}, the differential cross-sectional ratios are also given. Values of [S] are calculated from knowledge of the silicide density ρ, stopping powers of the metal and Si, and Bragg's rule.[57,58] The subscripts on [S] refer to the species from which scattering is considered and the superscripts refer to the media in which the energy loss is experienced. The values are calculated for an incoming beam of 2.0 MeV ^{4}He ions and a detector angle of 170°. Values of stopping powers were obtained from J.F. Ziegler and W.K. Chu.[57]

CHAPTER II. Experimental

A. Sample Preparation

1. Si-Ni, Si-Cr, Si-Pd-Cr and Si-Pd-Cr-Al

Substrates of single crystal <100> and <111> oriented, amorphous (evaporated) and polycrystalline silicon (poly Si) were used in the studies of the interactions of Ni with Si. The studies of chromium silicide were made on single crystal <100> and <111> oriented Si and on palladium silicide grown on <100> Si. The chemically polished single crystal Si substrates and poly Si were cleaned ultrasonically with TCE, acetone, methanol, rinsed in doubly-distilled H_2O and then etched in concentrated (diluted for poly Si) HF and rinsed again in doubly-distilled H_2O just prior to evacuation. The SiO_2 substrates on which amorphous Si was evaporated were cleaned only with TCE, acetone and methanol and then rinsed in doubly-distilled H_2O before being place in a vacuum. Depositions were made with an electron gun in an oil free deposition system. A vacuum of about 2×10^{-6} to 7×10^{-7} Torr or better was maintained during deposition. The vacuum during annealing was maintained, for all heat treatments, at a pressure between 5 and 7×10^{-7} Torr with an oil diffusion pump baffled with a LN_2 trap.

(a) Si-Ni

For the Ni evaporation, all of the substrates

were simultaneously loaded into an e-gun evaporator. The thicknesses of the Ni films vary from 1000 to about 5000Å. The samples were placed side by side in the same annealing boats under the same vacuum and annealed for the same lengths of time at the same temperatures. Annealing temperatures ranged from 200 to 325°C and lasted from about 1/2 to 24 hours.

(b) Si-Cr

Chromium films of about 800 to 2000Å were evaporated on single crystal Si, and Pd films ranging from 300 to 3000Å were deposited on single crystal Si before Cr was evaporated on top. Whenever both Pd and Cr films were deposited on a Si wafer both evaporations were made sequentially without breaking vacuum. Heat treatments were performed in a vacuum annealing furnace. Most of the Si-Cr and Si-Pd-Cr samples were heat treated together so that the resultant silicide thicknesses could be compared for identical process temperatures and times. Annealing temperatures ranged from 400 to 525°C and lasted from about 10 to 150 minutes.

Experimental procedures of radioactive Si tracer studies of the formation of $CrSi_2$ on Pd_2Si is given in detail in the Appendix.

(c) Pd-Al

The Pd-Al metallization scheme was investigated in two main stages. Sample preparations of the Si-Pd-Al ternary system was followed by the more complex Si-Pd-Cr-Al

system. All experiments were performed with single crystal <100> Si wafers as substrates. Cleaning procedures are similar to those earlier described for the investigation of nickel and chromium silicides. In the Si-Pd-Al system, evaporation of 300 to 2000Å of Pd followed by about 3000Å of Al were made in that order on <100> oriented Si without breaking vacuum. On some samples only thin films of Pd were deposited, annealed in vacuum at temperatures ranging from 275 to 300°C to form Pd_2Si with all of the Pd consumed before Al was vacuum deposited on top.

(d) Pd-Cr-Al

The more complex Si-Pd-Cr-Al samples were prepared by sequential evaporation of thin films of Pd, Cr and Al on <100> Si in a single pump down. Annealing temperatures were chosen between 275 and 550°C with times up to 2 hours. The heat treatments were essentially isothermal (± 1°C).

2. Polycrystalline Si-Metal Samples

Polished single-crystal Si wafers of about 4 Ωcm n-type conductivity and oriented in <100> direction were thermally oxidized at 950°C in steam to a thickness of 1000 ± 50Å. The substrates thus obtained were covered with a layer of undoped polycrystalline Si (poly Si) formed at 640°C by chemical vapor deposition. The grain size of the poly Si was found to be so small that no contrast could

be seen by conventional TEM imaging. Harris et al. found out by use of electron diffraction methods that the grain size is less than 300Å.[59] The thickness of this poly Si film ranged from approximately 0.4 to 0.5 μm. Metal layers of Al, Ag, Au, Pd, Ni and Cr were evaporated onto the unheated poly Si. Evaporation was performed by an electron gun for Al, Au, Pd, Ni and Cr and by a Mo resistance heater for Ag. Vacuum pressure during evaporation was maintained below 5×10^{-7} Torr. Heat treatments were performed in vacuum at pressures below 10^{-7} Torr. All annealings were performed below the lowest eutectic temperatures for each combination of metal and Si. Metal layers were chemically removed with aqua regia (1 HNO_3 + 3 HCl) for Al and Au, and with HNO_3 for Ag. Scanning electron microscopy (SEM) was used to monitor the change in morphology of the Si recrystallized in the metal matrices.

B. Backscattering Analysis

The primary tool used in this investigation was 2.0 MeV ^4He ion backscattering. The backscattering analysis was carried out on the 3 MeV Kellogg machine utilizing a solid state nuclear particle detector positioned at a scattering angle $\theta = 170°$. The detailed experimental technique of backscattering is given in a number of references.[35,50-55] A brief description of the basic

concepts has been given in Chapter I.

Basically, the method consists of placing a target in a monoenergetic beam of ions of light elements, ^4He ions in this investigation. Particles coming from the target are detected and analyzed. The schematic diagram of the backscattering chamber and electronics is shown in Fig. 5. The samples to be analyzed were mounted on a multiple target holder where they were sequentially rotated into normal incidence with the incoming beam. A beam spot of approximately 1 mm^2 was used to study the samples in this investigation. The basic concepts of this technique has been given in detail in Chapter I.

C. Read Camera Glancing Angle X-ray Diffraction

Phase identification of the silicides Ni_2Si, NiSi, Pd_2Si and $CrSi_2$ were made by using Read camera glancing angle x-ray diffraction technique. The Read camera configuration is basically a glancing angle diffraction setup with a fixed angle of incidence.[55,60-62] By use of glancing angles of incidence, a relatively large volume is examined even in thin film samples. For example, an incident angle of 6.4° will increase the length of the x-ray beam path in a thin specimen to about nine times the film thickness.[55]

The experimental geometries of the Read camera is shown in Fig. 6. X-ray diffraction patterns are obtained from monochromatic x-ray beam (CuKα at 45 keV and

Figure 5. This figure illustrated that experimental arrangement used to measure the backscattering spectra of the thin film structures in this investigation. The incoming beam strikes the sample at normal incidence and the ^{4}He particles scattered into an angle θ are analyzed with a solid state nuclear particle detector. The output of the detector is amplified and stored in a pulse height analyzer. A simple multi-target holder was used.

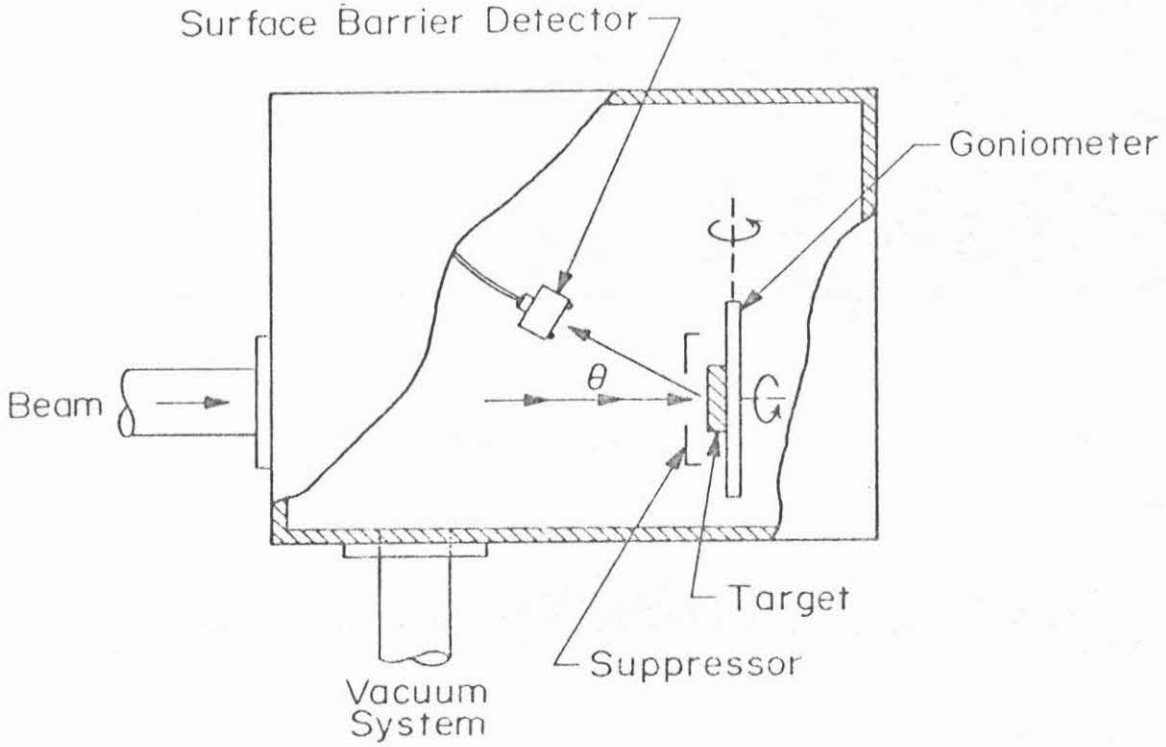
Surface Barrier Detector
Goniometer
Beam
θ
G
Target
Suppressor
Vacuum
System

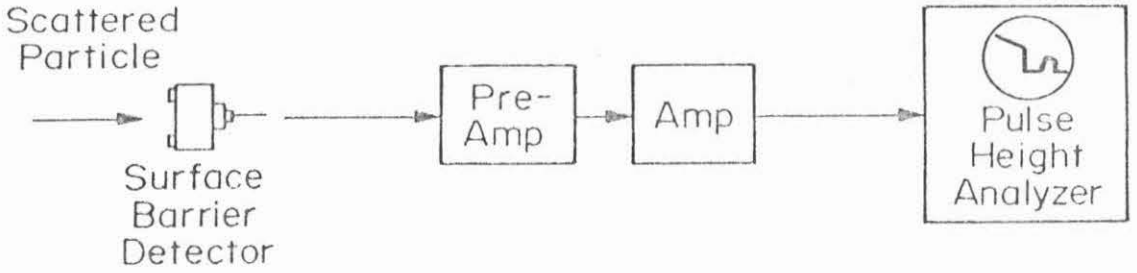
Scattered
Particle
Surface
Barrier
Detector
Pre-
Amp
Amp
Pulse
Height
Analyzer

Figure 6. Schematic diagram of the geometry of the Read camera. γ is the glancing angle of incidence and θ is the Bragg angle.

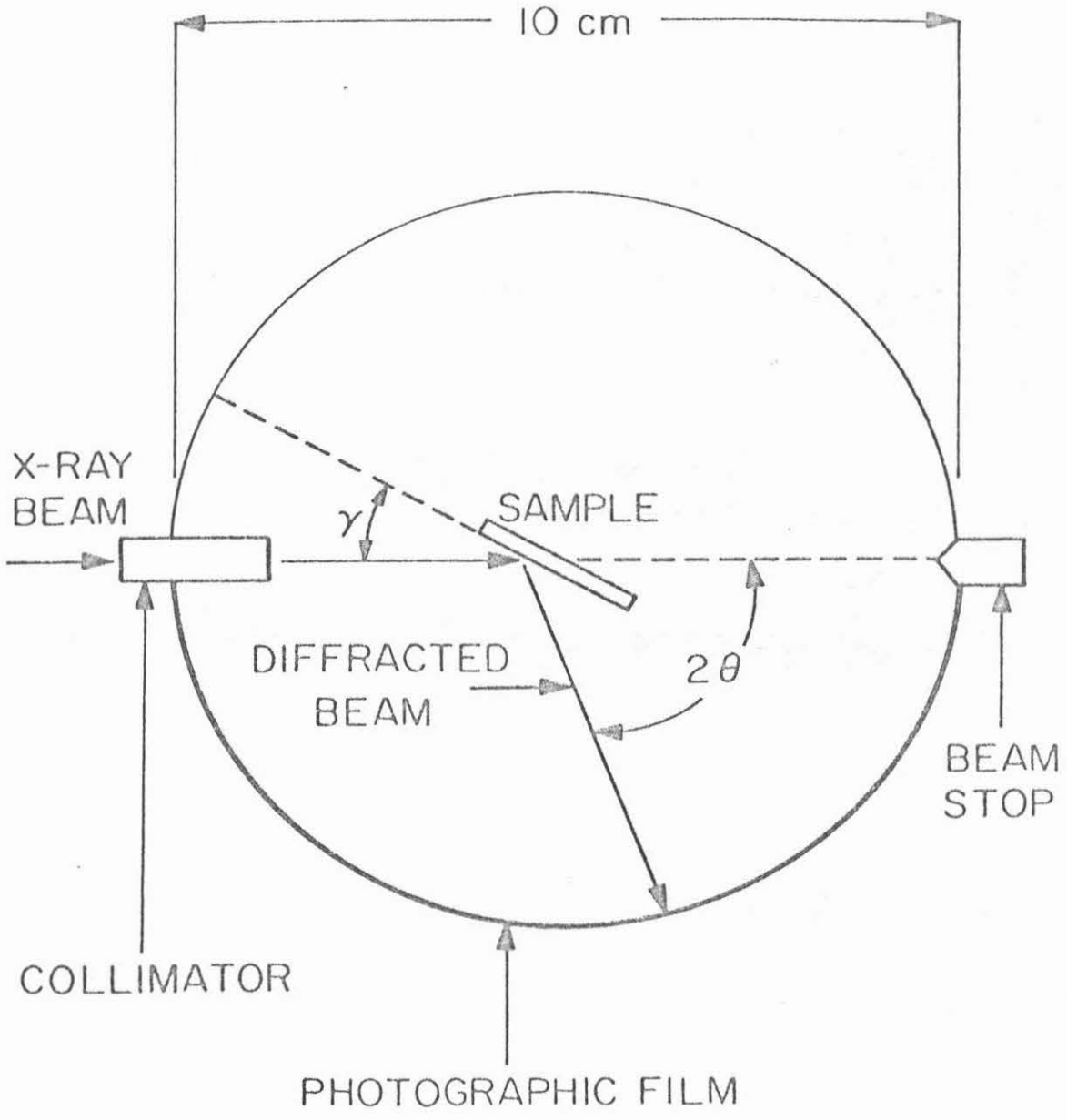
10 cm
X-RAY
BEAM
γ
SAMPLE
DIFFRACTED
BEAM
2θ
BEAM
STOP
COLLIMATOR
PHOTOGRAPHIC FILM

20 nA in the present studies), collimated through two pinholes and the patterns are recorded on polaroid film placed on a 5 cm radius from the sample center.

The Read camera diffraction technique gives spot patterns for diffractions from single-crystal Si and ring patterns from polycrystalline films. The components of the film are identified by measuring the angular positions of the rings and then comparing these positions with data in ASTM powder pattern compilation. The d-spacings, relative intensities, corresponding angles and crystallographic axes (hkl) are given for nickel, palladium and chromium silicides in the next few chapters. The details of the comparison of this experimental technique with backscattering has been given by S.S. Lau et al.[55]

D. Transmission, Scanning Electron and Optical Microscopy

The difference in the growth rate of nickel silicide, Ni_2Si, on <100> and <111> Si has been attributed to the structural differences of the compound layers. To verify this transmission electron microscopy was used to investigate the structure of the Ni_2Si on <100> and <111> Si substrates.

Scanning electron (SEM) and optical microscopy were used to analyze the surface topology and lateral uniformity of all the samples used in this work. Re-

crystallization of polycrystalline Si in Al, Ag and Au was monitored, after the metal layers were chemically removed with aqua regia, by using the SEM. The SEM was fitted with a two-axis goniometer. This allowed the sample surfaces to be viewed at their optimum angle.

CHAPTER III. Growth Rate, Compositon and Structure of Thin Film Nickel Silicide Layers

In this chapter, the growth kinetics, structure and composition of nickel silicides on different substrate orientations (<100>, <111>, amorphous [evaporated] and polycrystalline Si) substrates are described. So far, the substrate was believed to have only minor influence on the silicide formation. This chapter presents results obtained on thin films of nickel silicides which show that the state of the substrates can significantly affect the formation processes and the resultant phases of silicides observed.

Backscattering spectrometry is the primary technique used to investigate the growth rate and composition of the silicides.

The structure of Ni_2Si grown on <111> and <100> oriented Si is investigated by means of transmission electron microscopy (TEM). Read camera x-ray diffraction analysis identifies the compound phases on the different substrates.

A. Ni_2Si on Single-Crystal and on Poly Si Substrates

Annealing temperature varies from 200 to 325°C and from 1/2 to about 24 hours for all Ni films vacuum deposited on Si substrates. Over the whole temperature

range investigated, only the Ni_2Si phase was identified in the reaction product of thin Ni films of thicknesses ranging from 100 to 5000Å on single crystal Si and poly Si substrates. Figure 7 shows the backscattering spectra of 1600Å film of Ni on <100> and <111> Si annealed at 275°C for 4 hours. The film on the <100> substrate is almost fully reacted while that on the <111> substrate is mainly unreacted. Additional measurements were made for different temperatures and times. Only the phase Ni_2Si was observed and the rate of formation was always significantly faster on <100> then on <111> Si substrates.

The same silicide phase Ni_2Si is observed on Poly Si, as on single crystal substrates. Figure 8 shows the ^4He ion backscattering spectra of a Ni film on poly Si before and after annealing at 275°C for 2 hours.

The composition ratio of Ni to Si in the nickel silicide layer may be measured by using Eq. 16 rewritten here as

$$\frac{N_{Ni}}{N_{Si}} = \frac{A_{Ni}^{Ni_2Si}}{A_{Si}^{Ni_2Si}} \times \frac{\sigma_{Si}}{\sigma_{Ni}} \tag{20}$$

or

$$\frac{N_{Ni}}{N_{Si}} = \frac{H_{Ni}^{Ni_2Si}}{H_{Si}^{Ni_2Si}} \times \frac{\Delta E_{Ni}^{Ni_2Si}}{\Delta E_{Si}^{Ni_2Si}} \times \frac{\sigma_{Si}}{\sigma_{Ni}} \tag{21a}$$

Figure 7. ^{4}He ion backscattering spectra of a 1600Å film of Ni on <100> and <111> Si substrates after vacuum annealing at 275°C for 4 hours.

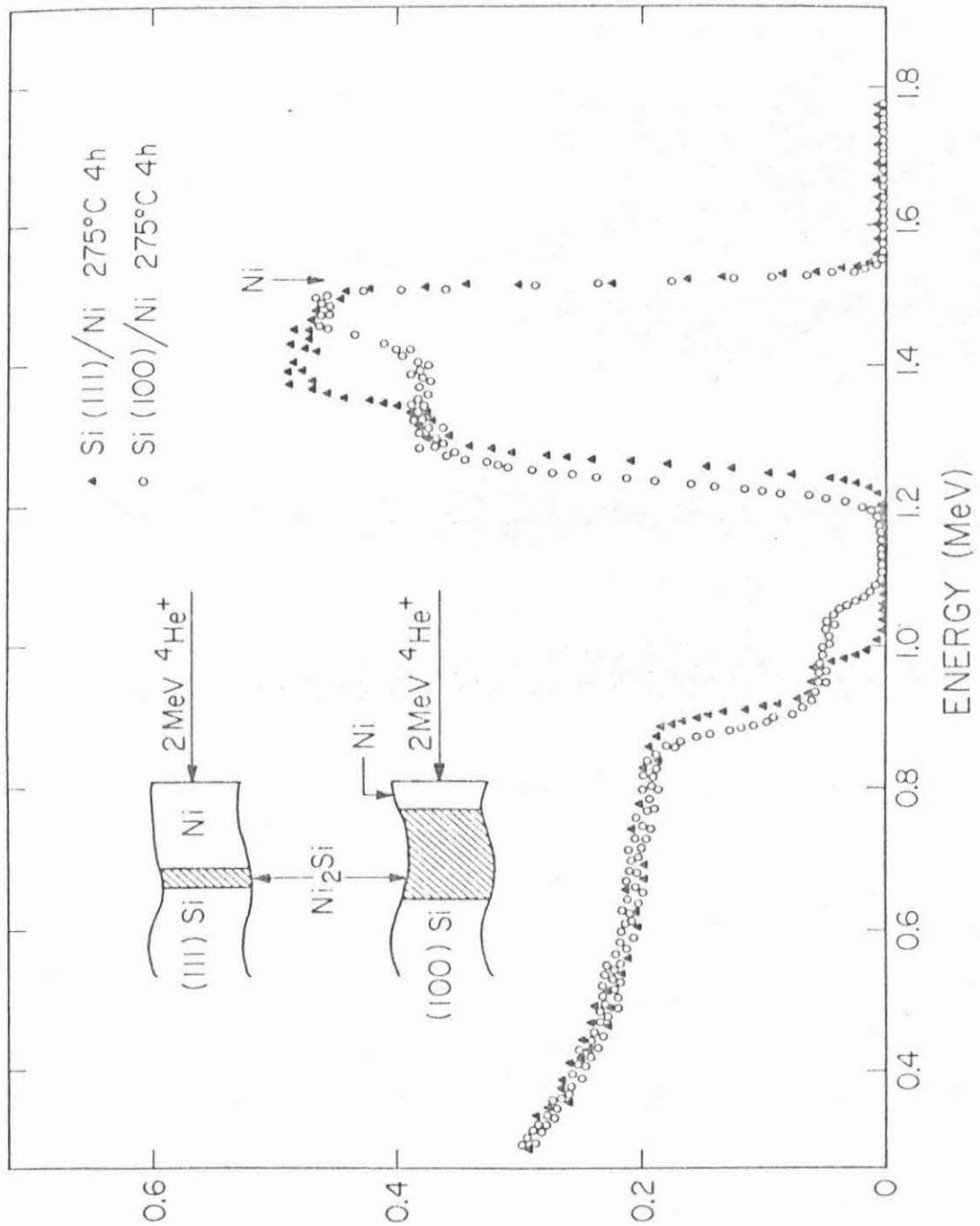
Si (111)/Ni 275°C 4h
Si (100)/Ni 275°C 4h
Ni
2MeV $^4He^+$
Ni
Ni_2Si
(111) Si
Ni
2MeV $^4He^+$
(100) Si
BACKSCATTERING YIELD (10^4 COUNTS)
ENERGY (MeV)
0
0.2
0.4
0.6
0.4
0.6
0.8
1.0
1.2
1.4
1.6
1.8

Figure 8. ^{4}He ion backscattering spectra of 4500Å Ni film on poly Si before (●) and after (o) vacuum annealing at 275°C for 2 hours.

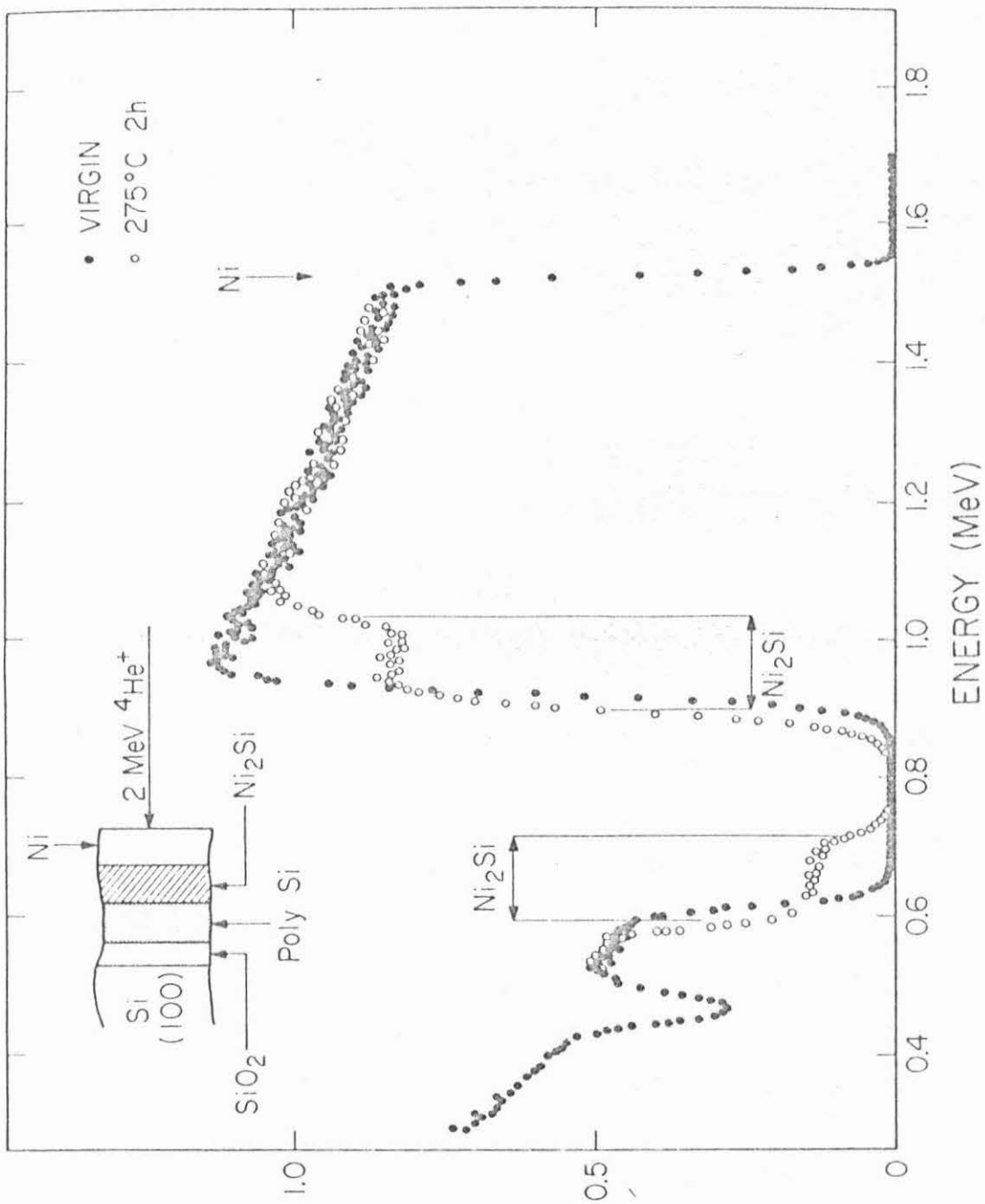
• VIRGIN
○ 275°C 2h
Ni
Ni₂Si
Ni₂Si
2 MeV ⁴He⁺
Ni
Ni₂Si
Poly Si
Si (100)
SiO₂
BACKSCATTERING YIELD (10⁴ COUNTS)
ENERGY (MeV)
0
0.5
1.0
0.4
0.6
0.8
1.0
1.2
1.4
1.6
1.8

Since $\Delta E = [S]t$ (Eq. 9),

$$\frac{N_{Ni}}{N_{Si}} = \frac{H_{Ni}^{Ni_2Si}}{H_{Si}^{Ni_2Si}} \times \frac{[S]_{Ni}^{Ni_2Si}}{[S]_{Si}^{Ni_2Si}} \times \frac{\sigma_{Si}}{\sigma_{Ni}} \qquad (21b)$$

where $A_{Si}^{Ni_2Si}$ and $A_{Ni}^{Ni_2Si}$ are the integratednumber of counts from each species within the compound. N_{Si} and N_{Ni} are as defined in the previous chapters. $H_{Ni}^{Ni_2Si}$ and $H_{Si}^{Ni_2Si}$ are the heights of the plateau in the backscattering spectrum corresponding to Ni and Si respectively in the compound layer. Values of the energy loss factors $[S]_{Ni}^{Ni_2Si}$ and $[S]_{Si}^{Ni_2Si}$ are 107 and 101 (eV/Å) as given in Table 2. Also $\sigma_{Ni}/\sigma_{Si}=4.13$ using these values and the calculated heights of Ni and Si in the compound layers, $N_{Ni}/N_{Si} = 2.0 \pm 0.5$.

Spectra similar to those in Figs. 7 and 8 were used to estimate the rate of formation of the silicide layer. From the energy loss ΔE, measured as the full width at half maximum of the contribution from the silicide, the thickness of the silicide layers can be obtained from the energy loss expression,

$$\Delta E = [S]t \qquad (22)$$

Using either the value of $[S]_{Ni}^{Ni_2Si}$ or $[S]_{Si}^{Ni_2Si}$, the thickness t of the silicide can be obtained.

A plot of the Ni_2Si layer thickness versus

(time)$^{1/2}$ is shown in Fig. 9 for <111> Si (four temperatures), <100> Si and poly Si (275°C only). The data for the <100> Si substrate agree well with the results of Tu et al. obtained also for Ni on <100> Si (dashed line in Fig. 9). The square-root-of-time dependence of the growth of the silicide layers holds in all cases. This indicates that the reaction process is limited by the transport of Ni across the silicide layer. The rate of the reaction, however, depends on the structure of the substrate. As can be seen, the reaction proceeds 2 to 3 times more slowly on a <111> than on a <100> or a poly Si substrate. At 275°C for one hour annealing, the rate on <100> Si corresponds to about 1000Å for Ni_2Si.

The Arrhenius plot for the formation of Ni_2Si on <111>, <100> and poly Si substrates is shown in Fig. 10. The corresponding activation energies are E_a = 1.6 ± 0.2, 1.5 ± 0.2 and 1.3 ± 0.2 eV respectively.

B. Structures of Ni_2Si on <100> and <111> Si Substrates by Transmission Electron Microscopy (TEM)

The dependence of the rate on the state of the substrates means that even though the process is transport-limited the substrate can still affect the process. This is a remarkable fact. A possible explanation is to assume that the silicide layers formed on different substrates are dissimilar in such a way as to alter the transport

Figure 9. Plot of Ni_2Si layer thickness versus $(time)^{1/2}$ for Ni evaporated on <100>, <111> and poly Si. For comparison, the work of Tu et al. on <100> Si (dashed line) is included.

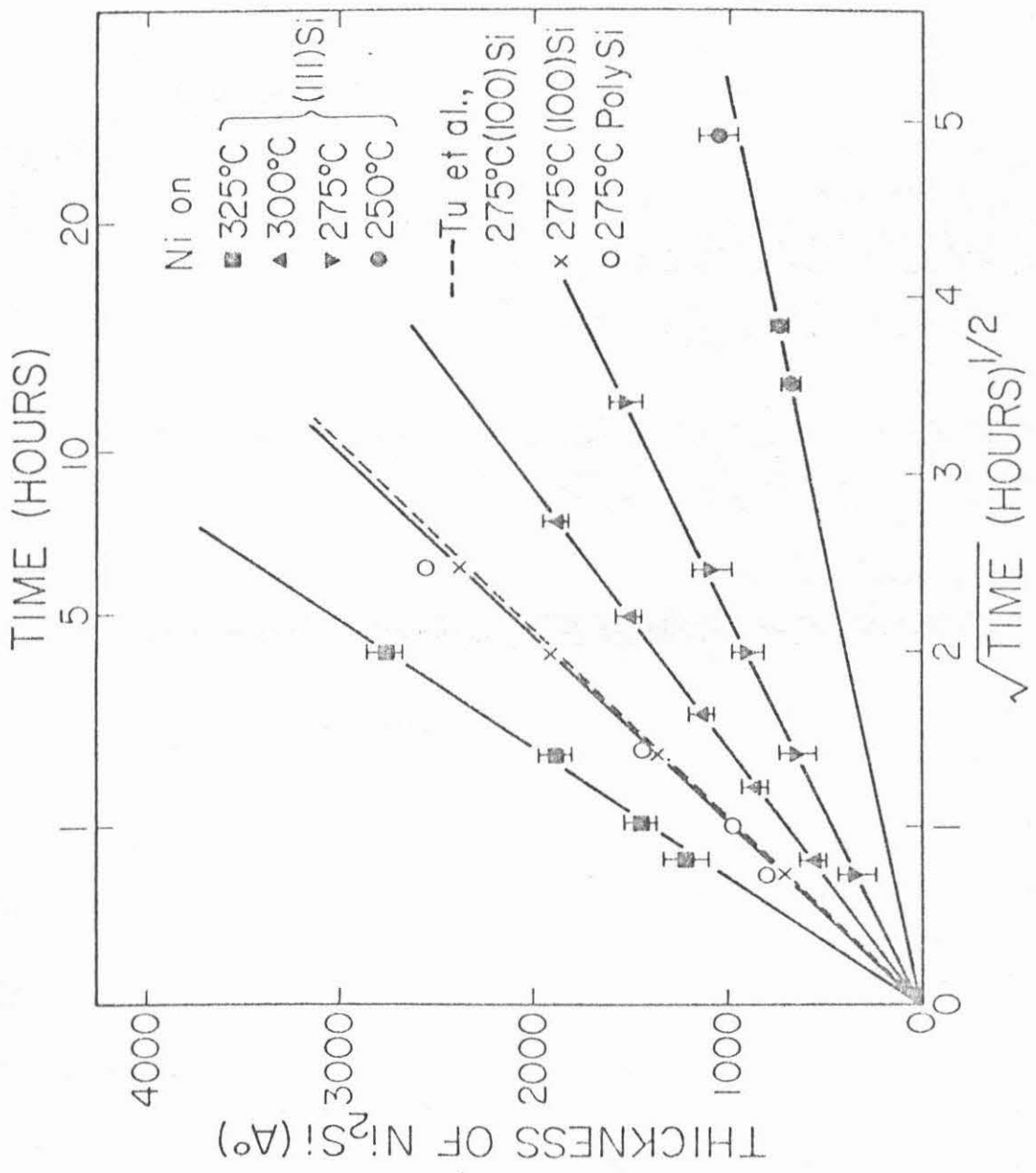
TIME (HOURS)
5
10
20
Ni on
325°C
300°C
275°C
250°C
(111)Si
---Tu et al.,
275°C(100)Si
× 275°C (100)Si
o 275°C Poly Si
4000
3000
2000
1000
0
THICKNESS OF Ni_2Si (A°)
0
1
2
3
4
5
$\sqrt{TIME}$ (HOURS)$^{1/2}$

Figure 10. Plot of activation energy for the Ni_2Si layer growth on <111>, <100> and poly Si substrates, and for the (Ni_2Si + NiSi) layer growth on amorphous (evaporated) Si. The dashed line is from Tu et al.

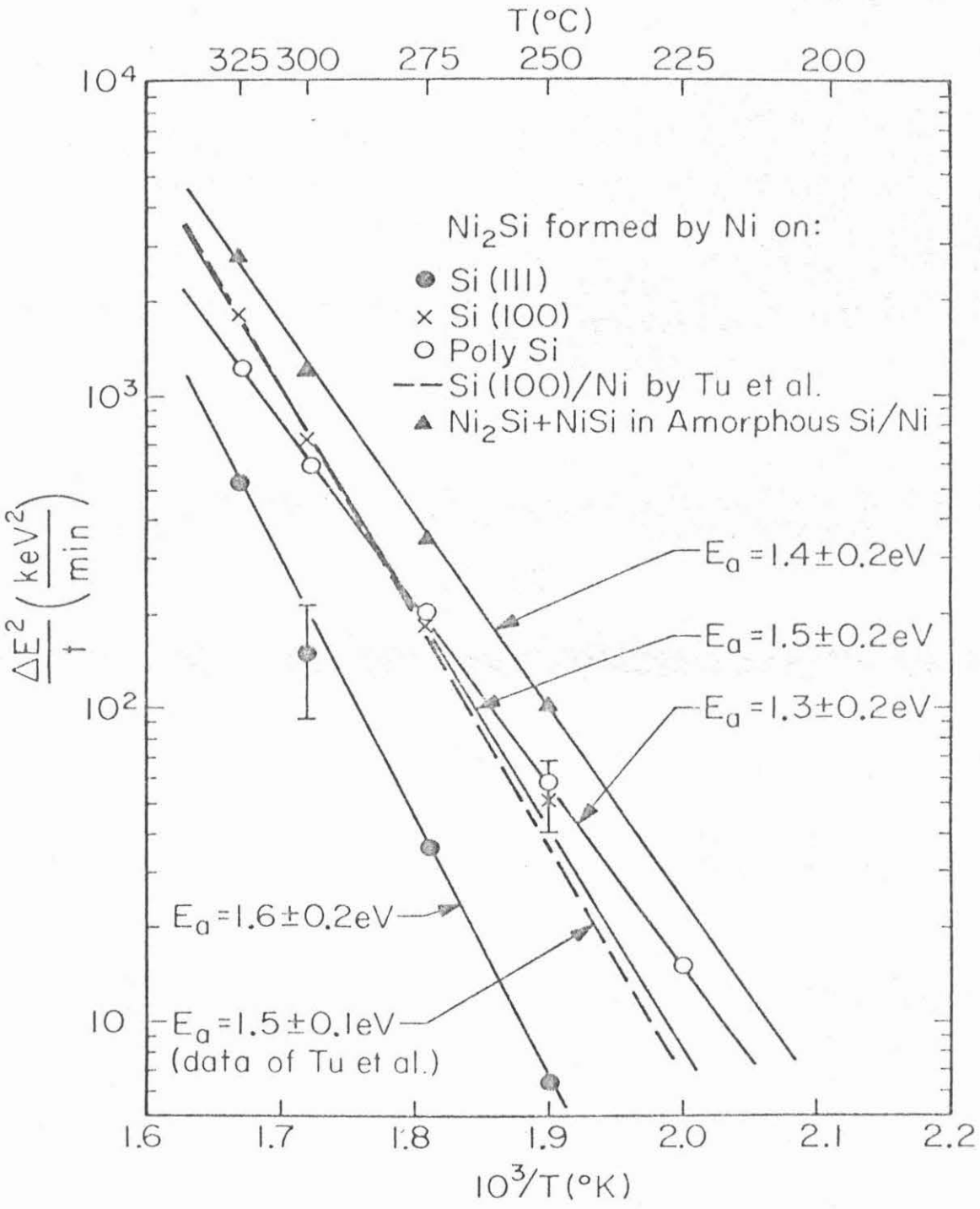
T(°C)
325 300 275 250 225 200
10^4
10^3
10^2
10
$\frac{\Delta E^2}{t}\left(\frac{keV^2}{min}\right)$
Ni_2Si formed by Ni on:
Si (111)
Si (100)
Poly Si
Si (100)/Ni by Tu et al.
Ni_2Si+NiSi in Amorphous Si/Ni
E_a = 1.4±0.2eV
E_a = 1.5±0.2eV
E_a = 1.3±0.2eV
E_a = 1.6±0.2eV
E_a = 1.5±0.1eV
(data of Tu et al.)
1.6 1.7 1.8 1.9 2.0 2.1 2.2
$10^3/T$(°K)

parameter for the atoms moving through the layer. To test this hypothesis, we have measured the grain size of silicide layers grown on <111> and <100> single crystal substrates. Figure 4 gives reproductions of TEM micrographs of one such layer each, as well as electron transmission diffraction patterns obtained on the same layers. The micrographs show tnat the average grain size of the Ni_2Si layer grown on a <100> Si substrate is about 600Å, while the layer grown on a <111> Si substrate is about 1300Å. The diffraction patterns have been analyzed and confirm the presence of Ni_2Si in the layers. This analysis was done by measuring the positions of the concentric diffraction rings from the center of the rings and from the knowledge of the camera constant λ_L, using the following[60]:

$$\lambda_L = dr \tag{23}$$

or

$$d = \frac{\lambda_L}{r} \tag{23a}$$

where d is the crystallographic diffraction spacing and r (cm) is the distance of the rings from the center of the concentric ring patterns. Table 3 gives the measured values of r, calculated values of d and the crystallographic axis (using ASTM data), for the Ni_2Si on <100> and <111> Si substrates. The patterns from the layer grown on the <100> Si substrate indicates randomly oriented grains. In contrast, we found evidence that layers grown on the

Figure 11. Transmission electron micrographs and electron diffraction patterns of Ni_2Si formed by 1600Å of Ni, (a) on <100> Si and annealed at 300°C for 5 hours, and (b) on <111> Si and annealed at 325°C for 580 minutes. All Ni was consumed in the reaction in both cases: the average grains size of Ni_2Si is about 600Å in (a) and 1300 to 1400Å in (b). The diffraction patterns in the latter case indicate that Ni_2Si is textured.

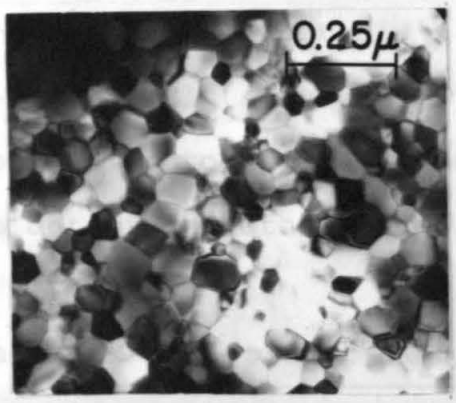

Ni_2Si on Si (100)

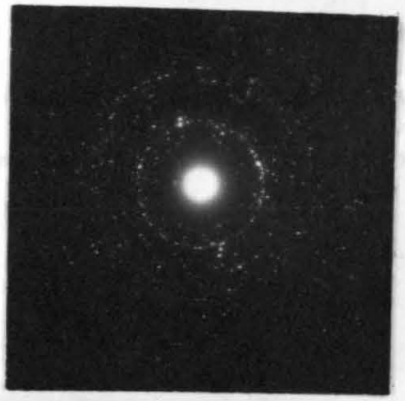

(a)

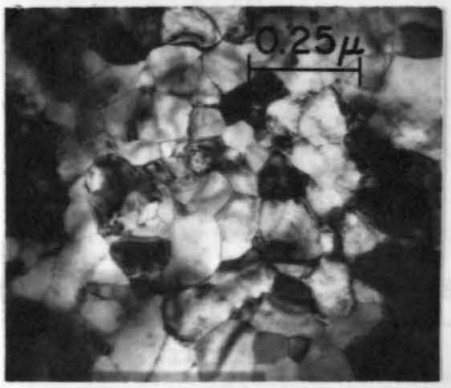

Ni_2Si on Si (111)

(b)

Table 3.

Values of d, calculated from measured values of r. These are compared with the d's on the ASTM data card number 5-0416 ($PbCl_2$ structure). Last column gives the axes corresponding to the d values. Some intensities are too weak to detect in both (a) and (b).

(a) TEM analysis of Ni_2Si on <100> Si

r (cm)	d (Å)	(hkl)
0.61	3.60	(002)
0.80	2.75	(111)
0.85	2.58	(020)
1.00	2.20	(112)
1.10	2.00	(120)
1.20	1.83	(200)
1.25	1.76	(004)
1.30	1.69	(014)
1.35	1.63	(202)
1.49	1.47	(220)
1.60	1.37	(222)
1.80	1.22	(034)
2.00	1.10	(320)

(b) TEM analysis of Ni_2Si on <111> Si

r (cm)	d (Å)	(hkl)
0.61	3.60	(002)
0.65	3.38	(101)
1.10	2.00	(120)
1.20	1.83	(200)
1.95	1.13	(224)
2.10	1.05	(026)

<111> Si substrate contain preferentially oriented grains. The <111> and <222> transmission electron diffraction lines are missing in the patterns of Ni_2Si on <111> Si substrates. This suggests that the <111> planes of the Ni_2Si crystallites lie preferentially parallel on the <111> Si substrate surface. The structural characteristics of the Ni_2Si layer thus depends indeed on the state of the substrate.

C. Ni_2Si plus NiSi Formation on Amorphous (Evaporated) Si

Thin Ni films were deposited on 3000 to 5000Å of evaporated Si on SiO_2 substrates. Silicon films were also deposited on Ni films evaporated on SiO_2 substrates. For both layer sequences, the two phases Ni_2Si and NiSi were observed simultaneously after heat treatments between 200 and 325°C. The backscattering spectrum of a thin (3500Å) Ni film deposited on amorphous (evaporated) Si on SiO_2 after annealing at 275°C for 4 hours is shown in Fig. 12. Two sublayers of differing atomic composition are clearly visible within the compound layer.

The rate of growth of the compound layers are investigated. The overall compound thicknesses as well as the individual sublayers were found to increase as the square root of the annealing time. The rate is roughly equal to that observed for the growth of Ni_2Si on <100> Si.

Figure 12. ^{4}He ion backscattering spectra of a thin (3500Å) Ni film vacuum-evaporated on an amorphous (evaporated) Si film on a SiO_2 substrate before (o) and after (o) annealing at 275°C for 4 hours.

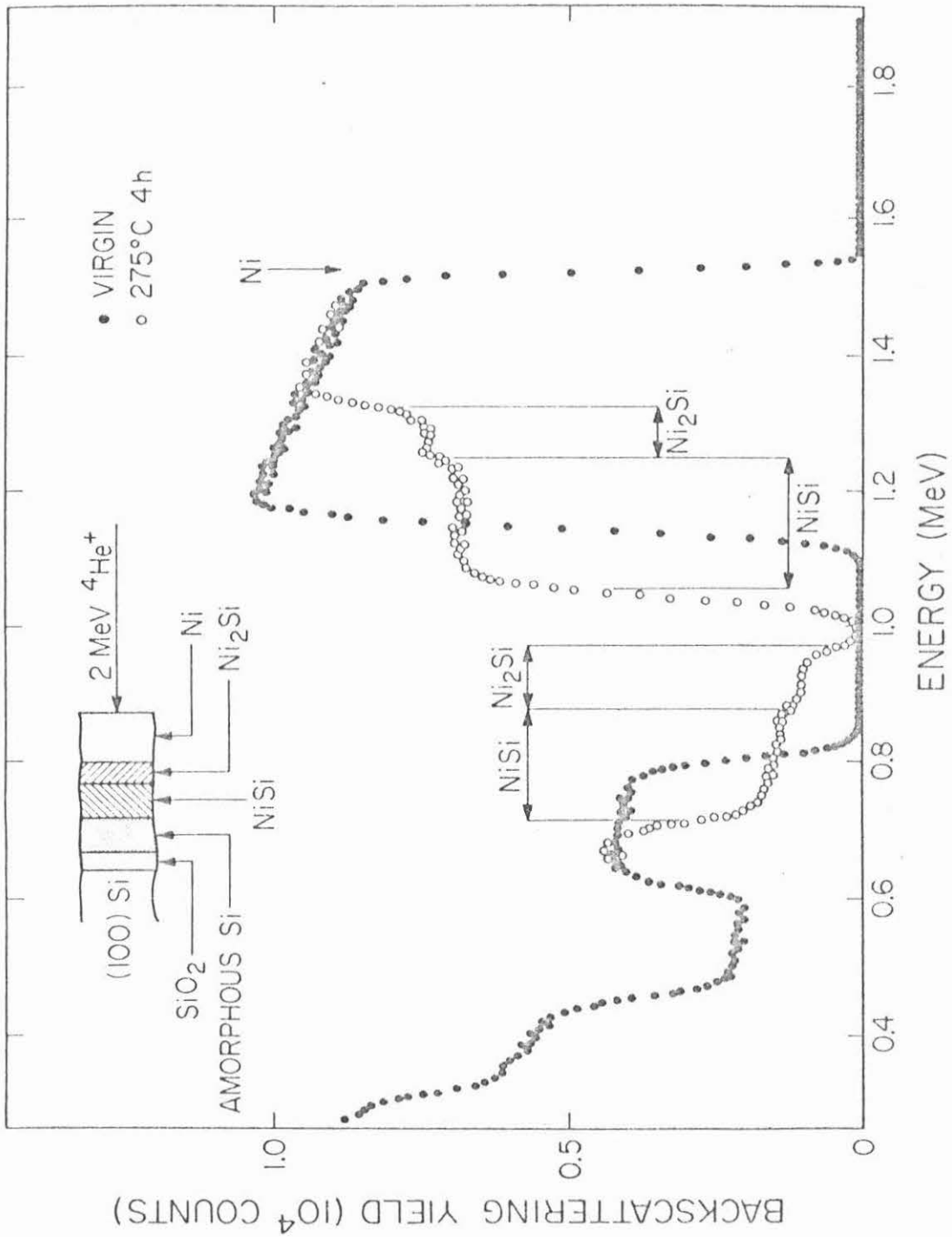
BACKSCATTERING YIELD (10^4 COUNTS)
ENERGY (MeV)
0
0.5
1.0
0.4
0.6
0.8
1.0
1.2
1.4
1.6
1.8
• VIRGIN
○ 275°C 4h
Ni
Ni_2Si
NiSi
NiSi
Ni_2Si
Ni_2Si
NiSi
2 MeV $^4He^+$
Ni
Ni_2Si
NiSi
(100) Si
SiO_2
AMORPHOUS Si

An Arrhenius plot for the growth of the overall compound layer of Ni_2Si plus NiSi is shown in Fig. 10. The activation energy was found to be $E_a = 1.4 \pm 0.2$ eV, which is quite similar to those found for the other substrates. A detailed analysis of x-ray diffraction patterns confirm that, indeed, these two phases coexist simultaneously.

The simultaneous existence of two silicides over an extended range of annealing times is unusual. Generally, only one phase is observed at a time in reactions of metal films with Si. Two phases were reported for platinum silicide,[33] But the growth of the first phase (Pt_2Si) ceases when the second phase (PtSi) appears. Two phases, Co_2Si and CoSi have also been reported recently for Co.[60]

D. Glancing Angle (Read Camera) X-ray Diffraction Analysis of Ni_2Si and NiSi

Identification of Ni_2Si and NiSi was made by using the Read camera glancing angle x-ray diffraction technique. A brief description of this anlaytical technique has been given in Chapter II. Details are given in other references.[55,60-62]

Figure 13 gives the diffraction patterns of thin Ni films evaporated on evaporated Si on SiO_2 substrates, annealed and unannealed. Analysis of these samples were made by comparing the measured angles of the

Figure 13. X-ray diffraction patterns of thin Ni film on amorphous (evaporated) Si before and after heat treatment at 275°C for 4 hours.

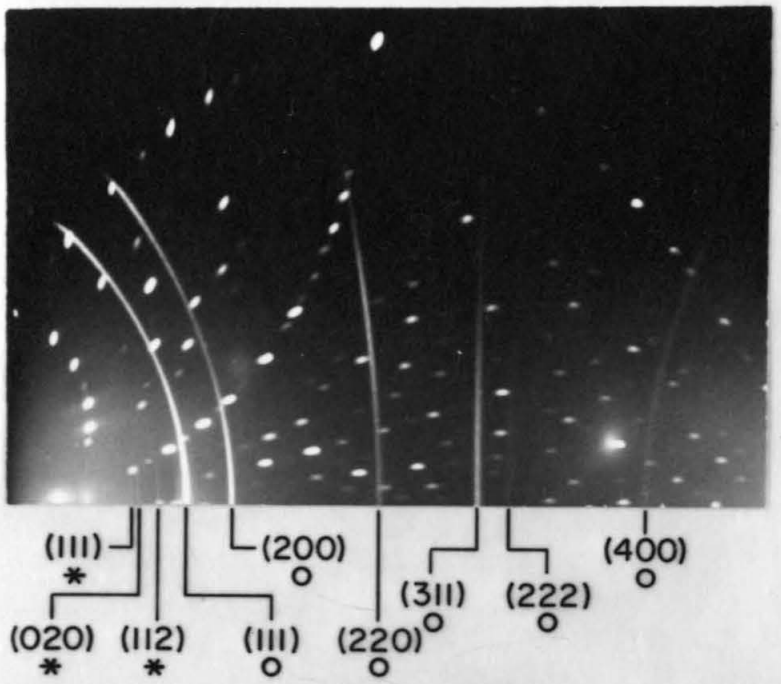

Ni on evap Si
as evaporated
* Ni_2Si
o Ni

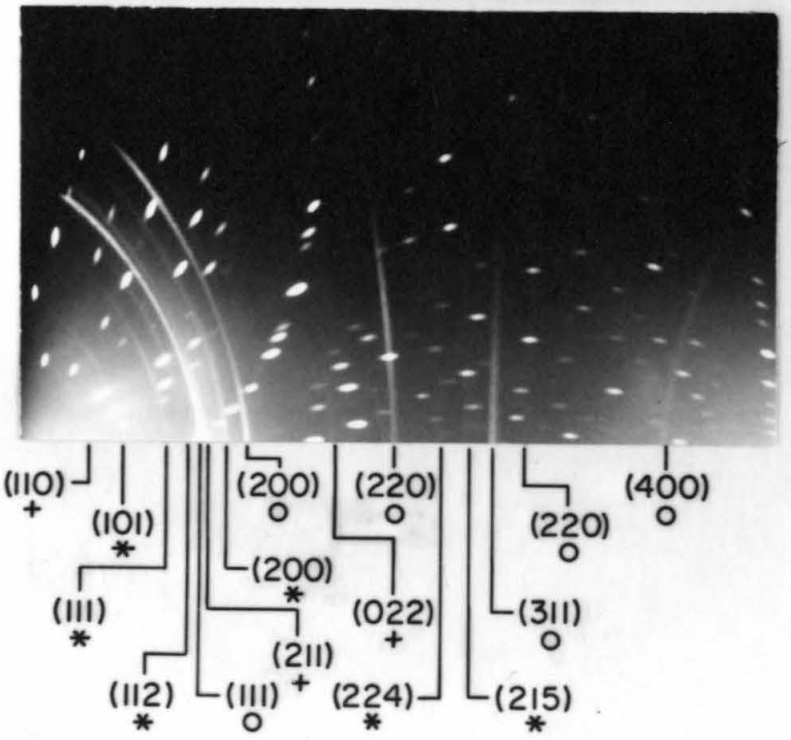

275°C 4h
* Ni_2Si
+ NiSi
o Ni

diffraction rings with the data in the ASTM compilation data. Ni_2Si and NiSi are known to have $PbCl_2$ and MnP orthorhombic structures respectively.[15,18] The ASTM data and the calculated d values (using the corresponding lattice parameters) corresponding to these compounds are used for the identification of Ni_2Si and NiSi. The listings for the x-ray diffraction data are given in Table 4.

Some reaction between thin Ni films and evaporated Si was found to have taken place even during the deposition of the Ni film on the evaporated Si, as indicated by the presence of Ni_2Si diffraction rings in the x-ray films of the as-deposited samples.

Table 4.

X-ray diffraction angles, the d-spacings calculated by using the lattice parameters for Ni_2Si and NiSi, the crystallographic axis (hkl) and relative intensities of diffraction patterns from ASTM cards for Ni, Ni_2Si and NiSi.

* indicates diffraction lines observed in the patterns. Most of the diffraction lines in the Ni_2Si and NiSi samples are not observed because of (i) they overlap with each other, and (ii) they are too weak to be detected. The resolution of the camera, operated at an incidence angle (see Chapter II) of 8° is about 2°.

Table 4

(a) Ni; ASTM number 4-850

2θ (°)	d (Å)	(hkl)	Relative Intensity
44.49	2.034	(111)	VS *
51.84	1.762	(200)	S *
76.37	1.246	(220)	S *
92.93	1.062	(311)	S *
98.43	1.017	(222)	W *
121.93	0.881	(400)	V
144.64	0.808	(331)	VW
155.66	0.788	(420)	VW

Crystalline Ni is FCC in structure, with lattice constant $a = b = c = 3.5238$ and $\alpha = \beta = \gamma = 90°$.

(b) Ni_2Si; ASTM number 5-0416 ($PbCl_2$ structure)

25.28	3.520	(002)	VW
27.03	3.296	(101)	M *
31.04	2.878	(012)	M
32.51	2.752	(111)	S *
35.89	2.500	(020)	W
39.51	2.279	(112)	W *
43.54	2.077	(120)	VW
44.41	2.038	(022)	W
45.50	1.912	(121)	M
45.63	1.986	(103)	M
48.79	1.865	(200)	M *
51.91	1.760	(004)	M
53.51	1.711	(023)	VW
55.29	1.660	(014)	VW
55.73	1.648	(202)	VW
58.96	1.565	(212)	VW
59.38	1.552	(123)	VW
61.04	1.517	(114)	VW
61.51	1.506	(032)	W
62.03	1.495	(220)	VW
62.38	1.487	(131)	VW
64.72	1.439	(024)	VW
68.08	1.376	(222)	VW
70.01	1.343	(124)	VW
73.99	1.280	(204)	VW
74.41	1.274	(115)	VW
76.80	1.240	(214)	VW
79.06	1.210	(034)	VW
80.73	1.189	(311)	VW
82.06	1.173	(006)	VW

Table 4 - continued

82.19	1.172	(232)	VW	
84.00	1.151	(134)	VW	
84.80	1.142	(016)	VW	
85.07	1.139	(224)	W	*
87.56	1.113	(320)		
89.26	1.096	(215)	W	*
92.96	1.062	(026)		

The crystal structure of Ni_2Si is orthorhombic with a = 3.73, b = 5, c = 7.04 and $\alpha = \beta = \gamma = 90°$.

(c) NiSi; ASTM number 7-384 (MnP structure)

23.33	3.809	(110)	VW	*
31.12	2.871	(101)	VS	*
31.81	2.810	(200)	S	*
34.60	2.590	(020)	VS	
35.72	2.511	(111)	VS	
36.34	2.470	(210)	M	
44.21	2.047	(021)	M	
45.64	1.986	(211)	VS	*
47.22	1.923	(121)	VS	
47.71	1.904	(220)	S	
51.85	1.762	(310)	S	
54.93	1.670	(002)	M	
55.49	1.654	(221)	VS	
55.64	1.651	(130)	M	
56.25	1.634	(311)	S	
59.25	1.558	(301)	VS	
60.99	1.518	(320)	W	
62.74	1.480	(131)	VS	
64.89	1.436	(202)	VW	
66.57	1.403	(022)	W	*
67.66	1.383	(212)	W	
69.23	1.356	(410)	W	
72.99	1.295	(040)	W	
74.70	1.270	(330)	W	
75.23	1.262	(140)	VW	
75.62	1.256	(411)	S	
75.68	1.256	(222)	VS	
77.17	1.235	(420)	VW	
78.92	1.212	(312)	S	
79.28	1.207	(041)	W	
81.46	1.180	(141)	VS	
81.83	1.176	(240)	M	
95.15	1.043	(511)	VW	
99.82	1.007	(142)	VW	

The crystal structure of NiSi is orthorhombic with a = 5.62, b = 5.18 and c = 3.34 and $\alpha = \beta = \gamma = 90°$.

CHAPTER IV. Formation Kinetics of Thin Films of $CrSi_2$ on Single Crystal Si and on Pd_2Si Grown on Si

In this chapter, the kinetic rate of formation and composition of $CrSi_2$ is reported. This part of the work starts by investigating the dependence of the growth rate of $CrSi_2$ on the orientation of the Si substrates, as was made for nickel silicides reported in the previous chapter. $CrSi_2$ was formed on <100> and <111> oriented Si and poly-crystalline Si. The growth and kinetics of the silicide was also investigated in a more complex Si-Pd-Cr system

The Pd-Si system has been well studied, but the interaction of Cr with silicon is less well known.[11] It is the objective of this investigation to study, in detail, the formation of $CrSi_2$ on single-crystal substrates with or without an interposed layer of Pd_2Si.

Read camera x-ray diffraction analysis were performed on both Si-Cr and Si-Pd-Cr samples, to confirm that, indeed, $CrSi_2$ was formed in both systems.

The interaction of Cr with Si required thorough investigation, particularly in the complex Si-Pd-Cr ternary system. This is found to be the key to the understanding of the Si-Pd-Cr-Al metallization scheme reported in Chapter V.

A. Behavior of Cr Films on Single-Crystal Si

Figure 14 shows 2 MeV $^4He^+$ backscattering spectra of samples with 2000Å Cr evaporated on <100> oriented Si substrates, annealed at 450°C for 50 minutes, and unannealed. The plateau at the higher energy part of Si signal and a corresponding one at the lower energy part of the Cr signal indicate that there has been an interaction between Si and Cr; indeed, a compound phase has been formed. Measuring the heights of the plateaus, $H_{Si}^{CrSi_2}$ and $H_{Cr}^{CrSi_2}$ for both Si and Cr signals respectively, and using the expression given in Eq. 16,

$$\frac{N_{Cr}}{N_{Si}} = \frac{H_{Cr}^{CrSi_2}}{H_{Si}} \times \frac{[S]_{Cr}^{CrSi_2}}{[S]_{Si}^{CrSi_2}} \times \frac{\sigma_{Si}}{\sigma_{Cr}} = \frac{1}{2}$$

Values of [S] (eV/Å) and σ ratios are given in Table 2 (Chapter II). Read camera x-ray analysis confirms that the compound layer is indeed $CrSi_2$. That the silicide $CrSi_2$, forms under these conditions was also reported by Bower et al. The compound phase develops at 450°C and is known to be stable beyond 1000°C. Measurements similar to those in Fig. 14 were made for different times and temperatures and the thickness of $CrSi_2$, calculated from the relationship $\Delta E = [S]t$ (Eq. 22), versus annealing time was plotted as shown in Fig. 15. The linearity of growth

Figure 14. $^{4}He^{+}$ backscattering spectrum of 2000Å Cr film evaporated on Si <100>, before (solid dots) and after (open circles) annealing at 450°C for 50 minutes.

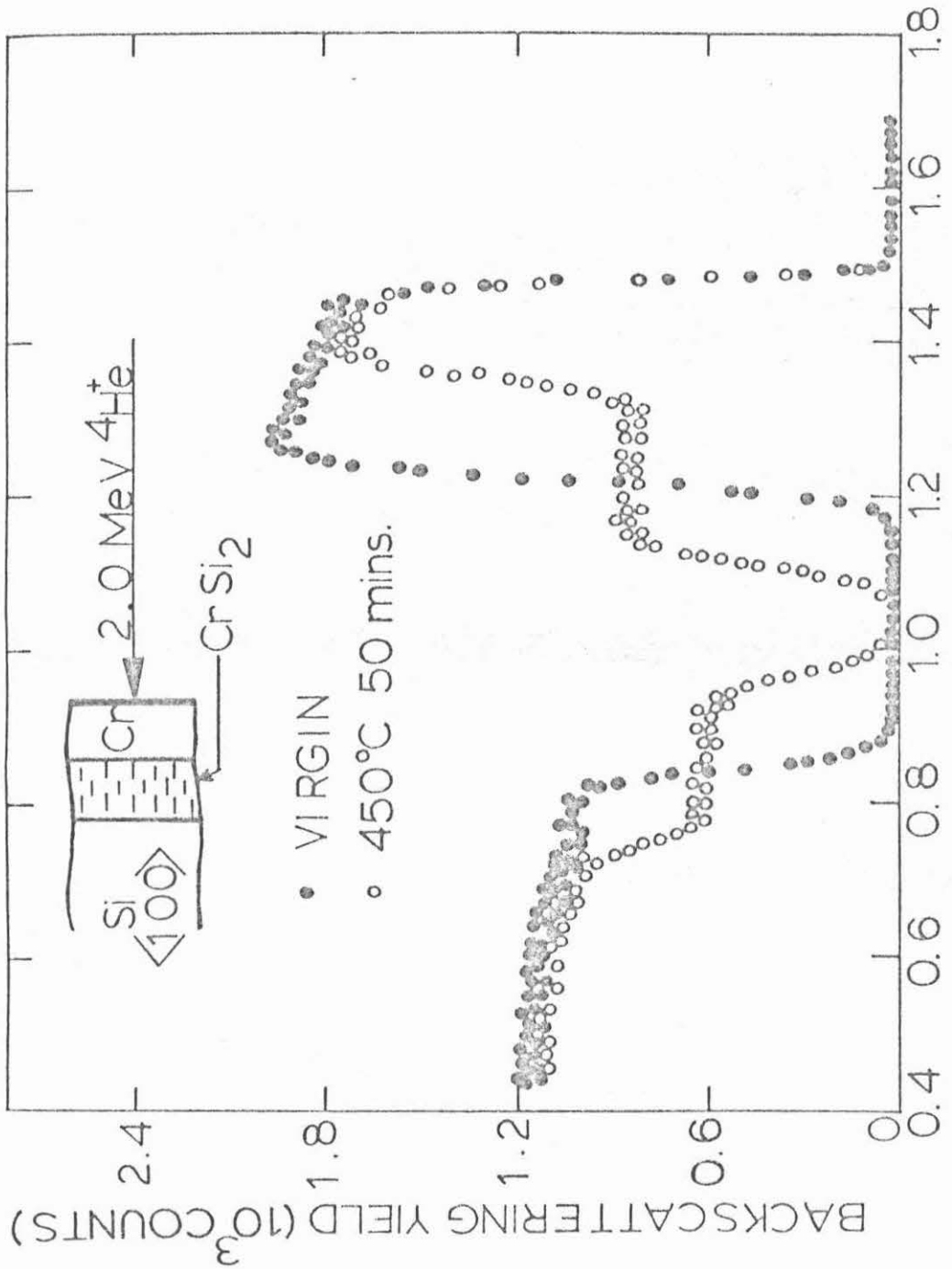
BACKSCATTERING YIELD (10^3 COUNTS)
2.4
1.8
1.2
0.6
0
0.4
0.6
0.8
1.0
1.2
1.4
1.6
1.8
ENERGY (MeV)
• VIRGIN
○ 450°C 50 mins.
2.0 MeV $^4He^+$
Cr
$CrSi_2$
Si
⟨100⟩

Figure 15. Thickness, W, of $CrSi_2$ formed in the reaction between Cr and Si <100> single crystal as a function of time. The nonlinear regime is due to contamination and oxygen is a prime suspect.

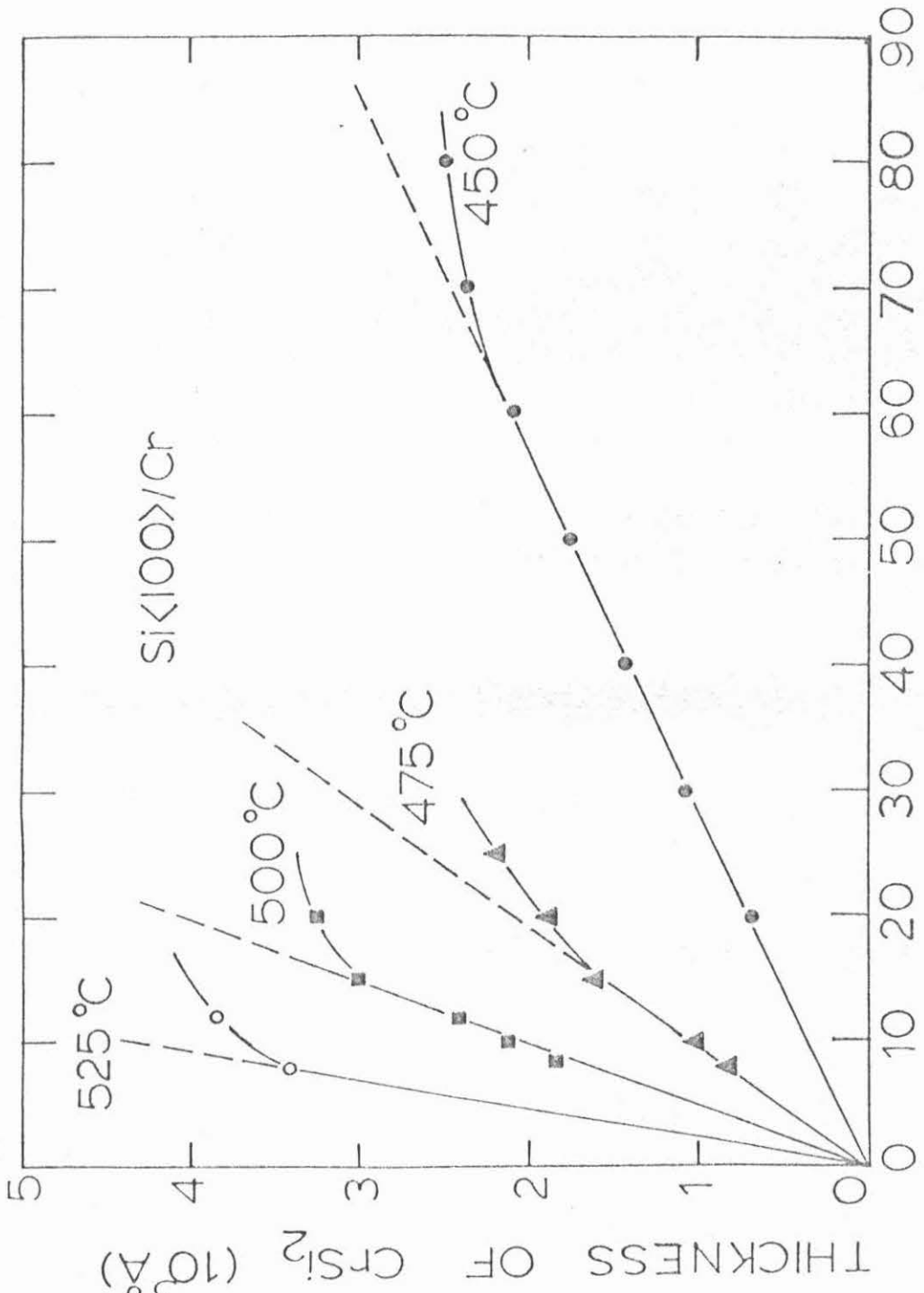
THICKNESS OF $CrSi_2$ (10^3 Å)
TIME, t (MINUTES)
Si<100>/Cr
525 °C
500 °C
475 °C
450 °C
0
1
2
3
4
5
0
10
20
30
40
50
60
70
80
90

of $CrSi_2$ with time indicates that the process is limited by the silicide reaction. This observation is also consistent with that reported by Bower et al.[11] It is worth noting also that $MoSi_2$ and VSi_2 exhibit the same linear type of growth.[11,14]

Samples of thin Cr films evaporated on <100> and <111> oriented single crystal Si were annealed side by side together in a vacuum furnace at 500°C for times up to 60 minutes. At this temperature and time, no dependence on the substrate orientation on the growth of $CrSi_2$ was observed. This nondependence of the growth of $CrSi_2$ on the orientation of the substrate has been reported for Pd_2Si and VSi_2, while the growth of Ni_2Si has been shown to be strongly dependent on the state of the substrate (Chapter III).

From the linear regime of Fig. 15, the Arrhenius plot shown in Fig. 16 was derived (open circles). The plot reveals a thermally activated process with an activation energy of $E_a = 1.7 \pm 0.1$ eV. This value coincides with that of 1.7 ± 0.2 eV quoted for the growth of VSi_2.[14]

1. Impurity Effects on the Growth Rate

It is observed (Fig. 15) that for long anneals (for example, 80 minutes at 450°C) at all temperatures investigated, a nonlinear growth regime exists. This nonlinear behavior is attributed to contaminations, probably oxygen, introduced during annealing. That choice is

Figure 16. Arrhenius plot for $CrSi_2$ formation in the reaction of Cr with Si <100> single crystal (open dots) and on Pd_2Si grown on Si <100> single crystal (solid dots). The agreement is very remarkable; it indicates that the only limiting process is the reaction of Cr with Si.

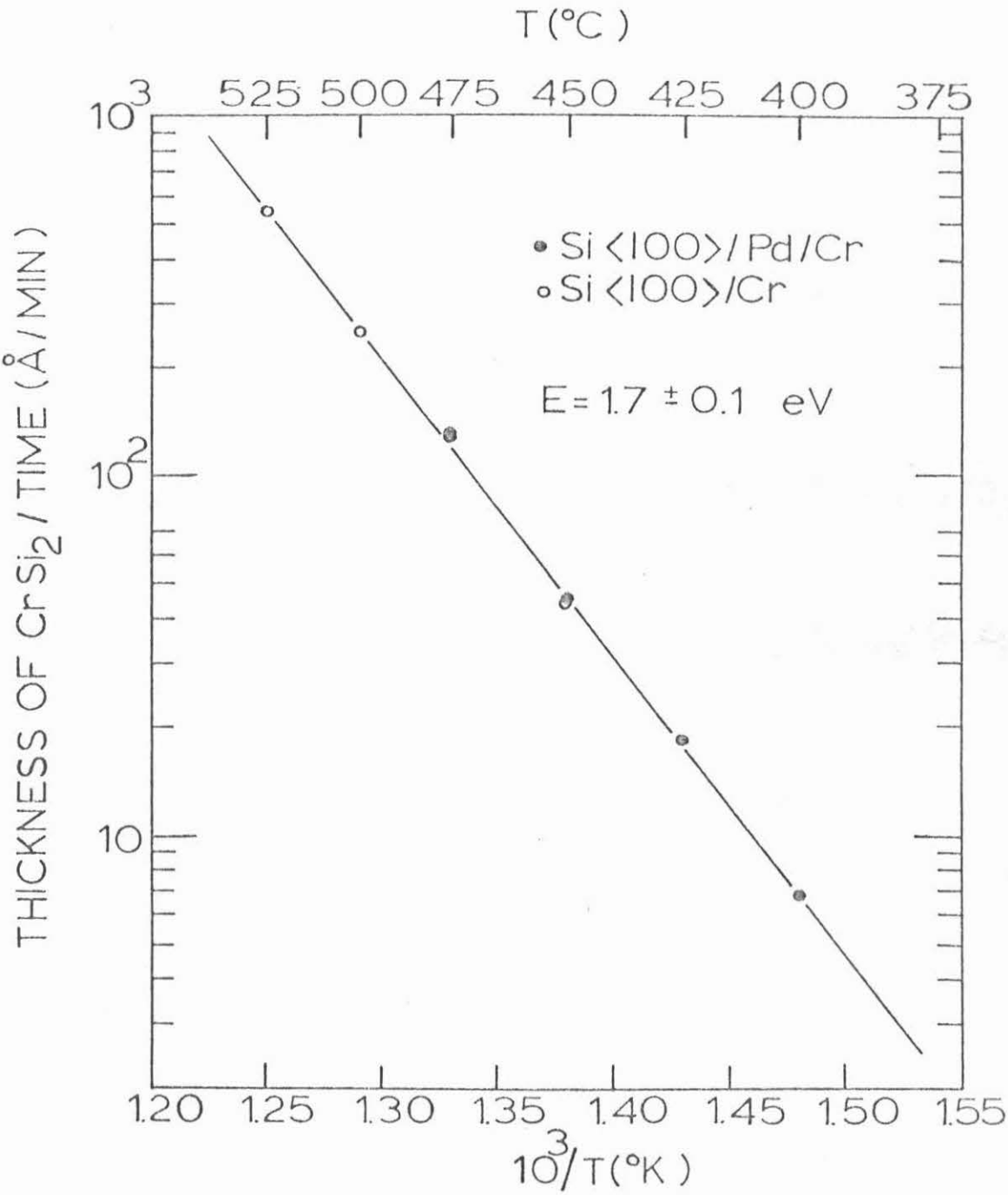
T(°C)
525 500 475 450 425 400 375
10^3
10^2
10
THICKNESS OF $CrSi_2$ / TIME (Å / MIN)
• Si <100> / Pd / Cr
○ Si <100> / Cr
E = 1.7 ± 0.1 eV
1.20 1.25 1.30 1.35 1.40 1.45 1.50 1.55
10^3 / T(°K)

suggested by the very similar observations made by Krautle et al. for VSi_2 where oxygen was shown to cause nonlinear growth.[14] In the presence of substrates such as Si, backscattering spectrometry is insensitive to oxygen. An amount of oxygen sufficient enough to retard the reaction could easily escape detection.

To investigate the presence of such impurities in the Cr film, an experiment was performed in which about 1000Å of Cr was re-evaporated on a film in which the top layer of about 500Å Cr was still unreacted. The Cr signal obtained by backscattering spectrometry from this sample was then compared with the Cr signal of an unannealed Si-Cr (Fig. 17). The unreacted part of the Cr film generates a signal of smaller height than that of the unannealed sample, while the signal height of the freshly evaporated Cr layer agrees quite well with that of the unannealed samples (solid line in Fig. 17). The decrease in yield of the unreacted part of Cr confirms that the Cr film is indeed contaminated. About 12-15% oxygen distributed uniformly in the unreacted portion of the Cr film is required to account for the reduction in the yield. The dip between the unreacted and the unannealed spectra is probably due to a layer of Cr oxide formed on the surface of the unreacted Cr.

2. Si-Cr Interface

For Si-Cr samples annealed between 400 and 425°C,

Figure 17. $^{4}He^{+}$ backscattering spectrum (open circles) of 2000Å Cr on Si <100> single crystal annealed at 450°C for 60 minutes and then covered with about 1000Å of deposited Cr. The solid line is the unannealed samples. About 12-15% oxygen contamination has resulted in the decrease in the yield of the unreacted Cr. The dip between the unreacted and the evaporated layers is likely due to a thin oxide layer on the vacuum-annealed sample. Samples were tilted 45° with respect to beam.

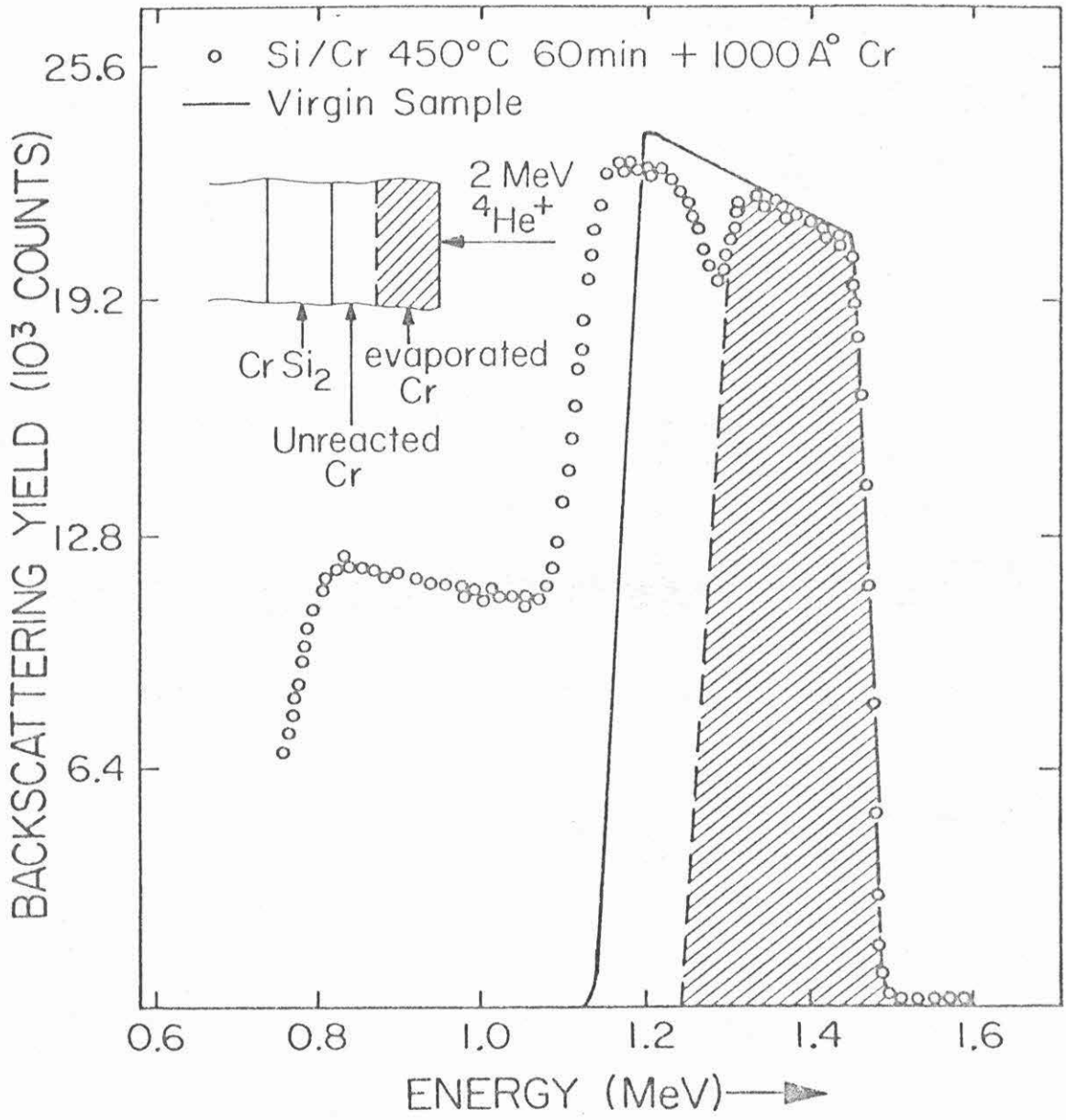
Si/Cr 450°C 60min + 1000A° Cr
Virgin Sample
2 MeV
4He+
Cr Si2
evaporated
Cr
Unreacted
Cr
25.6
19.2
12.8
6.4
BACKSCATTERING YIELD (10³ COUNTS)
0.6
0.8
1.0
1.2
1.4
1.6
ENERGY (MeV)

no measurable interaction of Cr with Si was observed. In fact, there was no measurable thickness of $CrSi_2$ for a sample annealed at 400°C for 120 minutes. A point plotted for the reaction is shown in Fig. 22 (point at origin) in the plot of $CrSi_2$ thickness versus Pd_2Si thickness. A similar sample quickly heat-treated at 500°C for 3 minutes and then annealed at 400°C for 120 minutes showed a measurable amount of $CrSi_2$, almost equal to that measured in the Si-Pd-Cr samples (arrowed point in Fig. 22). There was no measurable amount of $CrSi_2$ after the quick heat treatment at 500°C for 3 minutes. $CrSi_2$ starts to form on single crystal Si with an interposed Pd_2Si layer at 400°C. The absence of a reaction of Cr on bare Si at 400°C can thus be overcome by a quick exposure to higher temperatures. We suspect that the effect is due to contamination, such as a thin oxide layer, at the Cr-Si interface. The oxide layer may not withstand the brief thermal shock at 500°C. There is no corresponding effect of the oxide layer in the presence of Pd_2Si. We think that this is due to the elimination of the original interface by the formation of Pd_2Si at a relatively low temperature. This method of cleaning the surface by silicide formation at low temperature has been exploited also in the solid-phase epitaxial growth of Si through Pd_2Si.[63]

B. Behavior of Cr Films on Pd Films on Single-Crystal Si

Pd films of thicknesses between 300 and 3000Å were vacuum-deposited on <100> oriented Si and Cr films for thicknesses between 800 and 2000Å were in turn evaporated on the Pd film without breaking vacuum. Typical backscattering spectra of such a sample with about 1400Å Pd and 1200Å Cr before and after annealing at 280°C for 60 minutes are shown in Fig. 18. Palladium silicide, Pd_2Si, is known to form at about 200°C. Annealing the Si-Pd-Cr sample at 280°C for 60 minutes has, therefore, resulted in the formation of Pd_2Si (shaded region in Fig. 18) without any noticeable interaction of Pd with Cr. Samples annealed subsequently at 400°C develop a compound layer, at the Pd_2Si-Cr interface, identified by glancing angle x-ray (Read camera) diffraction to be $CrSi_2$. The same results are obtained for samples heat-treated directly at 400°C. This silicide layer increases in thickness with increase in temperature at constant time, or with increasing time for a given temperature. Figure 19 shows a backscattering spectrum of a sample identical to that of Fig. 18, but annealed at 450°C for 20 minutes. A compound layer has developed at the Pd_2Si-Cr interface, as indicated by a step on the high energy edge of the Si signal and a corresponding plateau at the low energy side of the Cr signal. Comparing Figs. 18 and 19, it is

Figure 18. $^{4}He^{+}$ backscattering spectrum of Pd (1400Å) and Cr (1200Å) evaporated in that order on Si <100> single crystal before (top) and after (bottom) annealing at 280°C for 60 minutes. The reaction between Pd and Si results in the formation of Pd_2Si while there is no apparent interaction between Pd and Cr.

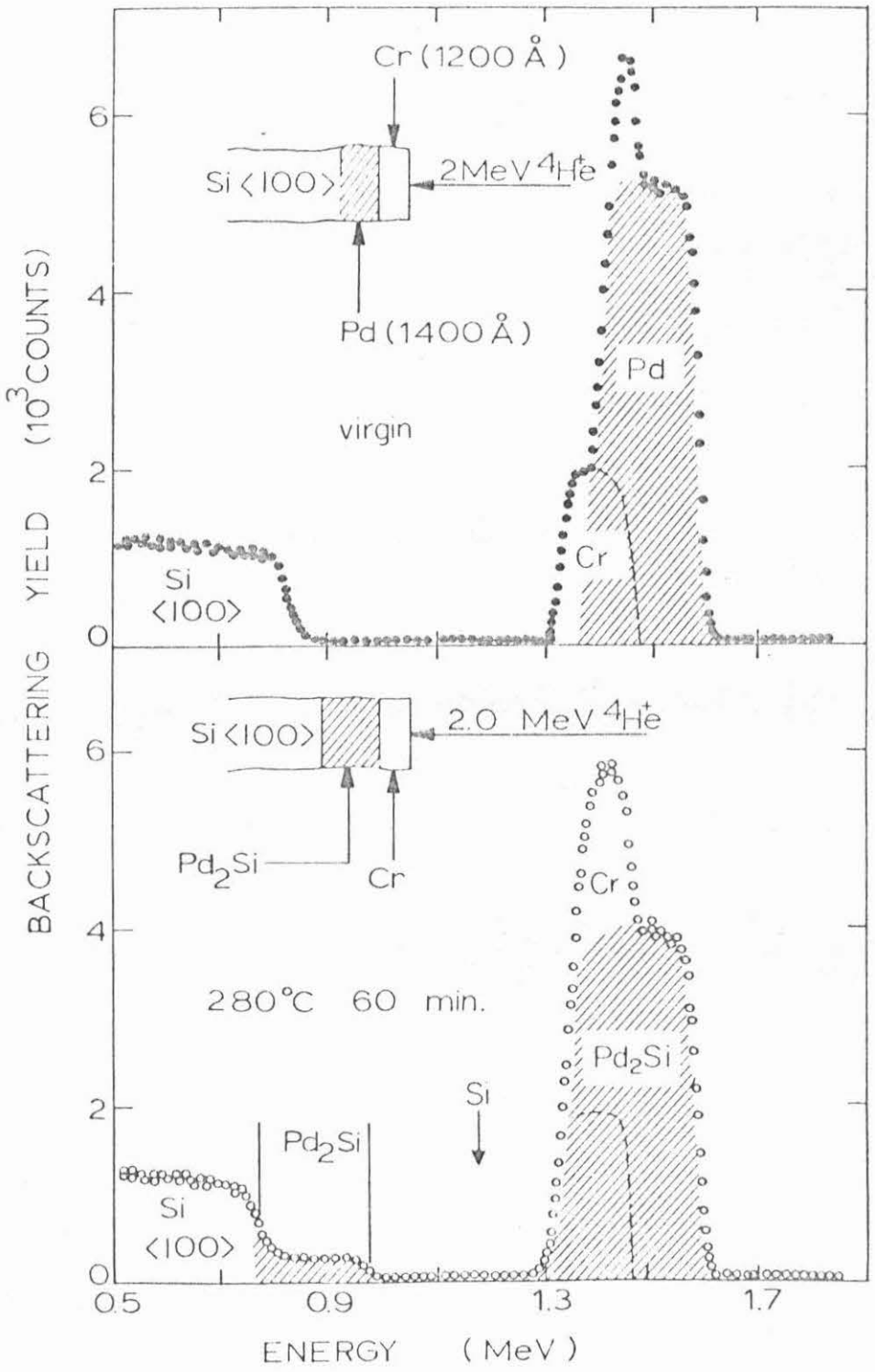
Cr (1200 Å)
Si ⟨100⟩
2MeV $^4He^+$
Pd (1400 Å)
virgin
Pd
Cr
Si
⟨100⟩
2.0 MeV $^4He^+$
Pd_2Si
Cr
280°C 60 min.
Si
BACKSCATTERING YIELD (10^3 COUNTS)
ENERGY (MeV)
0.5
0.9
1.3
1.7
0
2
4
6

Figure 19. $^{4}He^{+}$ backscattering spectrum of Pd (1400Å) and Cr (1200Å) evaporated in that order on Si <100> single crystal and annealed at 450°C for 20 minutes. All Pd has reacted with Si to form Pd_2Si before $CrSi_2$ was formed on top.

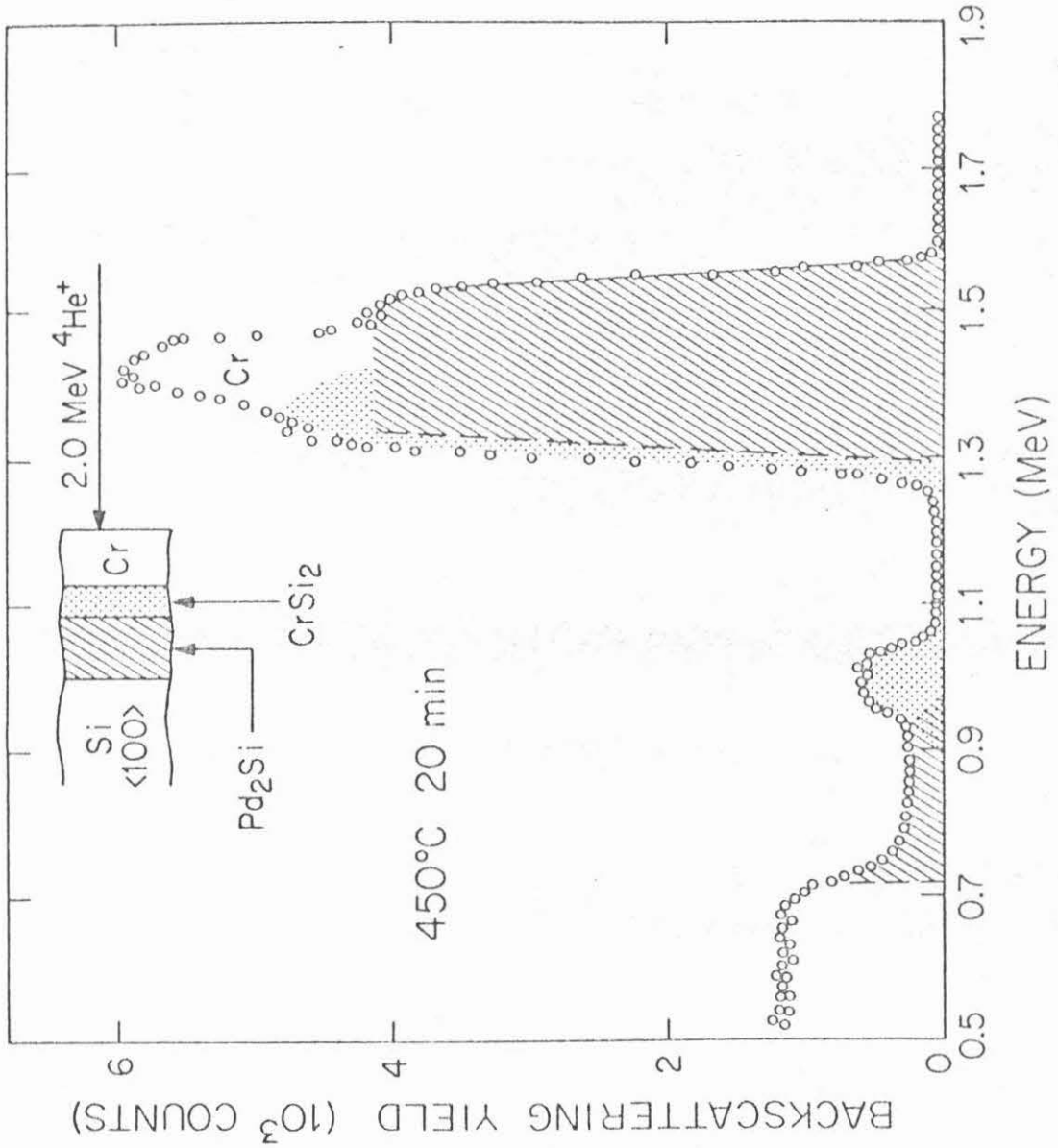
2.0 MeV $^4He^+$
Cr
$CrSi_2$
Pd_2Si
Si
<100>
450°C 20 min
Cr
BACKSCATTERING YIELD (10^3 COUNTS)
ENERGY (MeV)
0
2
4
6
0.5
0.7
0.9
1.1
1.3
1.5
1.7
1.9

observed that the thickness of Pd_2Si layer remains unchanged as $CrSi_2$ grows on top.

1. Kinetics and the Effects of Impurities

Figure 20 shows parts of three spectra for the same samples as in Fig. 19, annealed isothermally at 475°C for 7, 10 and 15 minutes. Using the expression $\Delta E = [S]t$ and the value of $[S]_{Si}^{CrSi_2} = 95.57$ (eV/Å) (Table 2) a plot of the $CrSi_2$ layer thickness versus time is obtained to give the growth kinetics of this process (Fig. 21). As for the Si-Cr system, the growth of $CrSi_2$ is linear with time, indicating that the process is reaction-limited. Again, a nonlinearity is observed at long annealing times which is attributed to contamination, with oxygen as a prime suspect. A plot of the reaction rate versus reciprocal temperature gives an activation energy of 1.7 ± 0.1 eV (Fig. 16) which is the same value obtained for $CrSi_2$ on Si. This indicates that the intermediate layer of Pd_2Si does not affect the mechanism responsible for the growth process of $CrSi_2$. For both Si-Cr and Si-Pd-Cr samples, the $CrSi_2$ thicknesses are almost equal at temperatures where they can be compared. For example, the $CrSi_2$ thickness is about 1500Å at 450°C for 40 minutes in both cases, which corresponds to a formation rate of about 0.7 Å/sec.

2. Growth of $CrSi_2$ versus Thickness of Pd_2Si

To investigate the effect of the thickness of

Figure 20. $^{4}He^{+}$ backscattering spectrum of isothermal growth of $CrSi_2$ on top of Pd_2Si. Anneals were done at 475°C for 7, 10 and 15 minutes. Only the Si part of the spectra is shown.

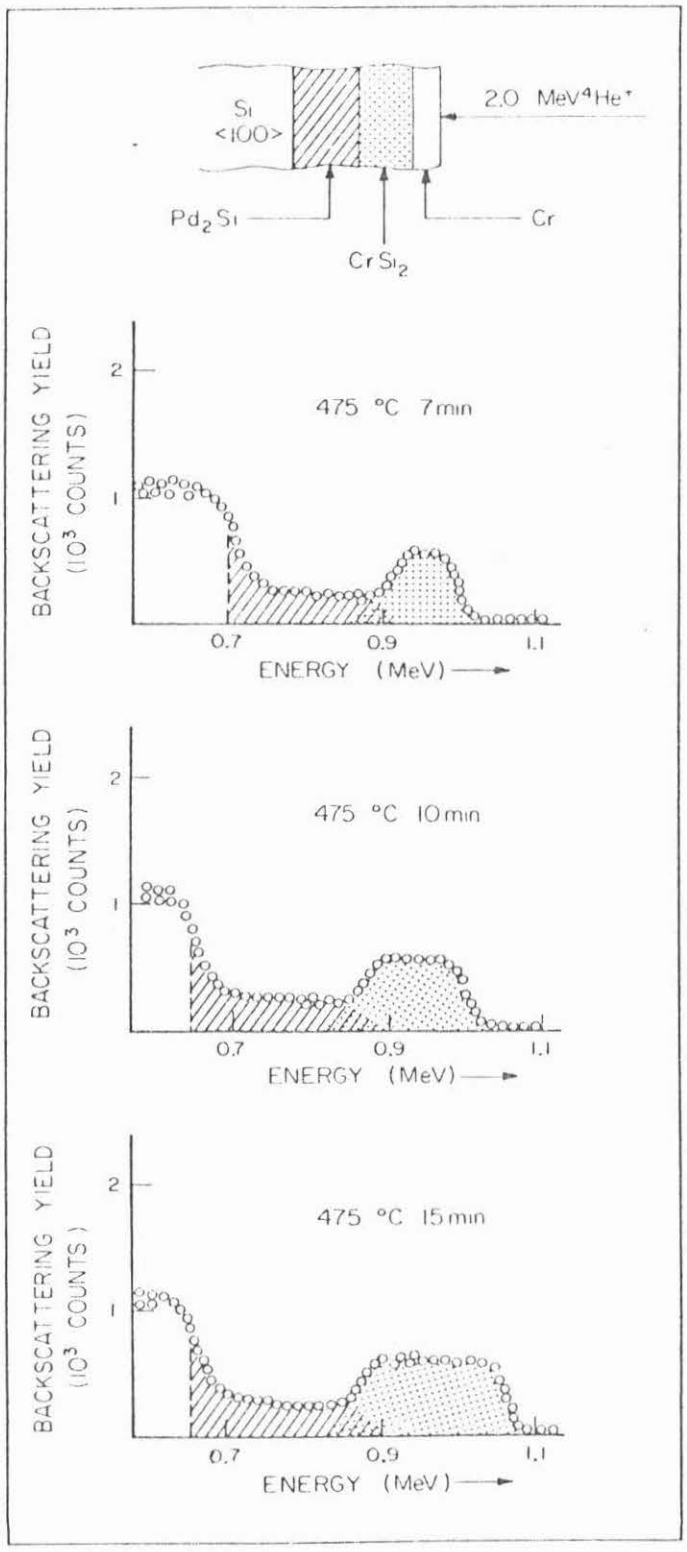
Si
<100>
2.0 MeV 4He+
Pd2Si
Cr
CrSi2
BACKSCATTERING YIELD
(10³ COUNTS)
475 °C 7min
ENERGY (MeV)
475 °C 10min
475 °C 15min
0.7
0.9
1.1
1
2

Figure 21. Thickness, W, of $CrSi_2$ formed on Pd_2Si grown on Si <100> single crystal as a function of time. The nonlinear regime is attributed to oxygen contamination.

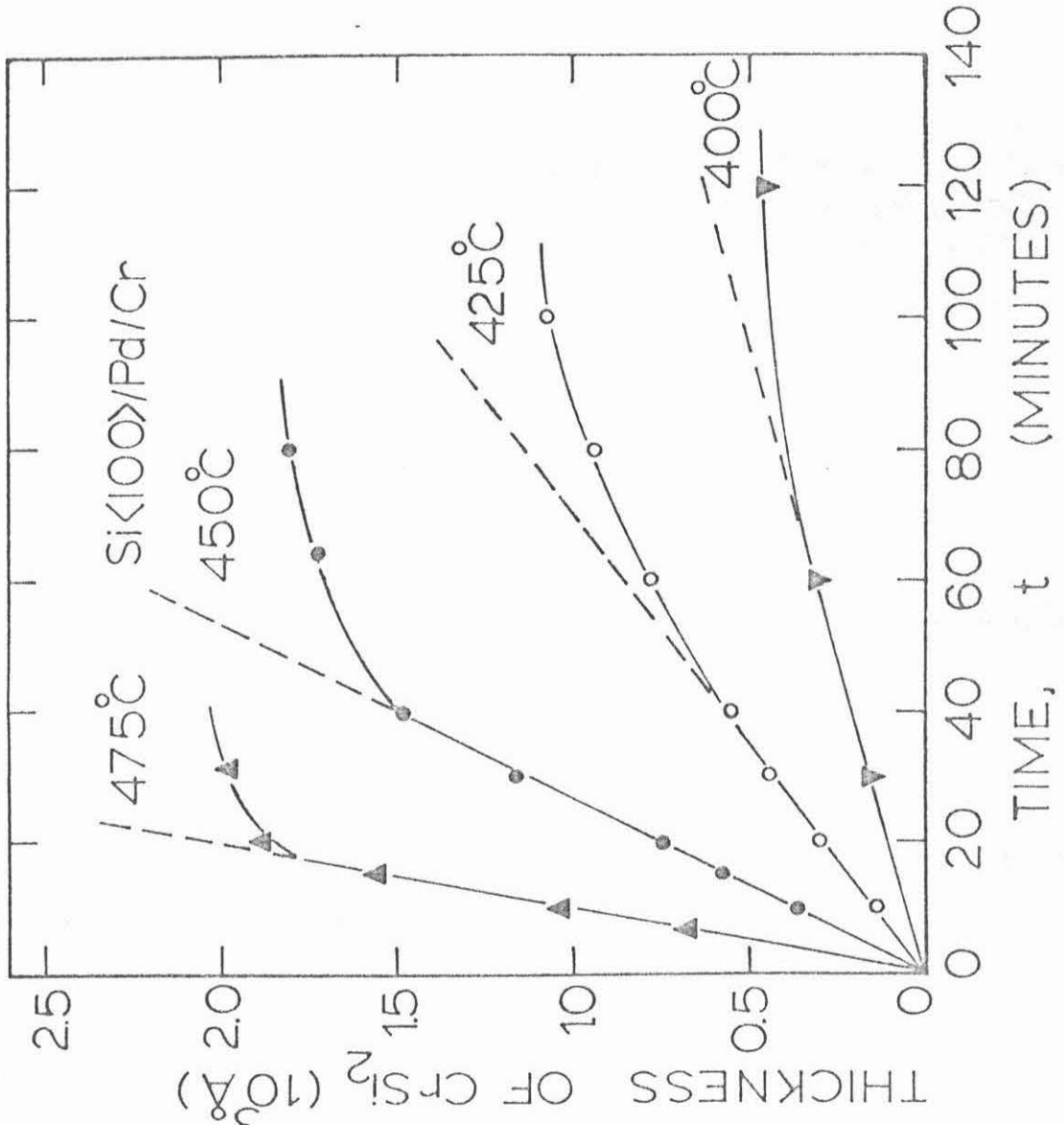
Si<100>/Pd/Cr
475°C
450°C
425°C
400°C
THICKNESS OF $CrSi_2$ (10^3 Å)
TIME, t (MINUTES)
0
0.5
1.0
1.5
2.0
2.5
0
20
40
60
80
100
120
140

Pd_2Si on the growth rate of $CrSi_2$, Pd films of different thicknesses were evaporated on single crystal Si and Cr was sequentially evaporated on top. The thickness of Cr was such that it would not be completely reacted in the process of $CrSi_2$ formation at the temperatures and times chosen for the experiment (400°C for 120 minutes, 450°C for 30 minutes and 475°C for 15 minutes). A plot of $CrSi_2$ thicknesses versus Pd_2Si thicknesses is shown in Fig. 22. Within the experimental errors, the thickness of $CrSi_2$ remains constant regardless of the thickness of Pd_2Si. Points along the $CrSi_2$ axis in Fig. 22 are those corresponding to the interaction of Cr with Si without an interposed Pd_2Si layer. The point at origin and the arrowed point have been explained in detail in Part B, Section 2, and in the figure caption.

C. Radioactive Si Tracer Studies of $CrSi_2$ on Pd_2Si

In Fig. 23 Rutherford backscattering spectra of $CrSi_2$ formation on Pd_2Si is shown. When the as-deposited virgin sample (23a) was heated at 400°C for 5 minutes the Pd film reacts with the amorphous radioactive Si and with the <100> Si substrate to form Pd_2Si. It can be seen (23b) that all the radioactive Si is consumed during Pd_2Si formation and that the Cr signal remains unchanged indicating that no $CrSi_2$ forms at this temperature and time. Upon annealing at higher temperatures (480 to 650°C) $CrSi_2$

Figure 22. A plot of the thickness of $CrSi_2$ as a function of the thickness of Pd_2Si for various annealing conditions. The ordinate (zero Pd_2Si thickness) gives the $CrSi_2$ thickness obtained for Cr films deposited directly on the Si substrate. A short time annealing at high temperatures (500°C, 3 minutes) "cleans" the Si-Cr interface for the reaction between Cr and Si at 400°C (arrowed point on $CrSi_2$ axis).

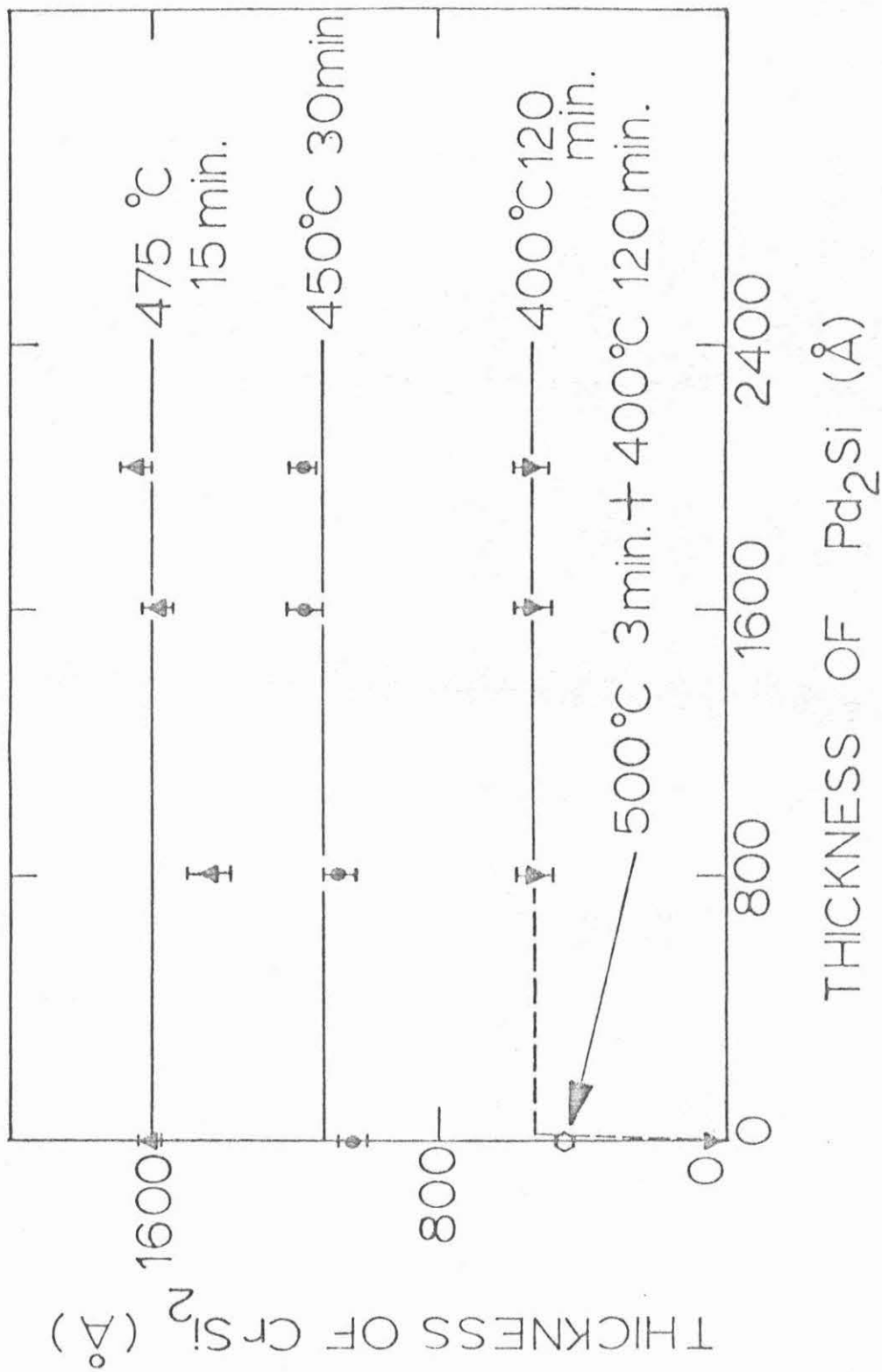
THICKNESS OF $CrSi_2$ (Å)
1600
800
0
0
800
1600
2400
THICKNESS OF Pd_2Si (Å)
475 °C 15 min.
450°C 30min
400 °C 120 min.
500°C 3min. + 400°C 120 min.

Figure 23. Rutherford backscattering spectra of Si<100>/Pd/Si(radioactive)/Cr sample (a) without heat treatment. (b) Annealed at 400°C for 5 minutes to form Pd_2Si, (c) annealed further at 600°C for 20 minutes to form $CrSi_2$ and (c) with $CrSi_2$ etched in 1 HF to 4 H_20, leaving only Pd_2Si on Si<100>.

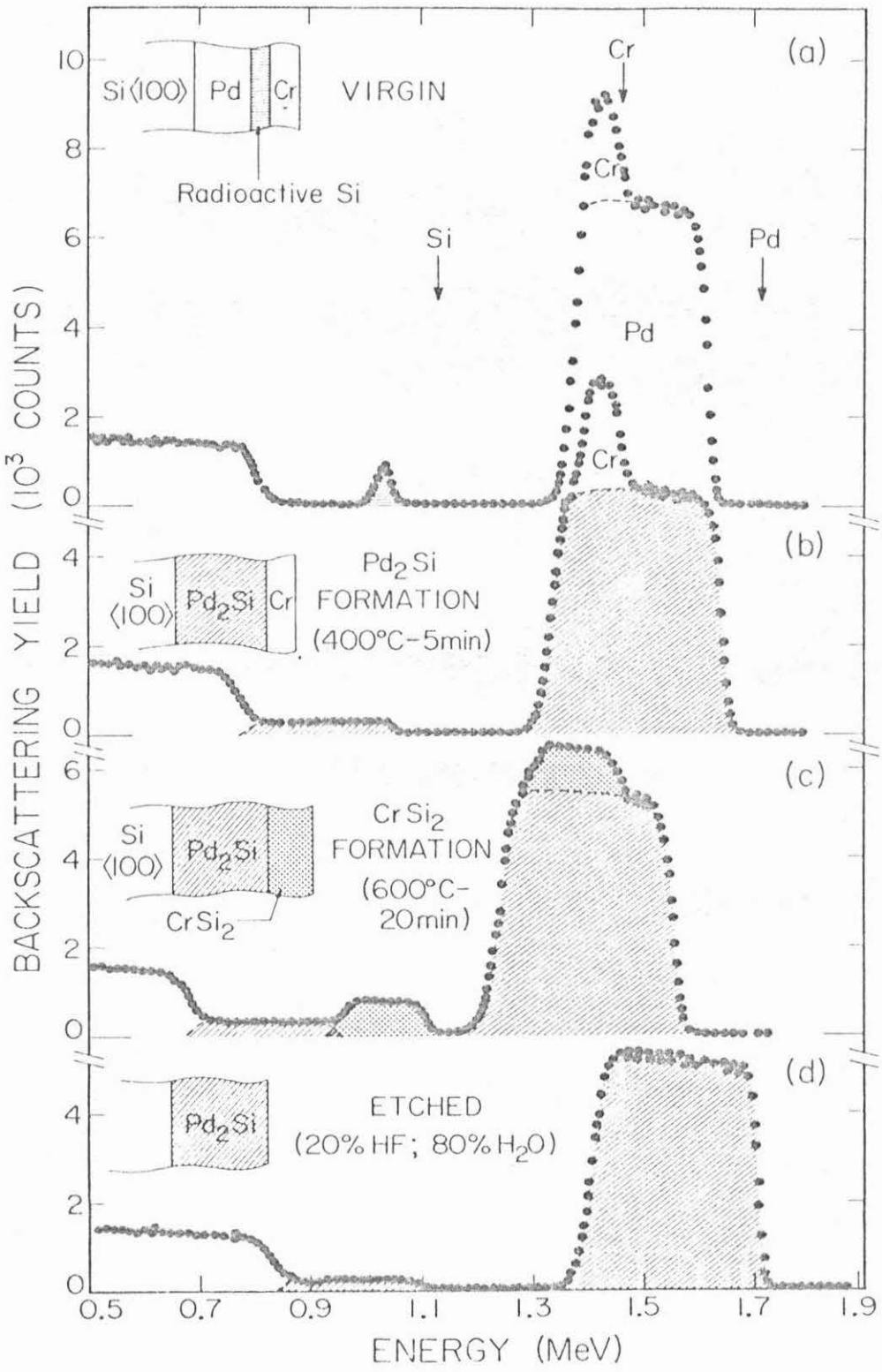
(a)
Si⟨100⟩ Pd Cr
VIRGIN
Radioactive Si
Cr
Cr
Si
Pd
Pd
Cr
(b)
Si ⟨100⟩ Pd2Si Cr
Pd2Si FORMATION (400°C-5min)
(c)
Si ⟨100⟩ Pd2Si
CrSi2
CrSi2 FORMATION (600°C-20min)
(d)
Pd2Si
ETCHED (20% HF; 80% H2O)
BACKSCATTERING YIELD (10^3 COUNTS)
ENERGY (MeV)
0.5
0.7
0.9
1.1
1.3
1.5
1.7
1.9

forms on top of Pd_2Si (23c), using all Cr in this reaction process. The $CrSi_2$ surface layer is then removed by etching the sample in 1 HF to 4 H_2O. From the Rutherford backscattering spectra (23d), it is clear that the $CrSi_2$ is removed completely and that the etchant does not attack the underlying Pd_2Si layer. Because HF forms gaseous SiF_4 with the silicon in $CrSi_2$ the activity in the etchant solution could not be measured. Silicon radioactivity left in the Pd_2Si layer was thus determined by measuring the activity in the sample before and after the $CrSi_2$ layer was removed.

The percentage activity left in the Pd_2Si after etching off $CrSi_2$, is shown in Fig. 24 for different thicknesses of $CrSi_2$ as a function of formation temperature of $CrSi_2$. For all the measurements the Pd_2Si thickness was kept constant at about 3000Å while the $CrSi_2$ thicknesses are expressed in terms of D, the ratio of the total number of Si atoms in the $CrSi_2$ layer, to the number of Si atoms in the Pd_2Si layer. The D values are determined from Rutherford backscattering thickness measurements and from the densities of Pd_2Si and $CrSi_2$. From these results it can be seen that the activity in the Pd_2Si layer decreases with increasing temperature of $CrSi_2$ formation and also becomes less when thicker layers of $CrSi_2$ are grown. For measurements where the radioactive Si is deposited directly on the Si substrate the same trends in the results are obtained as a function of $CrSi_2$ thickness

Figure 24. A plot of percentage activity in Pd_2Si for different $CrSi_2$ thickness as a function of formation temperature. Activity was counted after $CrSi_2$ layer had been removed.

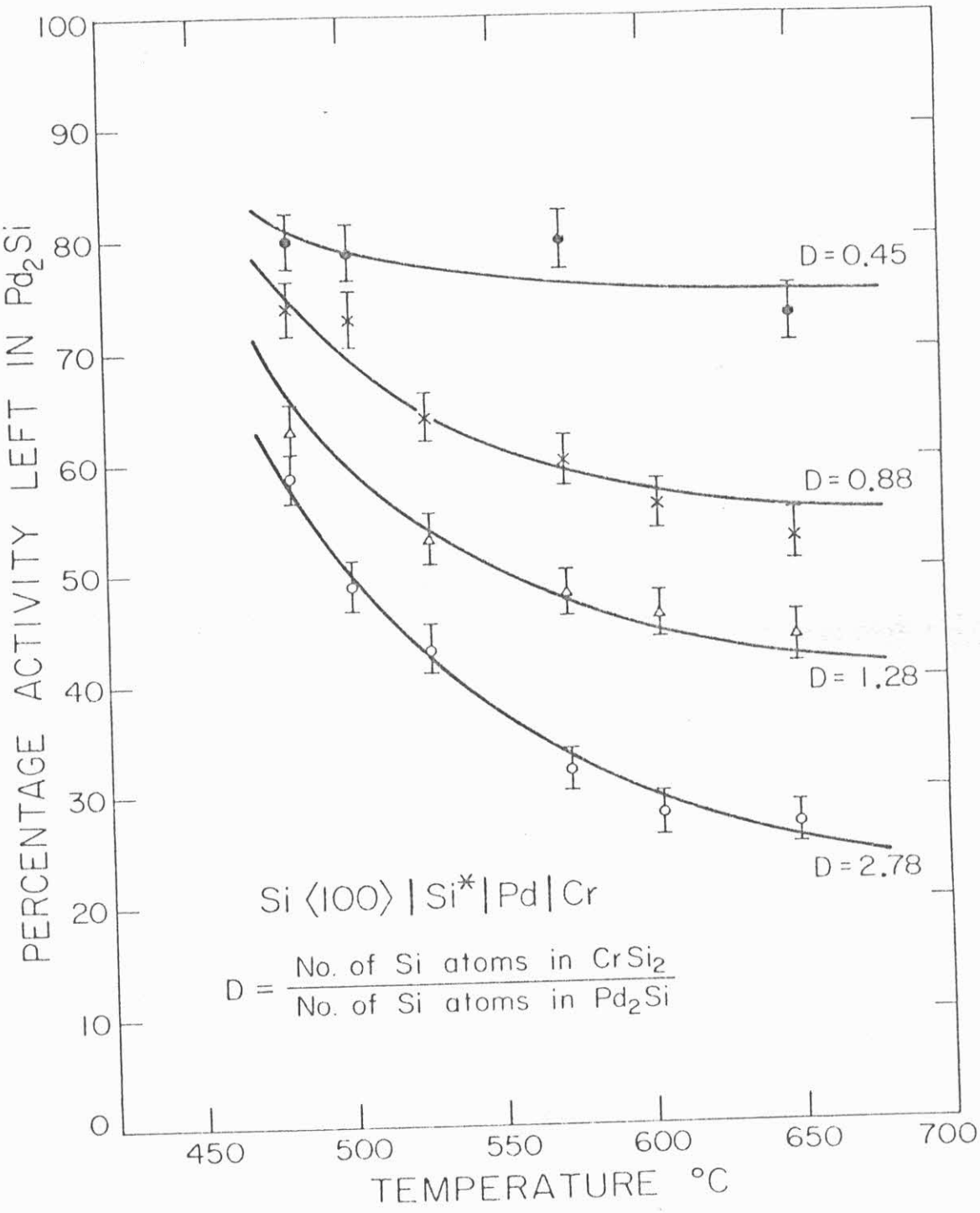
PERCENTAGE ACTIVITY LEFT IN Pd_2Si
TEMPERATURE °C
100
90
80
70
60
50
40
30
20
10
0
450
500
550
600
650
700
D = 0.45
D = 0.88
D = 1.28
D = 2.78
Si ⟨100⟩ | Si* | Pd | Cr
$D = \frac{\text{No. of Si atoms in } CrSi_2}{\text{No. of Si atoms in } Pd_2Si}$

and temperature of formation. For instance, the percentage activity left in Pd_2Si after $CrSi_2$ formation at 600°C for 20 minutes was found to be 37% and 30% for D-values of 1.9 and 3.0 respectively.

In Fig. 25 the percentage activity left in the Pd_2Si layer after $CrSi_2$ formation is plotted as a function of D-values (ratio of Si atoms in $CrSi_2$ to Si atoms in Pd_2Si). The activity profile in 3000Å of Pd_2Si formed on a Si <100> substrate with approximately 400Å of radioactive amorphous Si on top of single-crystal Si has been measured at 400°C.[64] From such an activity profile the percentage activity left in the Pd_2Si layer during $CrSi_2$ growth has been calculated for the case where silicon is supplied by substitutional (vacancy) diffusion through the Pd_2Si layer (curve A in Fig. 4). In this case, as could be expected, all the radioactive silicon atoms will be displaced from the Pd_2Si layer for D = 1. At temperatures higher than about 560°C, the self-diffusion rate of silicon in Pd_2Si layer is so high that complete intermixing of radioactive and nonradioactive Si atoms in the Pd_2Si layer takes place within 10 to 20 minutes.[64] It is clear that for $CrSi_2$ formation on Pd_2Si at such temperatures, all the radioactivity in the Pd_2Si layer can never be removed completely during substitutional diffusion of Si regardless of the thickness of the $CrSi_2$ layer (curve B in Fig. 25). Curve B, Fig. 25 was calculated for $CrSi_2$ growth by substitutional diffusion of Si under temperature

Figure 25. A plot of percentage activity left in the Pd_2Si after $CrSi_2$ formation as a function of $CrSi_2$ (D-value) thickness. Curve A is calculated assuming the activity distribution in Pd_2Si layer as presented by Pretorius et al.[64] and assuming that the supply of Si in $CrSi_2$ formation is by substitutional (vacancy) diffusion only. Curve B is calculated assuming self-diffusion of Si atoms in Pd_2Si and assuming that the supply of Si is by substitution of (vacancy) diffusion. Line C is calculated assuming that the supply of Si from the substrate is by grain-boundary or interstitial diffusion only.

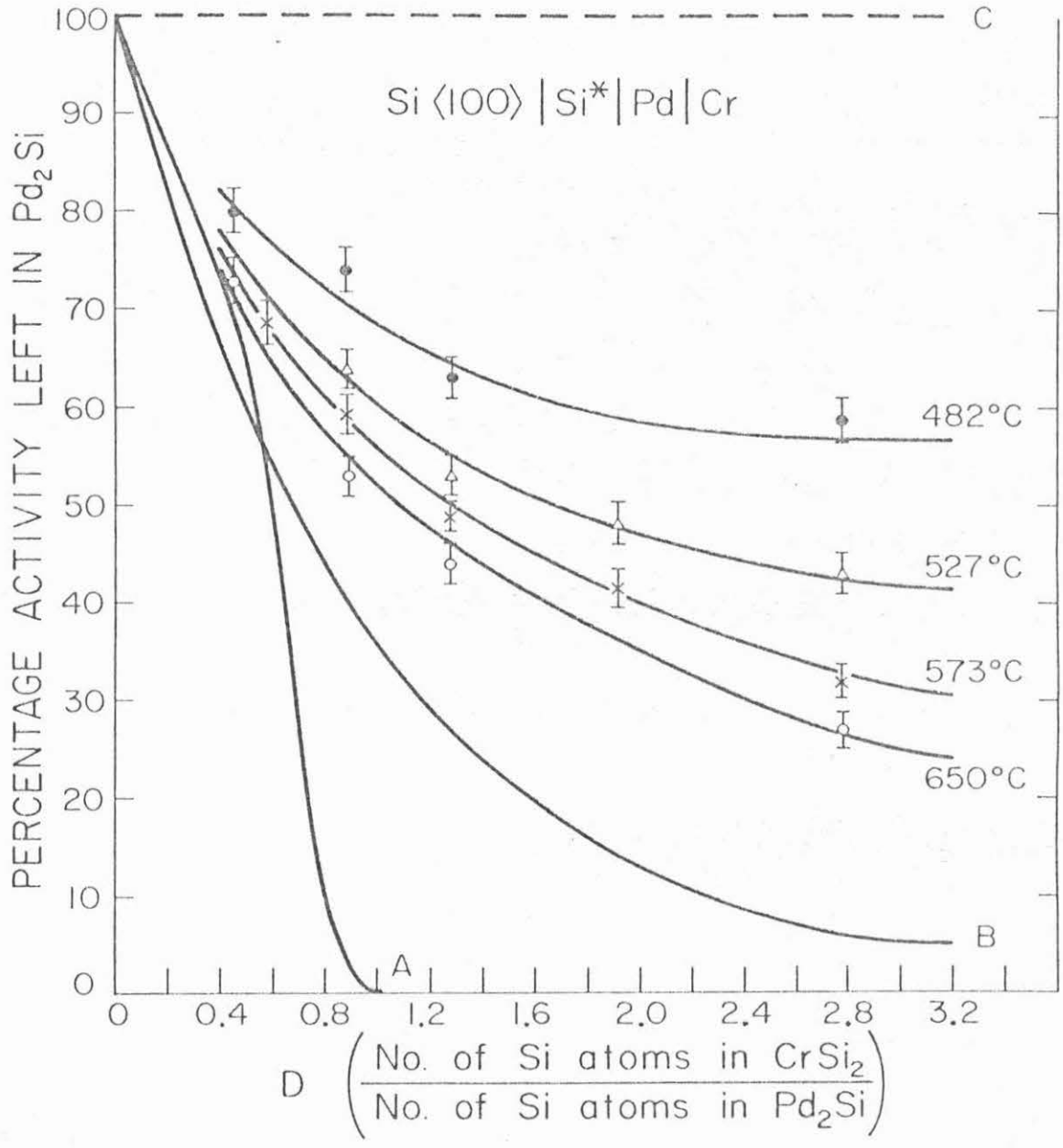
C
Si ⟨100⟩ | Si* | Pd | Cr
482°C
527°C
573°C
650°C
B
A
PERCENTAGE ACTIVITY LEFT IN Pd_2Si
100
90
80
70
60
50
40
30
20
10
0
0
0.4
0.8
1.2
1.6
2.0
2.4
2.8
3.2
D $\left(\frac{\text{No. of Si atoms in } CrSi_2}{\text{No. of Si atoms in } Pd_2Si}\right)$

conditions where the self-diffusion of Si is so high that complete equilibrium is immediately obtained between radioactive Si atoms and non-radioactive Si atoms entering the Pd_2Si layer from the Si substrate during $CrSi_2$ growth. Another possible mechanism of Si supply to the growing $CrSi_2$ layer would be by grain-boundary or "pure" interstitial (no interaction with Si atoms in the Pd_2Si lattice) diffusion of non-radioactive Si atoms directly from the single-crystal substrate. In this case, no radioactive Si atoms will be incorporated into the $CrSi_2$ layer (line C, Fig. 25). In Fig. 25 it can be seen that our measurements are located between B and C, which indicates that silicon atoms for $CrSi_2$ growth were being supplied from both the single-crystal Si substrate and from the Pd_2Si layer.

CHAPTER V. Chromium Thin Film as a Barrier to the Interaction of Pd_2Si and Al

The work reported in this chapter deals with a Pd-Al metallization scheme on Si and shows how a thin Cr layer can be used to prevent Pd_2Si from interacting with Al and thereby preserving the integrity of the Si-Pd_2Si interface. Heat treatments of Al films on Si substrates at temperatures used in integrated circuits (IC's) metallization results in the migration of Si into the overlying Al layer. Bower has used a Ti film layer between Si and Al to prevent Si erosion during heat treatments.[40] Nakamura et al.[41] have deferred the recrystallization of polycrystalline Si (poly Si) in contact with an Al film by placing a buffer layer of V or Ti between poly Si and the Al film. In a similar way we have interposed Cr film layers between Pd and Al in a more complex Si-Pd-Cr-Al system, as reported in this chapter.

In the preceding chapter, a detailed investigation on the formation kinetics of $CrSi_2$ on Pd_2Si grown on <100> oriented Si substrates was presented. The growth of the $CrSi_2$ proceeds at a linear rate with time, with an activation energy of 1.7 eV.

Howard et al.[65] report the kinetics of compound formation for the interaction of thin films of Cr with Al. They state that the compounds $CrAl_7$ (for Al thickness great-

er than Cr thickness) and Cr_2Al_{11} (for Cr thickness greater than or equal to the Al thickness) form between 300 and 450°C. From these results one should expect that at about 400°C Cr film placed between layers of Pd_2Si and Al will react at both interfaces.

Backscattering spectrometry with 2.0 and 2.3 MeV $^4He^+$ has been used in this investigation, to study the Pd_2Si-Al interaction, the interaction of Cr with Si and with Al, and to establish the barrier effect of the $CrSi_2$ and $CrAl_x$ formed in the metallization scheme.

A. Interaction of Pd_2Si with Al without an Interposed Cr Layer

Backscattering spectrum with 2.0 MeV $^4He^+$ of a sample with about 600Å of Pd_2Si plus 3500Å Al is shown in Fig. 26 (full dots). The sample was annealed at 450°C for 15 minutes and a second backscattering spectrum was taken (open circles). The annealed samples shows a substantial interdiffusion of Pd_2Si and Al, which destroys the Si-Pd_2Si interface. The same situation occurs for Si-Pd-Al samples which are obtained by sequentially evaporating Pd and Al on Si and then annealing at 450°C for 15 minutes. Since these changes during annealing are undesirable phenomena in Al metallization,s we have introduced a layer of Cr (300 to 1500Å) between the Al and Pd_2Si.

B. Barrier Effects of Cr

In Chapter IV, it is reported that in the absence

Figure 26. 2 MeV $^4He^+$ backscattering spectra of a sample consisting of a layer of about 600Å Pd_2Si formed on a single crystal <100>-oriented Si substrate and covered with a film of 3500Å Al deposited on top before (o) and after (o) annealing at 450°C for 15 minutes in vacuum.

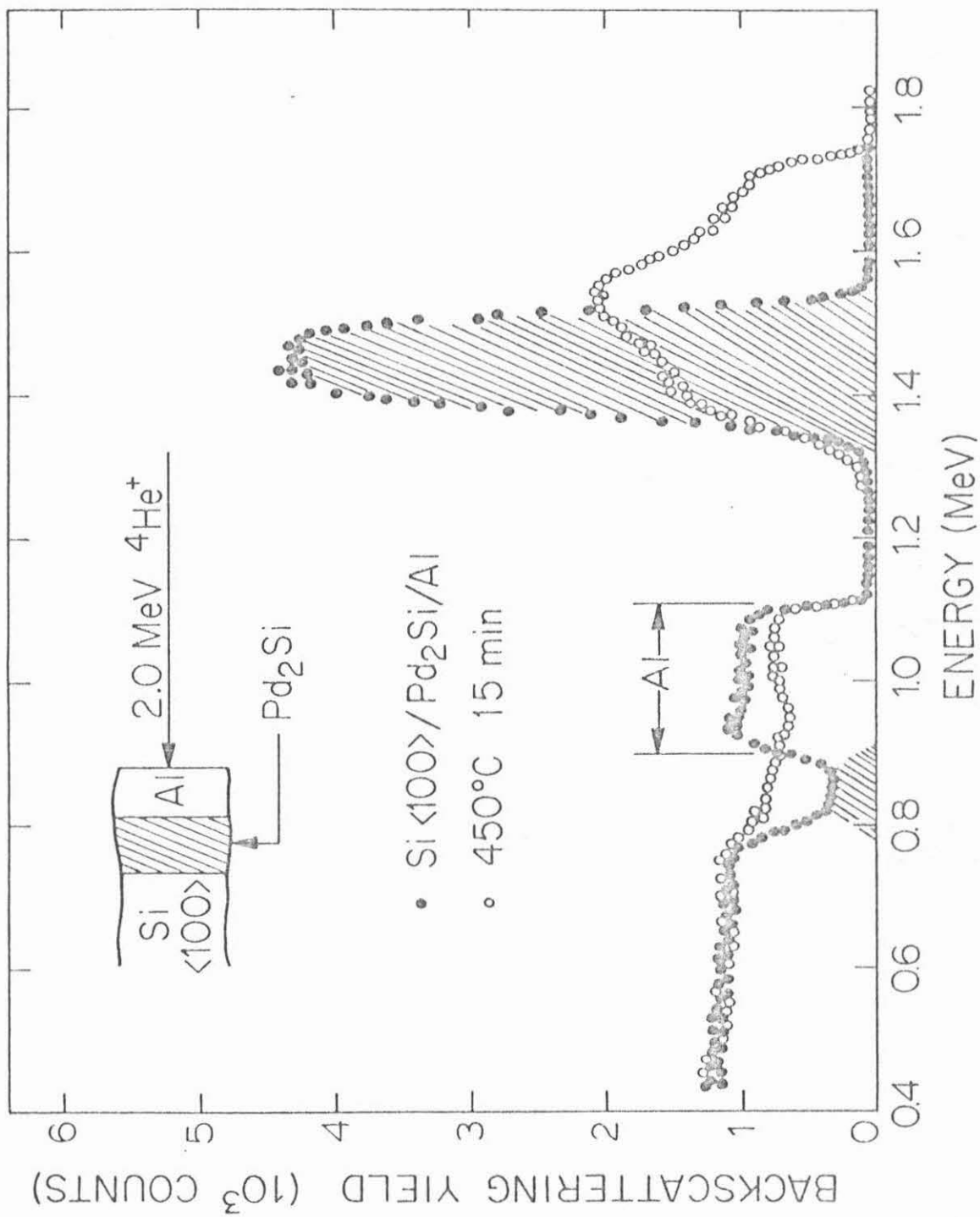
BACKSCATTERING YIELD (10³ COUNTS)
ENERGY (MeV)
0
1
2
3
4
5
6
0.4
0.6
0.8
1.0
1.2
1.4
1.6
1.8
Si <100>
Al
Pd₂Si
2.0 MeV ⁴He⁺
• Si <100>/Pd₂Si/Al
∘ 450°C 15 min
Al

of Al, Cr reacts with Si and forms $CrSi_2$ on top of Pd_2Si. Both Pd_2Si and $CrSi_2$ are formed in distinct sublayers as confirmed by x-ray diffraction and backscattering. Thus, so far, one can assume that the binary Si-Pd and the ternary Si-Pd-Cr systems are relatively well understood. We need to determine what is obtained when a layer of Al is deposited on the latter, giving a more complex Si-Pd-Cr-Al system in a metallization scheme.

The backscattering spectrum with 2.3 MeV $^4He^+$ for a sample in which Pd, Cr and Al were sequentially evaporated on single crystal Si is shown in Fig. 27 before and after annealing at 450°C for 10 minutes. In this particular example, the layer thicknesses were about 800Å for Pd, 500Å for Cr and 3000Å for Al. These thicknesses were calculated and chosen for convenience of a clear interpretation of the two spectra is shown in Fig. 28. During the annealing, all of the Pd reacts with the Si substrate to form Pd_2Si. Chromium silicide, $CrSi_2$, is formed at the interface between Cr and Pd_2Si (as expected from reports in Chapter IV). A $CrAl_x$ compound is formed at the interface between Cr and Al (as expected from the report of Howard et al.[65]). At this temperature and time, not all the Cr is consumed in the reaction process and about 1200Å Al is still unreacted.

For samples annealed up to 500°C and times not greater than 90 minutes, the integrity of Pd_2Si and of the interface between Si and Pd_2Si are maintained. Above

this temperature or for longer annealing times, substantial mixing of Si, Pd, Cr and Al sets in and the backscattering spectra become difficult to interpret.

Figure 27. 2.3 MeV $^{4}He^{+}$ backscattering spectrum of Pd, Cr and Al layers deposited, in that order, on a single crystal <100>-oriented Si substrate before (o) and after (●) annealing at 450°C for 10 minutes.

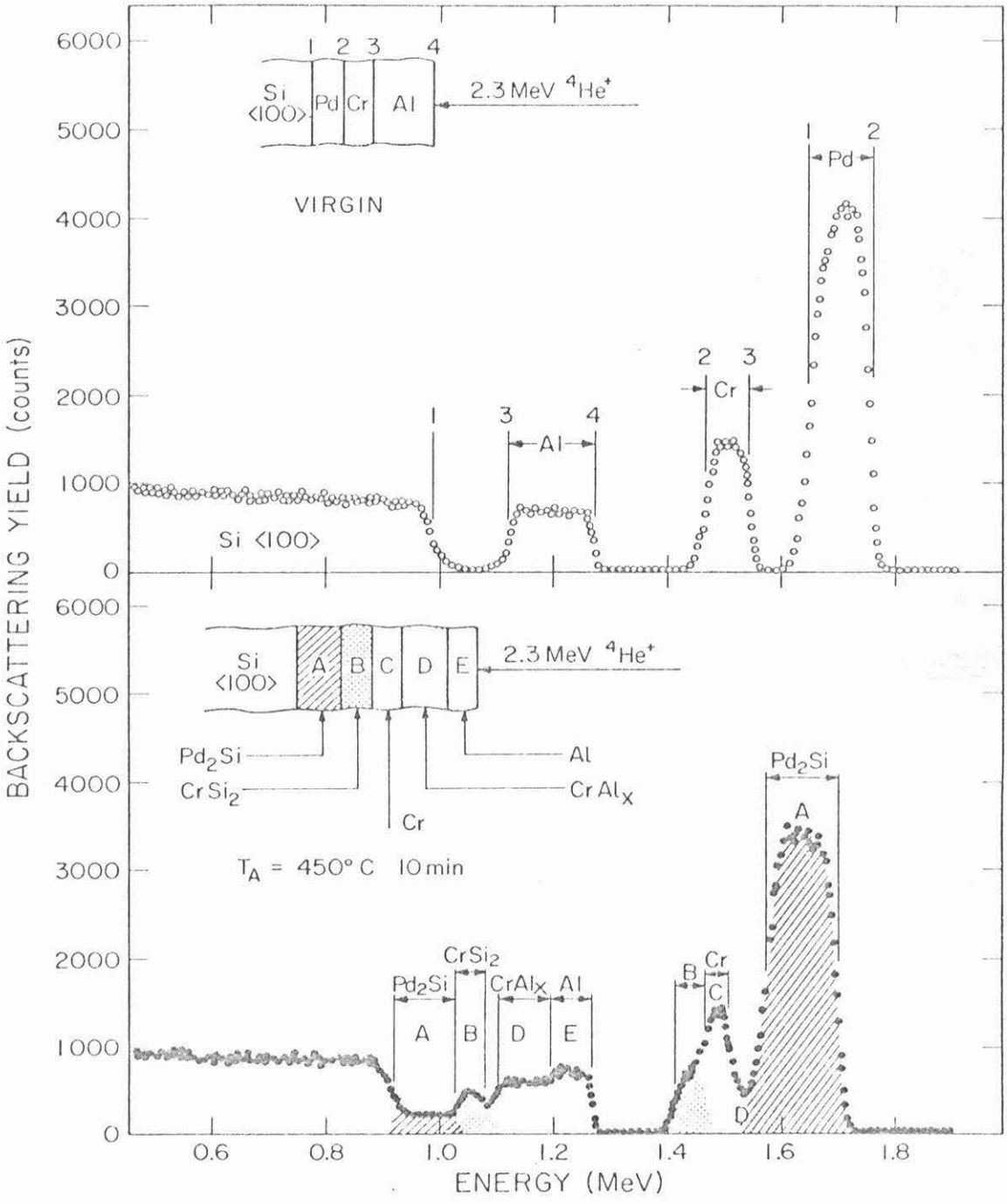
BACKSCATTERING YIELD (counts)
ENERGY (MeV)
Si <100>
Pd
Cr
Al
2.3 MeV $^4He^+$
VIRGIN
Pd_2Si
$CrSi_2$
$CrAl_x$
T_A = 450° C 10 min

Figure 28. Schematic representation of backscattering spectra of Figure 24.

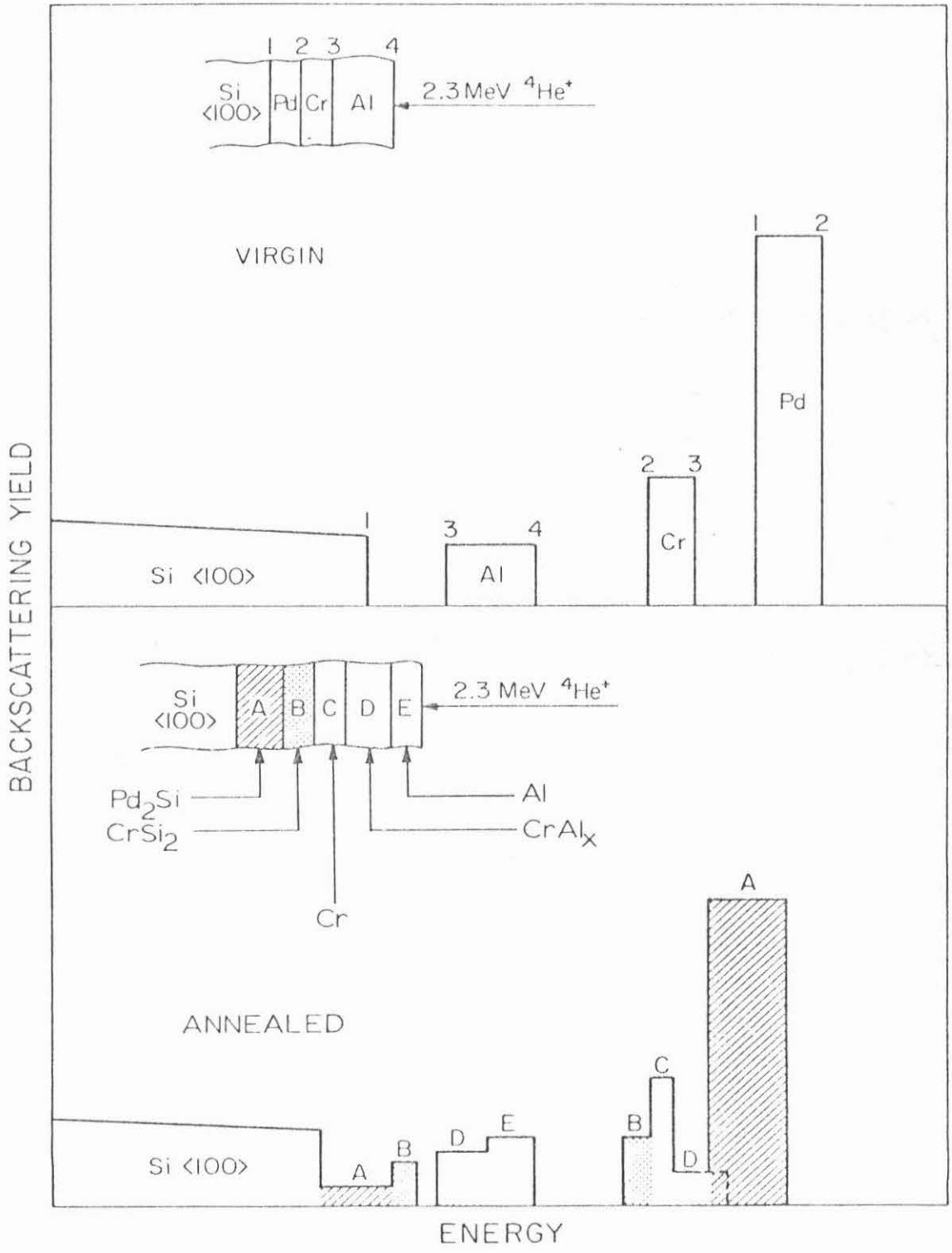
1 2 3 4
Si <100>
Pd
Cr
Al
2.3 MeV $^4He^+$
VIRGIN
1 2
Pd
2 3
Cr
1
3 4
Al
Si <100>
Si <100>
A B C D E
2.3 MeV $^4He^+$
Pd_2Si
$CrSi_2$
Cr
Al
$CrAl_x$
ANNEALED
A
C
B
D
E
Si <100>
A
B
D
E
BACKSCATTERING YIELD
ENERGY

CHAPTER VI. Interaction of Metal Layers with Polycrystalline Si

It has been demonstrated as mentioned in Chapter I, that the interaction of Al layers with polycrystalline Si at temperatures between 400 and 560°C results in the dissolution and recrystallization of poly Si in the metal film.[45] This chapter is a generalization of this phenomenon to other metals.

The last three chapters have laid emphasis on the interaction of single-crystal Si with silicide-forming transition metals. The present chapter presents results obtained when transition metals interact with polycrystalline Si (poly Si). The metals studied include Al, Ag and Au, which form simple eutectics with Si, and Pd, Ni and Cr which form intermetallic compound phases (silicides) with Si. Nakamura et al. reported on the interaction of Al layers with poly Si and found that poly Si dissolves and recrystallizes in the Al matrix at a temperature (400 - 560°C)[45] well below the Si-Al eutectics (577°C). The schematics of the dissolution and recrystallization mechanisms for Al thickness greater or less than poly Si thickness is shown in Fig. 29.

One of the purposes of the present study is to determine if the same dissolution and recrystallization phenomena occur in other metals, which either form simple

Figure 29. Schematic diagrams showing the changes which occur during annealing for samples with original Al layer thinner than the poly Si layer (a), (b) and (c), for samples with original Al layer thicker than the poly Si layer [(d), (e) and (f)].

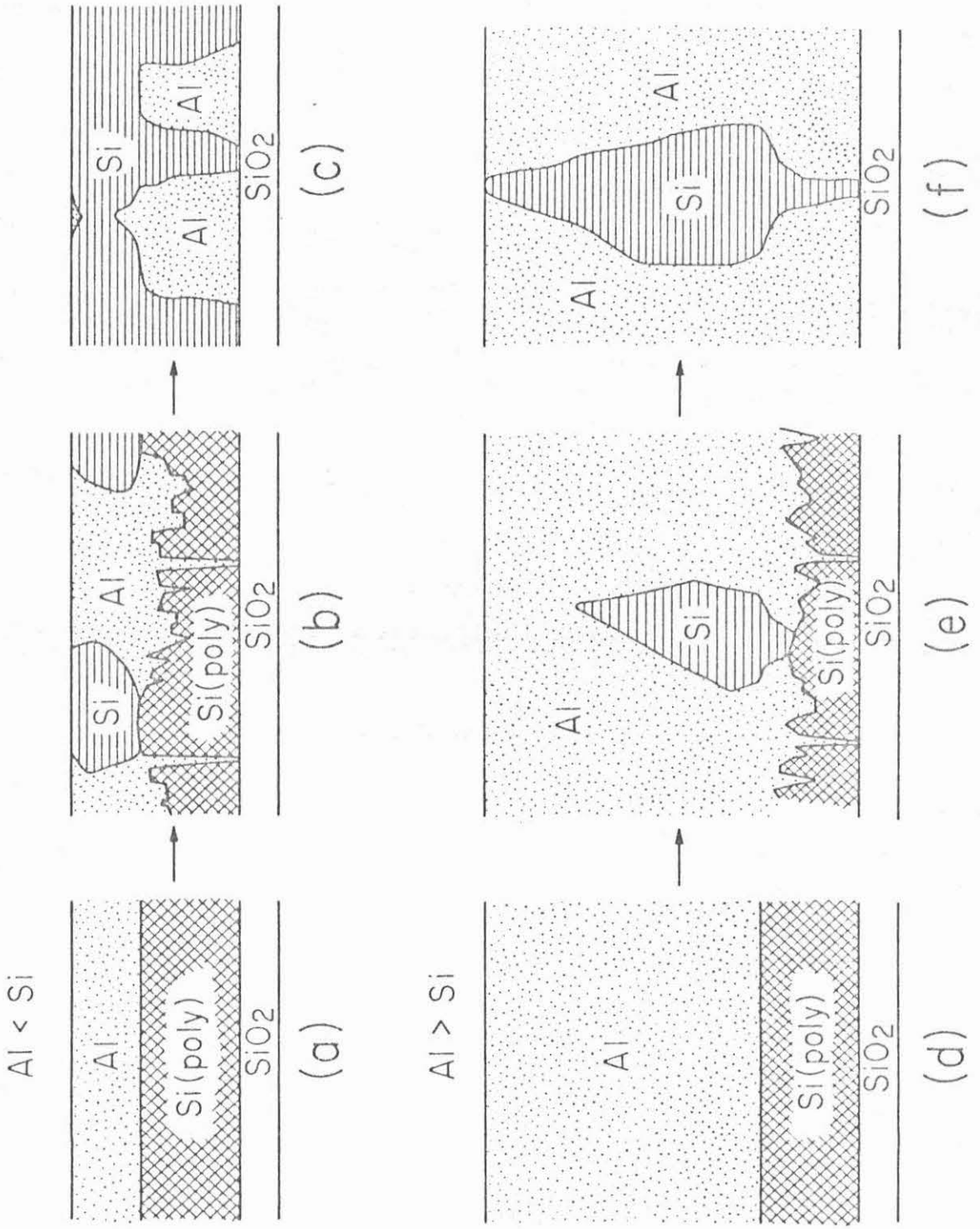
Al < Si
Al
Si(poly)
SiO2
(a)
Si
Al
Si(poly)
SiO2
(b)
Si
Al
Al
SiO2
(c)
Al > Si
Al
Si(poly)
SiO2
(d)
Al
Si
Si(poly)
SiO2
(e)
Al
Al
Si
SiO2
(f)

eutectics or silicides with Si. Au and Ag provide metals with eutectics below (Si-Au eutectic at 370°C) and above (Si-Ag eutectic at 830°C) that for the Si-Al system. For the other purpose, metals were chosen which form silicides at the relatively low temperatures of 200 to 250°C (Pd and Ni) and at the higher temperatures of 450 to 550°C (Cr) on single-crystal Si crystals.

Following heat treatments, the morphological changes and crystallites formation in the poly Si metal structures were observed by scanning electron microscopy (SEM) and glancing angle x-ray diffraction. The composition and kinetics of the silicide-forming metals were studied by MeV $^{4}He^{+}$ backscattering. Another point of interest was to determine if the polycrystalline nature of the Si layer in contact with the metal film results in a change in the growth kinetics or the identity of the initial phases of the silicides as compared to those observed with single-crystal Si.

A. Simple Eutectic Systems

1. Scanning Electron Microscopy (SEM)

When an Al layer covers poly Si, the Si migrates into Al and forms crystalline precipitates within the Al during annealing below the Si-Al eutectic temperature (577°C). The process of this recrystallization can be observed with SEM by etching away the Al layer after annealing. The scanning electron micrographs were taken

on an Akaski-Seisakusho model MSM-2 Mini-SEM.

The sequence of scanning electron micrographs in Fig. 30 shows the recrystallization process of Si in Al as a function of time at 535°C. In this sample the Al layer (1.2 μm) was much thicker than the poly Si (0.5 μm). The reaction begins with the formation of tiny crystallites at the interface between the Al layer and the poly Si substrates (Fig. 30a). With time, the crystallites grow bigger (Fig. 30b) and, eventually, all of the original poly Si substrate is converted to distinct Si crystallites (Fig. 30c). Beyond this point, some crystallites continue to grow at the expense of others (Fig. 30d). However, the growth is confined to the lateral direction; the height of each crystallite is limited by the thickness of the Al layer. Similar dissolution of poly Si and formation of crystallites was observed at temperatures as low as 400°C. However, at the lower temperatures the crystallites growth rate was substantially reduced. For example, the morphology of a sample heated at 400°C for 30 minutes was similar to that shown in Fig. 30b.

A similar recrystallization phenomenon is also observed when a Ag or Au layer is in contact with poly Si (see Fig. 31). The reaction can occur at temperatures as low as 550°C for the poly Si-Ag system and 200°C for poly Si-Au system. The corresponding eutectic temperatures are 830°C for Si-Ag and 370°C for Si-Au respectively. The difference in the shape of the crystallites in Figs. 31a

Figure 30. Scanning electron micorgraphs of samples with 1.2 μm Al on 0.5 μm poly Si after annealing at 535°C for (a) 1 minute, (b) 5 minutes, (c) 1 hour, and (d) 55 h. The Al was chemically removed before examination. The incident angle of the electron beam with respect to the normal of the sample is 60°.

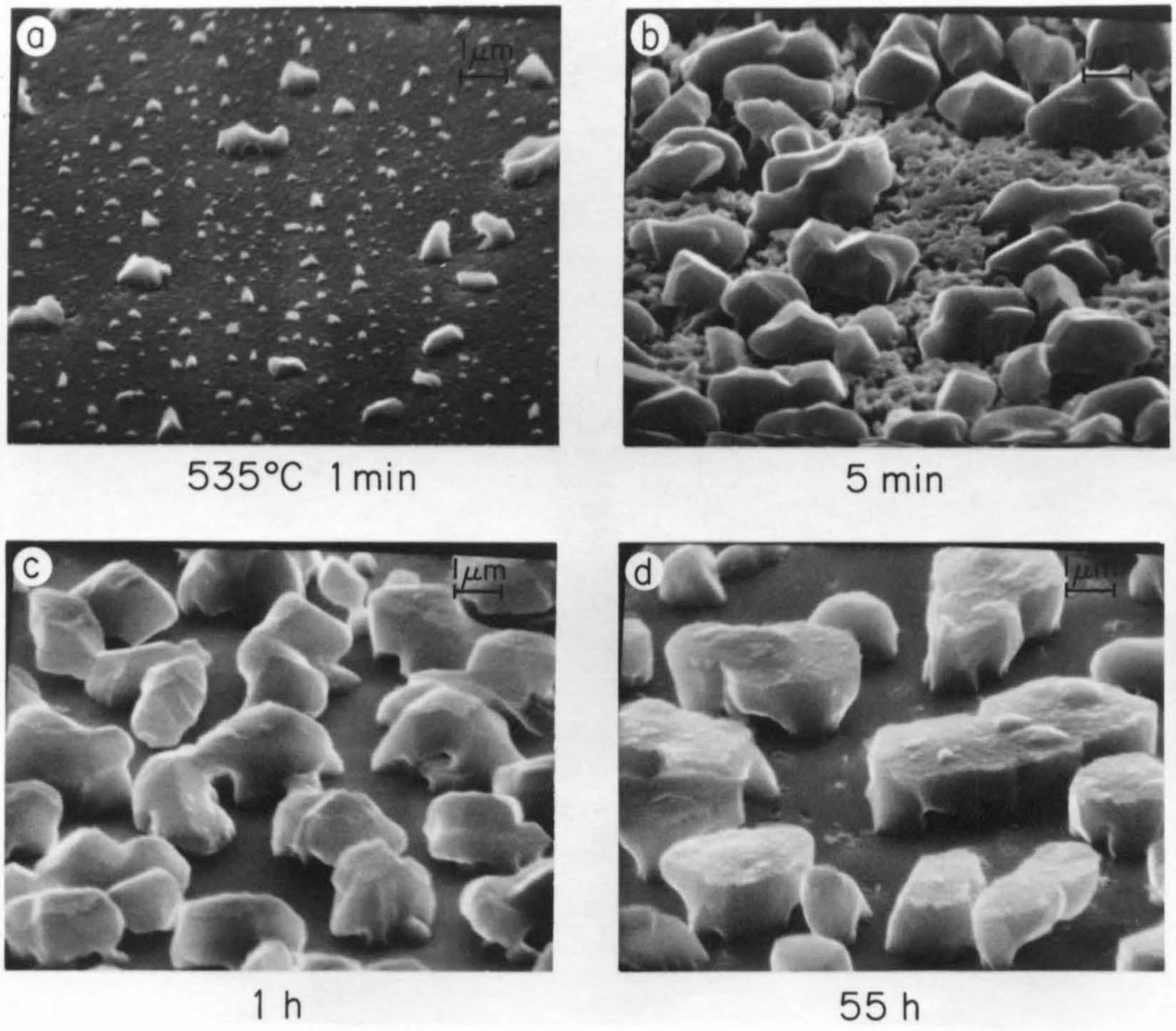
a
1μm
535°C 1 min
b
5 min
c
1μm
1 h
d
55 h

Figure 31. Scanning Electron micrographs of samples with (a) 0.7 μm Ag on 0.5 μm poly Si annealed at 600°C for 15 hours, and (b) 1.5 μm Au on 0.5 μm poly Si annealed at 250°C for 48 hours. The Ag and Au were chemically etched by HNO_3 and aqua regia (1 part of HNO_3 to 3 parts of HCl), respectively, before examination. The incident angle of the electron beam with respect to the normal of the sample is 60°.

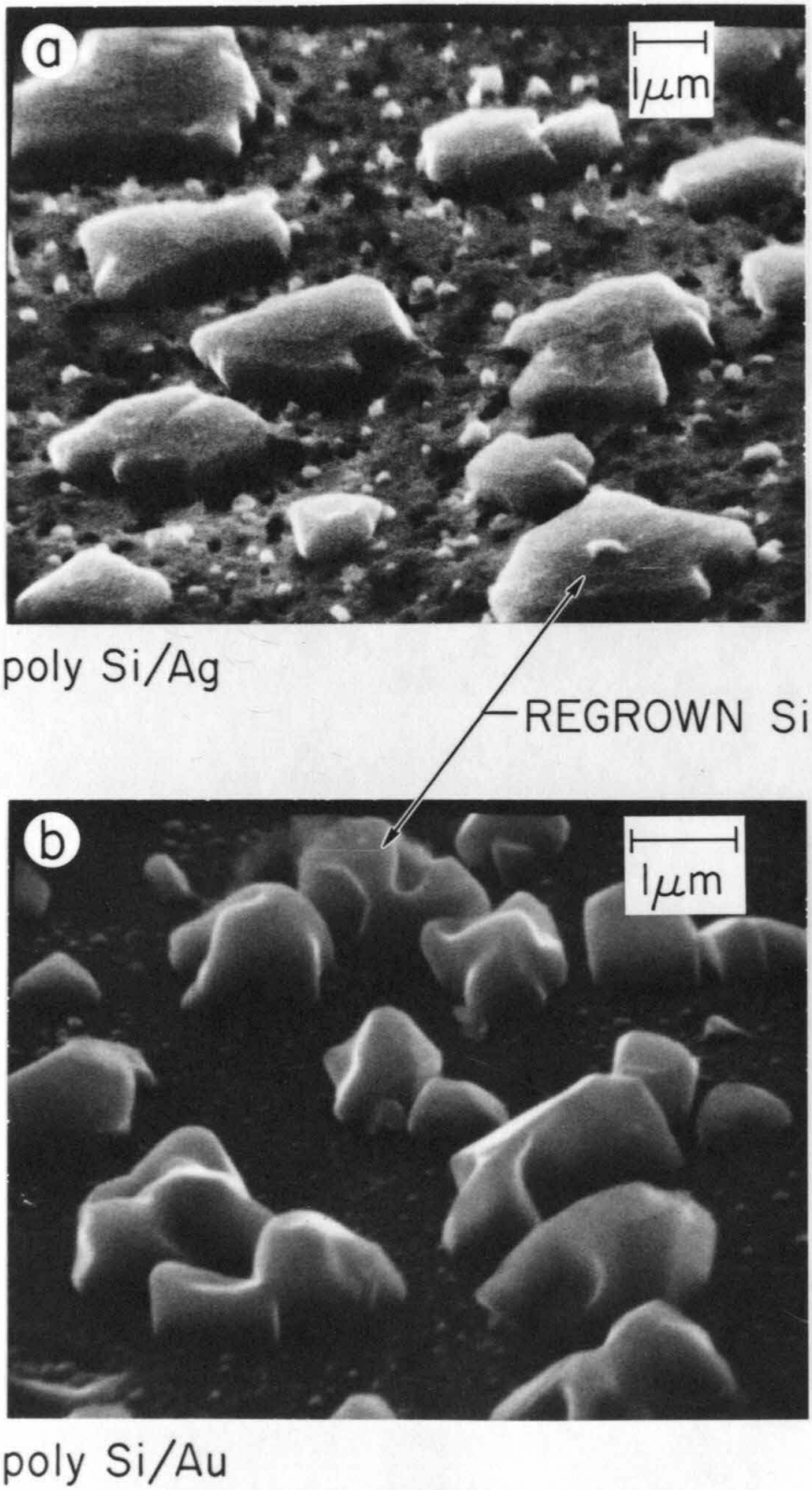
a
1μm
poly Si/Ag
REGROWN Si
b
1μm
poly Si/Au

and 31b is due to the fact that the Ag layer was thin enough to geometrically confine the growth, while the thicker Au layer did not.

2. X-ray Diffraction

The crystal growth process of Si in Al, Au and Ag was monitored by glancing angle (Read camera) x-ray diffraction at each stage of the reaction. Before annealing, Debye-Scherrer rings are absent in the x-ray diffraction pictures of the original poly Si substrate which indicates that the grain size of the original poly Si substrates is small and below the detection limit (Fig. 32a). After annealing a poly Si-Al sample Debye-Scherrer rings of Si appear (Al etched), confirming the presence of Si crystallites (Fig. 32b). All diffraction lines shown are Si lines.

Observation of the patterns reveals that each diffraction line consists of a multitude of individually resolved spots. This multi-spot feature of each diffraction line becomes more perceptible after long annealing (Fig. 32b) proving that the Si crystallites grow bigger with time.

B. Silicide-Forming Systems

Chapters III through V discuss in detail the formation of Ni, Cr and Pd silicides on single crystal Si. This part of the work is to determine if crystallite growth

Figure 32. X-ray diffraction patterns obtained from (a) 0.5 m poly Si as-deposited on SiO_2, and (b) 1.2 m Al on 0.5 m poly Si annealed at 535°C for 120 hours. In (a) the spot pattern is due to the single crystal Si substrate. (b) The ring pattern is due to small Si crystallites. The Al was removed before exposing the sample to x-rays.

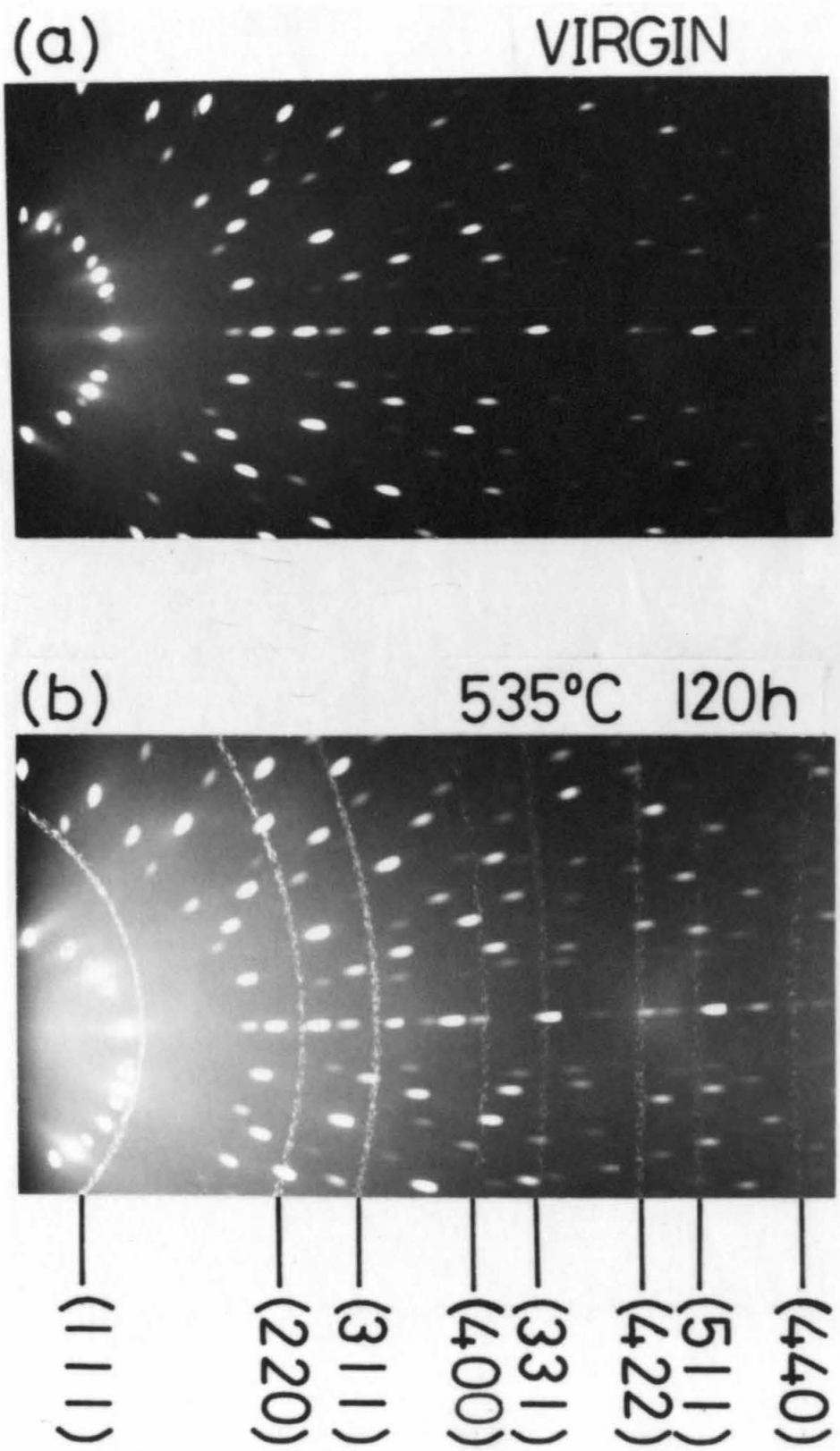
(a)
VIRGIN
(b)
535°C 120h
(111)
(220)
(311)
(400)
(331)
(422)
(511)
(440)

occurred for Pd, Ni and Cr, metals which form silicides, when brought in contact with poly Si. Alternatively, if silicides are formed (as it is with these metals on single crystal Si, Chapters III, IV and V), it is of interest to find out if the polycrystalline nature of the Si layer in contact with the metals alters the formation processes of the silicides compared to those observed with single-crystal Si.

To investigate the behavior of poly Si in contact with silicide forming metals (such as Pd, Ni and Cr), the samples were first annealed at temperatures where a silicide was known to form between these metals and single crystal substrate, i.e., 200 to 325°C for Pd and Ni, and 450 to 500°C for Cr.

1. Poly-Si-Pd

Figure 33 shows the backscattering spectra of a sample with 3700Å of Pd on 5000Å of poly Si before and after annealing at 250°C. After the heat treatment, the formation of an intermediate layer is revealed by the presence of the steps on the low-energy side of Pd signal and the high-energy side of Si signal (see Chapters III and IV). The amplitude ratio of these steps, normalized by the appropriate energy loss factors and differential scattering cross sections (values of these are given in Table 2 for Ni, Pd, Si and Cr), gives the atomic concentration ratio in this layer, which is found to be Pd:Si = 2.0:1.0.

Figure 33. Backscattering spectra of a 3700Å film of Pd evaporated on 5000Å poly Si before (●) and after annealing at 250°C for 35 minutes (o) and 128 minutes (x). The arrows indicate the energy corresponding to scattering from atoms at the surface.

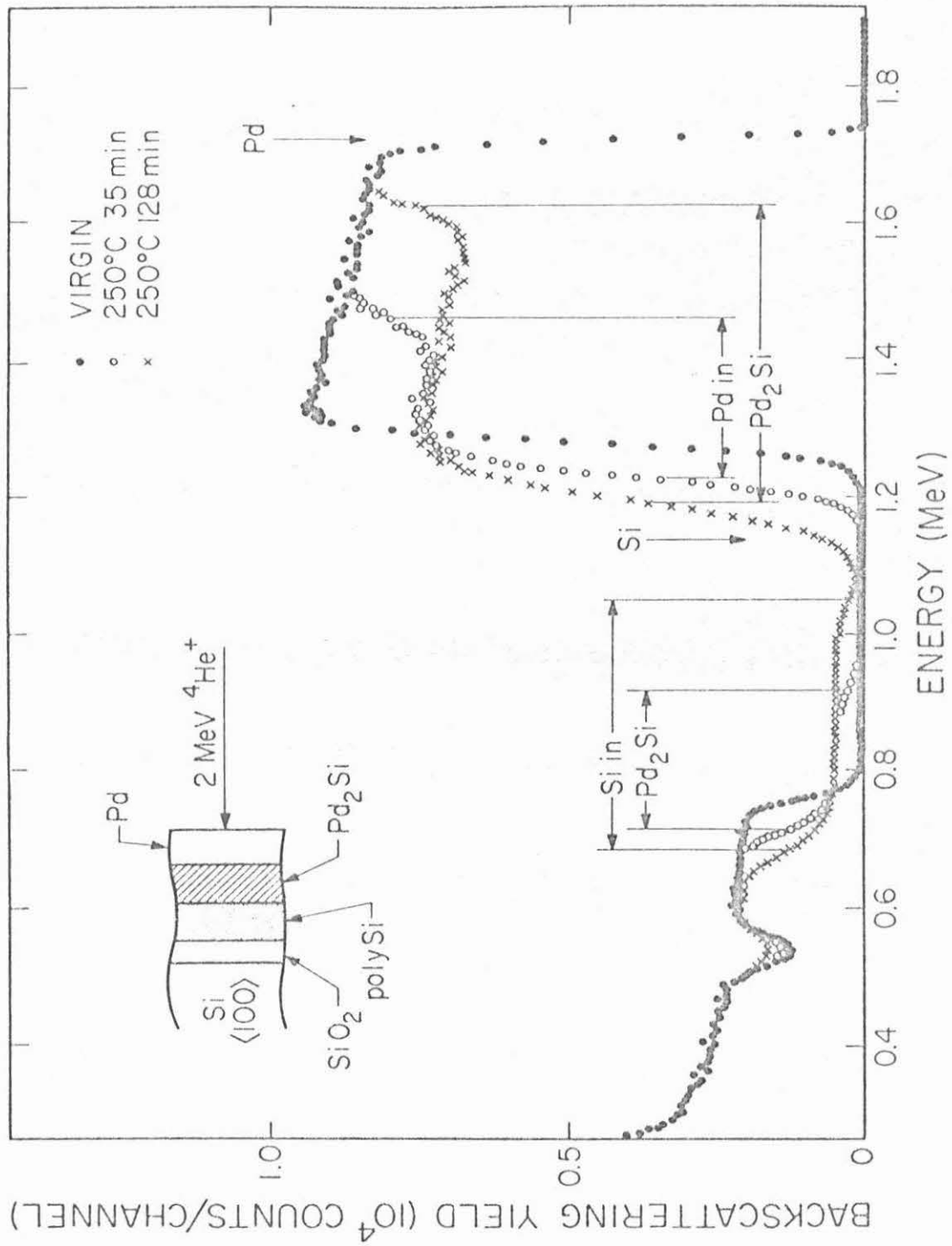
VIRGIN
250°C 35 min
250°C 128 min
Pd
Pd in
Pd$_2$Si
Si
Si in
Pd$_2$Si
2 MeV ^{4}He$^+$
Pd
Pd$_2$Si
Si
⟨100⟩
SiO$_2$
polySi
BACKSCATTERING YIELD (10^4 COUNTS/CHANNEL)
ENERGY (MeV)
0
0.5
1.0
0.4
0.6
0.8
1.0
1.2
1.4
1.6
1.8

X-ray diffraction analysis establishes that the phase of this layer is Pd_2Si as is also found for the reaction of Pd on single crystal Si at 250°C.

By measuring the width of the steps one can determine the thickness of the silicide layer (see Chapters III and IV). Figure 34 shows the thickness of Pd_2Si as a function of time at four different temperatures. The abscissa is scaled in square root of time. Measured points are well fitted by straight lines through the origin. This shows that the rate-limiting process is the diffusion of the species through the silicide layer, as is the case for silicide formation on a single-crystal Si substrates.

Figure 35 shows the Arrhenius plot of the rate of Pd_2Si formation on the poly Si substrate together with the results quoted by Bower et al.[11] for a single crystal substrate. An activation energy of about 1.2 eV is obtained in the case of the poly Si substrate. This value is 0.3 eV lower than the value obtained by Bower et al, but is similar to the value of 1.27 eV reported by Hutchins and Shepala.[6]

2. Poly-Si-Ni

The poly-Si-Ni samples were annealed at temperatures between 225 and 325°C and analyzed by backscattering. Figure 36 shows spectra of a sample with 5400Å of Ni on 5000Å of poly Si before and after annealing at 275°C. As in thecase of Pd, a silicide is formed. The amplitude ratio

Figure 34. Thickness of Pd_2Si formed in the reaction between Pd and poly Si as a function of time. The abscissa is scaled in square root of time.

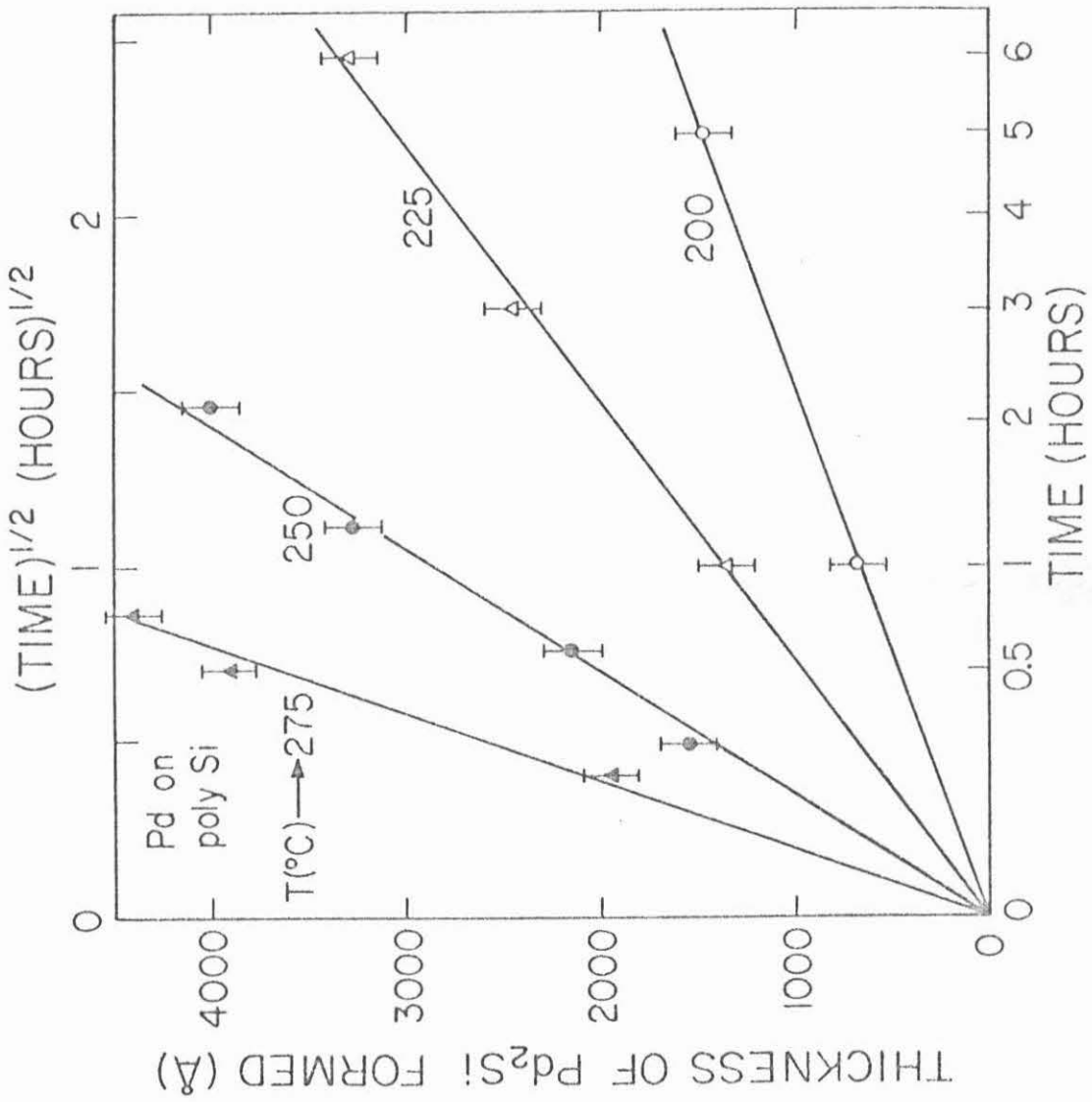
THICKNESS OF Pd_2Si FORMED (Å)
TIME (HOURS)
(TIME)$^{1/2}$ (HOURS)$^{1/2}$
Pd on poly Si
T(°C)→275
250
225
200
0
1000
2000
3000
4000
0.5
1
2
3
4
5
6

Figure 35. Arrhenius plot for Pd_2Si and Ni_2Si formation in the reaction of poly Si with Pd and Ni. The formation rates for the case of a single-crystal substrate are also shown for reference purposes.

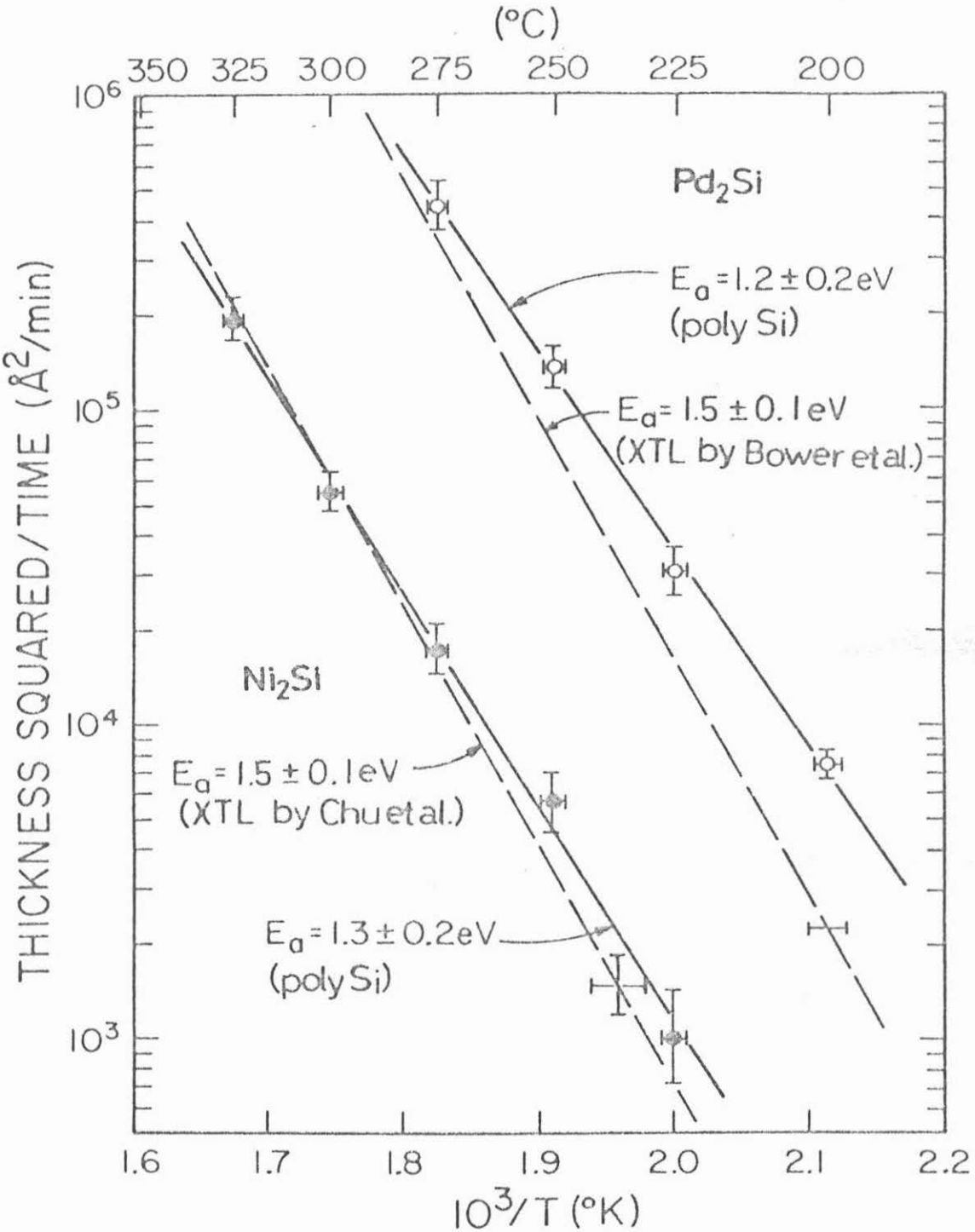
(°C)
350 325 300 275 250 225 200
10^6
10^5
10^4
10^3
THICKNESS SQUARED/TIME (Å²/min)
Pd_2Si
E_a = 1.2 ± 0.2eV
(poly Si)
E_a = 1.5 ± 0.1eV
(XTL by Bower et al.)
Ni_2Si
E_a = 1.5 ± 0.1eV
(XTL by Chu et al.)
E_a = 1.3 ± 0.2eV
(poly Si)
1.6 1.7 1.8 1.9 2.0 2.1 2.2
$10^3/T$ (°K)

Figure 36. Backscattering spectra of a 5400Å film of Ni evaporated on 5000Å of poly Si before (o) and after annealing at 275°C for 2 hours (o), and 6 h (x). The arrows indicate the energy corresponding to scattering from atoms at the surface.

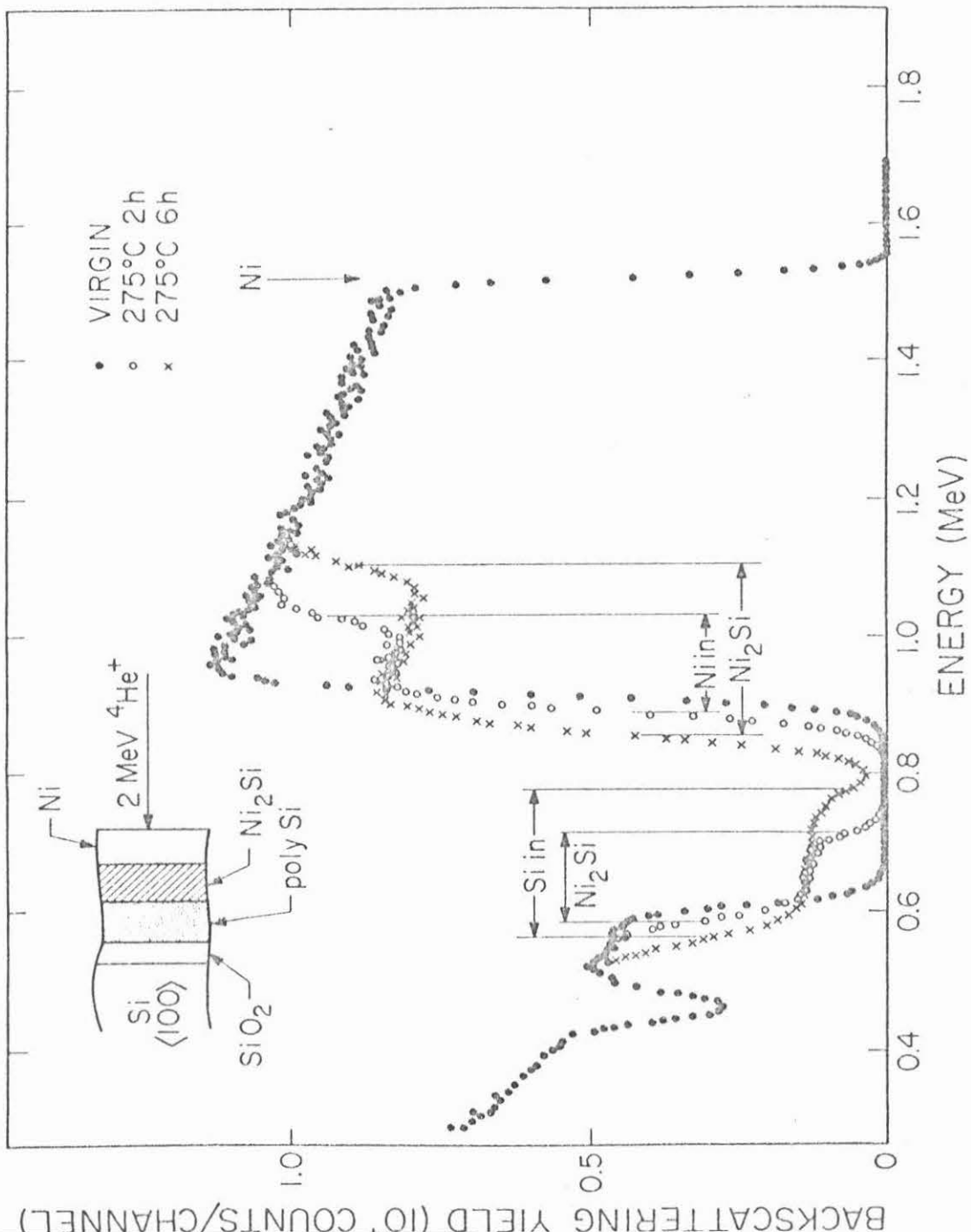
BACKSCATTERING YIELD (10^4 COUNTS/CHANNEL)
ENERGY (MeV)
VIRGIN
275°C 2h
275°C 6h
Ni
Ni in
Ni_2Si
Si in
Ni_2Si
2 MeV $^4He^+$
Ni
Ni_2Si
poly Si
Si ⟨100⟩
SiO_2

of the elements in the compound layer is found to be Ni:Si = 2.0:1.0. X-ray diffraction analysis identifies the phase as Ni_2Si as is found for the reaction of Ni on single-crsystal Si in this temperature range. Growth curves as shown in Fig. 37. The silicide, Ni_2Si, forms on the poly Si substrate according to a parabolic time dependence, as is the case for a single-crsystal Si substrate (see Chapter III). An Arrhenius plot of the formation rate of Ni_2Si is given in Fig. 35 and yields an activation energy of about 1.3 eV. This value is 0.2 eV lower than that found by Tu et al.[15] for <100> Si and 0.3 eV lower than that found for <111> Si (Chapter III).

3. Poly-Si-Cr

Figure 38 shows the backscattering spectra of the sample with 1700Å of Cr on 5000Å of poly Si before and after annealing at 500°C for 40 minutes. Analysis of this spectrum and x-ray diffraction measurements made on the sample after annealing indicate that $CrSi_2$ is formed, as in the case of single crystal substrate (see Chapter IV). The growth kinetics of this system was not studied in detail, but silicide formation is observed in the same temperature range (450 to 500°C) as that for single crystal Si.

In all the three silicide forming systems there was no evidence of Si crystallite formation in the temperature range where growth of the silicide layers occurred.

Figure 37. Thickness of Ni_2Si formed in the reaction between Ni and poly Si as a function of time. The abscissa is scaled in square root of time.

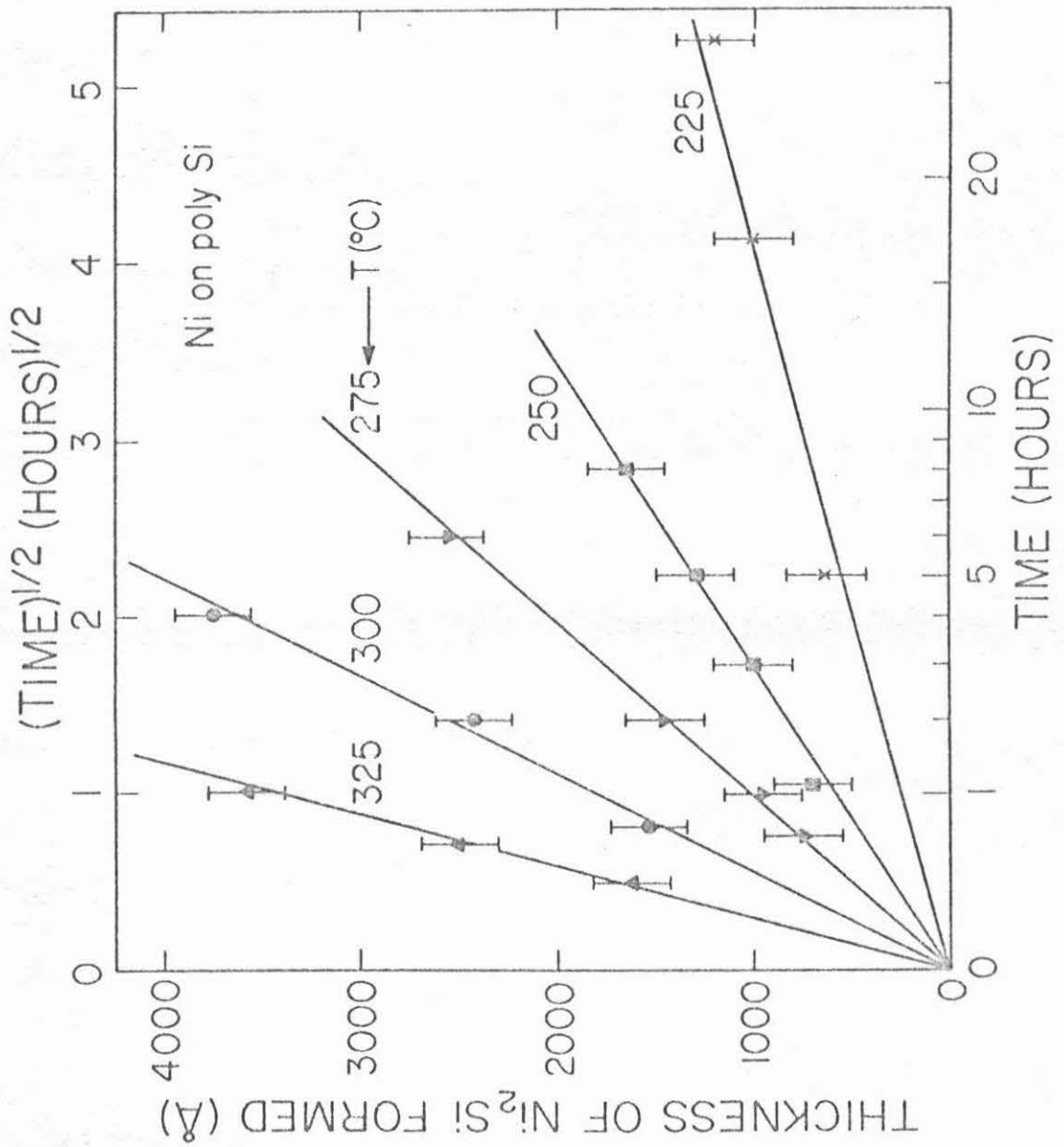
THICKNESS OF Ni2Si FORMED (Å)
4000
3000
2000
1000
0
0
1
2
3
4
5
(TIME)1/2 (HOURS)1/2
0
5
10
20
TIME (HOURS)
Ni on poly Si
T (°C)
325
300
275
250
225

Figure 38. Backscattering spectra of 1700Å film of Cr evaporated on 5000Å of poly Si before (o) and after annealing at 500°C for 40 minutes (o). The arrows indicate the energy corresponding to scattering from atoms at the surface.

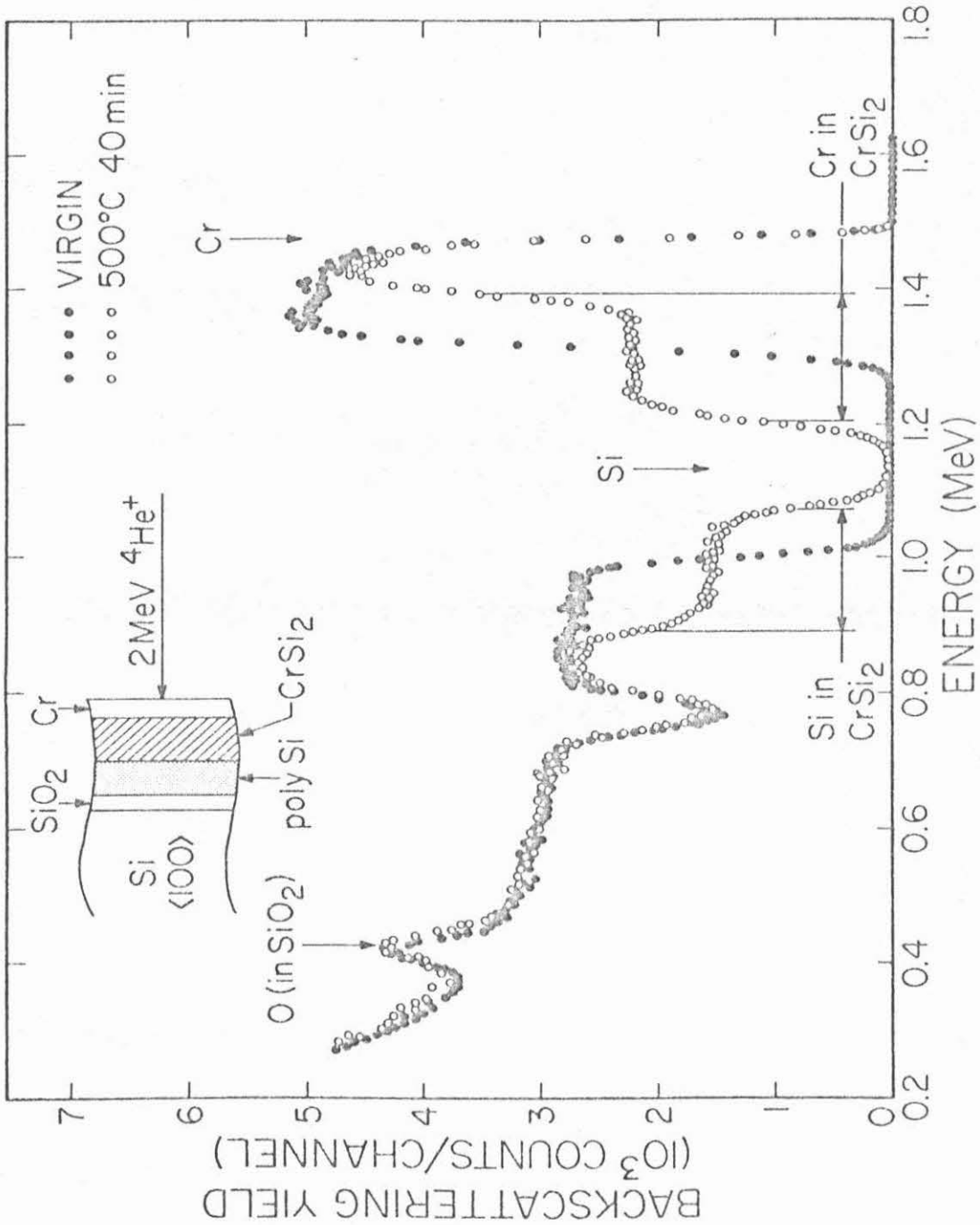
BACKSCATTERING YIELD
(10³ COUNTS/CHANNEL)
ENERGY (MeV)
VIRGIN
500°C 40 min
2MeV ⁴He⁺
Cr
SiO₂
Si
⟨100⟩
O (in SiO₂)
poly Si
CrSi₂
Si
Cr
Si in CrSi₂
Cr in CrSi₂

This is based on the absence of Debye-Scherrer rings corresponding to Si in the diffraction patterns and the presence of near-stoichiometric composition of metal to Si within the silicide layer.

CHAPTER VII. Conclusion and Speculations

By using MeV ^{4}He ion backscattering, glancing angle x-ray (Read camera) diffraction techniques, transmission, scanning electron and optical microscopy I have investigated the interactions of metals (Ni, Cr, Pd, Al, Au and Ag) with single-crystal and polycrystalline Si. The unique capacity of backscattering of ^{4}He ions as a quantitative tool in analyzing the composition, kinetics and growth rates of compounds and multilayer metallization structures has been demonstrated.

The formation, composition, structure and kinetic rate of formation of Ni silicides are strongly influenced by the orientation and nature of the Si substrates. While no orientation effects were found in the reaction of Cr with Si, the rate of formation of $CrSi_2$ is strongly influenced by small traces of impurities and the nature of the Si-Cr interface.

In the reaction of Ni with single-crystal Si, the growth rate of Ni_2Si on <111>-oriented Si substrates annealed between 200 and 325°C is about 2 to 3 times lower than the growth rate observed on <100>-oriented Si substrates. In both cases, the Ni_2Si layer grows proportional to the square root of time, therefore implying that the rate is transport-limited. This work presents a positive example to illustrate that a transport-

limited silicide formation
can indeed be influenced by the orientation of the substrates. The transmission electron micrographs of the polycrystalline Ni_2Si on <100> and <111> Si substrates indicate that the grain size of Ni_2Si on the latter is twice that on the former. This merely indicates that there are more grains and, hence, more grain boundaries per unit volume in Ni_2Si on <100> Si. Since it has been observed by a marker experiment that Ni is the moving species in the formation of Ni_2Si,[31,32] one could speculate that grain boundary diffusion plays a role in the diffusion of the Ni atoms through the silicide layer. If it is assumed that grain boundary diffusion is the major transport mechanism, which, indeed, I think it is, one clearly observes that more diffusion paths are available for Ni motion in Ni_2Si on <100> Si which has more grains per unit volume. The faster Ni atoms are delivered to the Si-Ni interface the faster the growth of Ni_2Si. It is, therefore, hypothetically and logically consistent that the growth of Ni_2Si on <100> Si is much faster than on <111> Si.

On poly Si substrates, the silicide formed is Ni_2Si as observed on <100> oriented Si substrates; the value of its reaction rate and its activation energy are quite similar in both cases. Harris[59] later discovered that the grain size of the poly Si used in these studies is

very small, less than 300Å. It might be speculated, therefore, that if these small grains are oriented in a particular low index direction with each other, the poly Si substrates would behave like a single crystal. Since the interaction of the poly Si substrates with Ni, Pd and Cr is similar to what is found for single crystal Si, one might conclude that the grains of this poly Si are arranged in a somewhat crystalline fashion. It might be expected that it forms silicides with Ni, Pd and Cr, with growth rate similar to that found for single crystal Si.

On evaporated Si substrates, the two compound phases Ni_2Si and NiSi are formed simultaneously in distinct sublayer. Read camera x-ray diffraction analysis identifies the two phases to be Ni_2Si and NiSi, backing up the composition and depth profiling analysis of backscattering. The growth rate and activation energy for the composite layer are similar to those measured on <100> oriented and poly Si substrates. In general, only one equilibrium phase is observed in the reaction of transition metals with Si, but that does not necessarily preclude the coexistence of another phase. It has been postulated[16,21] that the frequency of nucleation and growth rate of a silicide phase are the necessary conditions for a particular phase to exist. The high energy state of amorphous Si could be viewed as providing a driving force for an enhanced frequency of nucleation and a fast growth rate for NiSi; a situation similar to the

driving force in the epitaxial growth of Si in Si(amorphous)-metal-Si system.[63]

Unlike the Ni-Si systems, and very much like Pd-Si and V-Si,[13,14] no orientation effects of the substrates were found in the interaction of Cr with Si. Two different approaches were taken to study the properties of formation of $CrSi_2$. One is the formation of $CrSi_2$ in the Si-Pd-Cr thin film structure and the other is the Si-Cr system. For both samples the rate of $CrSi_2$ formation is the same, and is linear in time with an activation energy of 1.7 ± 0.1 eV. For each temperature, the rate slows down and becomes nonlinear at long annealing times. The nonlinearity effect has been proved to be due to contaminant distributed uniformly in the Cr film, most probably oxygen.

The $CrSi_2$ formation was investigated for temperatures between 400 and 525°C and times up to 2½ hours. There is formation of Pd_2Si in the Si-Pd-Cr system at about 280°C and $CrSi_2$ starts to form at about 400°C on top. No $CrSi_2$ formation was observed for Si-Cr below 450°C. The absence of $CrSi_2$ in the Si-Cr reaction below 450°C is attributed to the presence of an interfacial layer between the Cr film and Si substrate, quite probably a thin oxide layer. The thin oxide layer must have been "cleaned" in the process of Pd_2Si formation.

Samples prepared with different thicknesses of Pd_2Si all show the same thickness of $CrSi_2$ after the same

annealing. This independence of the $CrSi_2$ formation on the existence of a Pd_2Si layer proves that the formation of $CrSi_2$ is only limited by the Si-Cr reaction.

Palladium silicide forms on single crystal Si at a temperature much less than 200°C while no reaction of Si with Cr has been observed below 450°C. Once Pd_2Si is formed it is stable up to 800°C. It is speculated that the low temperature formation and the stability of Pd_2Si might be important factors in the formation of $CrSi_2$ on Pd_2Si in the Si-Pd-Cr system.

A tracer technique using radioactive ^{31}Si ($T_{1/2}$ = 2.62 h) was used to study the growth of $CrSi_2$ on Pd_2Si. Our results show that silicon atoms for $CrSi_2$ growth were partly coming from the single crystal Si substrate and partly from the Pd_2Si layer. As the thickness or formation temperature of $CrSi_2$ increased the amount of radioactive Si left in the Pd_2Si layer decreased. This probably indicates that there is more exchange between the radioactive Si atoms and the Si atoms from the substrate during passage through the silicide layer at higher temperatures. One cannot consider the silicide layer as a static lattice but that the Pd_2Si bonds are broken or reformed at the temperatures of $CrSi_2$ formation. Both curves A and B of Fig. 25 apply to such a bond-breaking diffusion mechanism. However, in the case of curve B the self-diffusion rate of Si is much higher than the growth rate of $CrSi_2$. We speculate that Si is primarily trans-

ported by grain boundary and/or interstitial diffusion. As the $CrSi_2$ formation temperature increases there is more exchange between this silicon and the radioactive silicon atoms present in the Pd_2Si layer. In effect, therefore, Si is supplied from the substrate directly and from the Pd_2Si layer, indirectly.

$CrSi_2$ has proved useful as a diffusion barrier in Si-Pd-Cr-Al metallization system. We observed that $CrSi_2$ forms on Pd_2Si before any grain-boundary diffusion of Al into Pd_2Si. It might be speculated, therefore, that the silicide-formation-before-grain-boundary-diffusion is a factor in the use of $CrSi_2$ as a diffusion barrier between Pd_2Si and Al in the Si-Pd-Cr-Al scheme.

Interaction of polycrystalline Si (poly Si) with Ni, Pd, Cr, Al, Ag and Au was also studied. For the case of Al, Ag and Au, metals which form simple eutectics with Si, our results demonstrate that poly Si crystallizes below the eutectic temperature when in contact with films of these metals during annealing. The process seems to be a general one for metals forming simple eutectics with Si.

The observation of the crystallites is plausible if one assumes that the force which drives this process originates from the growth of large-grain Si crystallites at the expense of the small grained poly Si material. It is known, furthermore, from experiments by Hiraki et al.[38] and from my work on the transport of Si in the Si-Au-Si system, that Au films constitute an efficient transport

medium for Si at very low temperatures. Similar observations nave been made on Ag films by Ottaviani et al.[44] It is worth noting also that the solubility of Si in Al is of the order of 1% at an anneal temperature of 500°C, while in Au it is less than 0.02% below the eutectic point. The processes responsible for the crystallization are thus only weakly dependent on the solubility of Si in the metal. Transport along grain boundaries is a mechanism compatible with this fact, but our observations do not allow a conclusion regarding the microscopic nature of the transport mechanisms involved.

In contrast to what is found for Al, Ag and Au films, the crystallization of poly Si is not the dominant process in films of Ni, Pd and Cr. Upon annealing, these metals form a silicide at the metal-poly-Si interface. There is no visible crystallization of Si. The silicides formed are the same as those observed on single crystal Si substrates. For the case of Pd and Ni, the growth kinetics also obeys the same time dependence ($\propto t^{1/2}$) found with single crystal substrates, and the rate constants and the activation energies are quite similar. The kinetics of $CrSi_2$ formation on poly Si is yet to be determined, but the temperature at which the compound begins to form on poly Si is close to that observed for single crystal Si substrates also.

Once all the metal is consumed in the silicide,

the structure is stable. No changes were observed after annealing for 20 hours at the formation temperature. More studies are required to investigate whether or not crystallization could be included at higher temperatures.

APPENDIX

1. Experimental Procedures and Analysis in Radioactive Tracer Studies of $CrSi_2$ on Pd_2Si

Bulk silicon chips of irregular shapes and sizes were first cleaned and then activated in a Triga nuclear reactor at the University of California, Irvine. During neutron activation radioactive ^{31}Si is formed from ^{30}Si (3.1 at %) by the reaction $^{30}Si(n,\gamma)^{31}Si$ which has a cross section of 0.10 barns. Silicon-31 decays with a half-life of 2.62 hours by emitting beta particles (max β^- energy = 1.48 MeV) for 99.93% of its disintegration.

The activated chips were first etched in HF, rinsed in double-distilled H_2O, blown dry and immediately placed into an electron-gun deposition system. Loaded simultaneously are palladium and chromium charges. Palladium, activated Si and Cr were sequentially deposited in that order onto <100> oriented single crystal Si wafers, giving Si<100>/Pd/Si(activated)/Cr samples. The Si substrates were first cleaned in organic solvents, etched in HF, rinsed in H_2O and blown dry before vacuum deposition. Activated Si with thicknesses varying between 300 and 1000Å was deposited on Pd before Cr was in turn evaporated on top. The thickness of Pd was kept constant at about 2000Å while the thickness of Cr varies between 300 and 3500Å/ Evaporations were done in a vacuum of 5-7

x 10^{-7} Torr.

Samples were first annealed at 400°C for 5 minutes to form Pd_2Si, by the reaction of Pd with both the Si substrates and with the radioactive Si. The thicknesses of the activated Si were such that it will be completely consumed in the process of silicide formation. After the Pd_2Si formation, the samples were annealed at higher temperatures up to 650°C to form $CrSi_2$ using all the Cr in the reaction process. All annealings were performed in a vacuum quartz-tube furance at pressures between 1 x 10^{-6} and 8 x 10^{-7} Torr.

The $CrSi_2$ layer was completely removed by etching the samples in 1 HF to 4 H_20 etchant solution. The silicon radioactivity in Pd_2Si was determined by counting the activity before and after $CrSi_2$ layer was removed. The presence of ^{31}Si was determined by measurement with an end-window Geiger-Muller counter having a mica window (1.8 mg/cm^2) with a cross sectional area of 6 cm^2.

To investigate whether or not the activity in the samples is coming from Si atoms only, activity decay curves were plotted for all the samples, as shown in Figure A1. If the number of radioactive atoms at time t = 0 (where the time t = 0 is defined in this case as the time the Si chips were removed from the reactor) is A_o, the number at any later time t is given as

Figure A1. A plot of activity (counts per minute) in Pd_2Si as a function of decay time in Si/Pd/Si(radioactive)/Cr samples. Time, t = 0, is taken as time when Si chips were immediately removed from the reactor. A5, A2 and B5 are samples with $CrSi_2$ layers unetched.

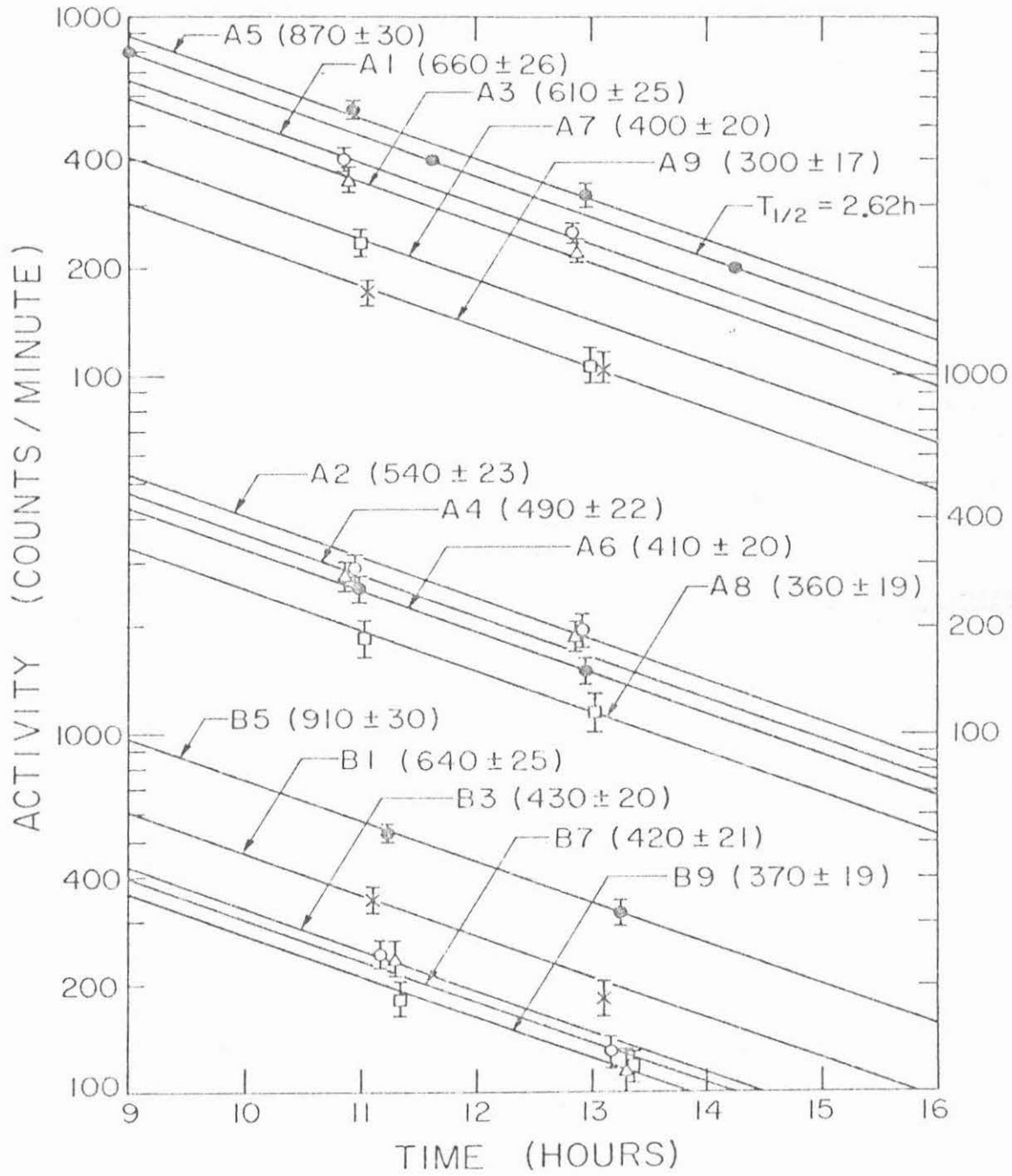
A5 (870 ± 30)
A1 (660 ± 26)
A3 (610 ± 25)
A7 (400 ± 20)
A9 (300 ± 17)
T1/2 = 2.62h
A2 (540 ± 23)
A4 (490 ± 22)
A6 (410 ± 20)
A8 (360 ± 19)
B5 (910 ± 30)
B1 (640 ± 25)
B3 (430 ± 20)
B7 (420 ± 21)
B9 (370 ± 19)
ACTIVITY (COUNTS / MINUTE)
TIME (HOURS)
1000
400
200
100
9
10
11
12
13
14
15
16

$$A = A_o e^{-\lambda t} \qquad (1)$$

where λ is the decay constant, which is the probability that an atom will decay within a unit time.[56] λ is related to the half-life, $T_{1/2}$, of the radioactive atoms as

$$T_{1/2} = \frac{\ln 2}{\lambda} = \frac{0.693}{\lambda} \qquad (2)$$

Equation 1 therefore becomes

$$A = A_o e^{-0.693 \frac{t}{T_{1/2}}} \qquad (3)$$

A plot of $\ln(A/A_o)$ vs t therefore gives a straight line with a negative slope defined by the half-life of the radiating atoms. The decay curve in Fig.A1 is drawn for three sets of samples, each set occupying a decade. The curves obey relationship 3, as expected if there is no contamination, with $T_{1/2} \approx 2.62$ h. The $T_{1/2} = 2.62$ h Si reference line is drawn, assuming an abitrary activity of 800 counts per minute (cpm) at time t = 9h(i.e origin in this figure). At 2.62 h later the activity would have dropped to 400 cpm; 2.62 h later this in turn would have dropped to 200 cpm etc. A5, A2 and B5 are samples with $CrSi_2$ layers unetched (i.e. "virgin"). We calculated the percentage activity in each of the samples with respect to the virgin (unetched) sample. The value of the percentage activity was then plotted as a function of tem-

peratures and of the ratio of Si atoms in $CrSi_2$ to Si atoms in Pd_2Si as shown in Chapter IV.

2. Proposal for Possible Future Experiments

The folliwng are proposed as possible future experiments.

1. Silicide formation in Si/single-crystal metals to investigate if crystallinity of metals plays any role in silicide formation.
2. Investigation of the effects of substrate orientation on the interaction of refractory metals (Ti, W, Mo, etc.) with Si.
3. Silicide formation on silicides in the following systems: Si/Pd/V, Si/Pd/Ti, Si/Pd/Zr, Si/Pd/Mo. It might be interesting to replace Pd with either Pt or Ni which are also low-temperature silicide-forming metals.
4. Neutron activation experiments to find out the source (or origin) of Si used in the formation of the Si-rich silicides in 3.
5. Use of refractory-metal silicides ($TiSi_2$, VSi_2, $MoSi_2$, etc.) as diffusion barriers in metallization.
6. Influence of the grain size of poly Si on dissolution and recrystallization of Si in metals, and on silicide formation.
7. The possibility of recrystallization of poly Si in silicides if the silicides are heat treated at temperatures above which the silicides are known to be stable.

REFERENCES

1. A. J. Khambata, Introduction to Integrated Semiconductor Circuits, John Wiley and Sons, Inc., New York (1963).
2. W. V. T. Rush and C. A. Burns, Solid-State Electron. 11, 1011 (1970).
3. C. J. Kircher, Solid-State Electron. 14, 507 (1971).
4. W. D. Buckley and S. C. Moss, Solid-State Electron. 15, 1331 (1972).
5. A. Shepala, Solid-State Electron. 10, 477 (1973).
6. G. A. Hutchins and A. Shepala, Thin Solid Films 18, 343 (1973).
7. T. Kawamura, D. Shinoda and H. Muta, Appl. Phys. Lett. 11, 101 (1967).
8. H. Muta and D. Shinoda, J. Appl. Phys. 43, 2913 (1972).
9. R. A. Tolla and R. P. Sopher, IBM J. Res. Dev. 13, 226 (1969).
10. J. M. Anderson and M. P. Lepselter, Solid-State Electron. 13, 1011 (1970).
11. R. W. Bower and J. W. Mayer, Appl. Phys. Lett. 20, 359 (1972).
12. J. F. Ziegler, J. W. Mayer, C. J. Kircher and K. N. Tu, J. Appl. Phys. 44, 3851 (1973).
13. R. W. Bower, D. Sigurd and R. E. Scott, Solid-State Electron. 16, 1461 (1973).

14. H. Krautle, M-A. Nicolet and J. W. Mayer, J. Appl. Phys. 45, 3304 (1974).

15. K. N. Tu, W. K. Chu and J. W. Mayer, Thin Solid Films 25, 403 (1975).

16. K. N. Tu, Appl. Phys. Lett. 27, 221 (1975).

17. J. W. Mayer and K. N. Tu, J. Vac. Sci. Technol. 11, 86 (1974).

18. M. Hansen, Constitution of Binary Alloys, McGraw-Hill, New York (1958).

19. H. J. Goldschmidt, Interstitial Alloys, Plenum Press (1967).

20. J. S. Kirkardy, Can. J. Phys. 36, 917 (1958).

21. G. V. Kidson, J. Nucl. Mat. 3, 21 (1961).

22. P. Duwez, Trans. ASM 60, 607 (1967).

23. K. E. Sundstrom, S. Petersson and P. A. Tove, Uppsala University Report No. UPTEC 73-29R (unpublished).

24. K. N. Tu, J. F. Ziegler and C. J. Kircher, Appl. Phys. Lett. 23, 493 (1973).

25. C. J. Kircher and J. F. Ziegler, private communication.

26. J. A. Borders and J. N. Sweet, private communication.

27. D. Sigurd, W. van der Weg, R. W. Bower and J. W. Mayer, Thin Solid Films 19, 319 (1974).

28. D. H. Lee, R. R. Hart, D. A. Leimet and O. J. Marsh, Phys. Status Solidi A15, 645 (1973).

29. A. Hiraki, M-A. Nicolet and J. W. Mayer, Appl. Phys. Lett. 18, 178 (1971).

30. S. S. Lau, J. S. Y. Feng, J. O. Olowolafe and M-A.

Nicolet, Thin Solid Films 25, 415 (1975).

31. W. K. Chu, H. Krautle, J. W. Mayer, H. Muller and M-A. Nicolet, Appl. Phys. Lett. 8, 454 (1974).

32. W. K. Chu, S. S. Lau, J. W. Mayer and H. Muller, Thin Solid Films 25, 393 (1975).

33. J. M. Poate, T. C. Tisone, Appl. Phys. Lett. 24, 391 (1974).

34. R. W. Bower, Thesis, California Institute of Technology, 1973.

35. R. Pretorius, Z. L. Liau, S. S. Lau and M-A. Nicolet, private communication.

36. J. O. McCaldin and H. Sankur, Appl. Phys. Lett. 19, 524 (1971).

37. J. O. McCaldin and H. Sankur, Appl. Phys. Lett. 20, 171 (1972).

38. H. Hiraki, E. Lugujjo, M-A. Nicolet and J. W. Mayer, Phys. Stat. Sol. A7, 401 (1971).

39. H. Sell, Elec. Chem. Soc. Ext. Abstr. 17, 2 (1968).

40. R. W. Bower, Appl. Phys. Lett. 23, 99 (1973).

41. K. Nakamura, S. S. Lau, M-A. Nicolet and J. W. Mayer, Appl. Phys. Lett. 28, 277 (1976).

42. G. J. van Gurp, J. Appl. Phys. 44, 2040 (1973).

43. S. R. Herd, P. Chandlari and M. H. Brodsky, J. Non-Cryst. Solids 7, 309 (1972).

44. G. Ottaviani, D. Sigurd, V. Marrello, J. W. Mayer and J. O. McCaldin, J. Appl. Phys. 45, 1730 (1974).

45. K. Nakamura, M-A. Nicolet, J. W. Mayer, R. J. Blattner and C. A. Evans, Jr., J. Appl. Phys. 46, 4678 (1975).

46. Hidenobu Mochizuki, Teruaki Aoki, Hisayoshi Yamoto, Masanori Okayama, Motoaki Abe and Tetsuo Ando, Semi-Insulating Polycrystalline-Silicon (SIPOS) Films Applied to MOS Integrated Circuits, to be published.

47. Takeshi Matsushita, Teruaki Aoki, Takaji Otsu, Hisayoshi Yamoto, Hisao Hyaski, Masanori Okayama and Yoshiyuki Kawana, Semi-Insulating Polycrystalline (SIPOS) Passivation Technology, to be published.

48. A. S. Grove, Physics and Technology of Semiconductor Devices, John Wiley and Sons, Inc., New York (1967).

49. K. Nakamura, private communication.

50. W. K. Chu, J. W. Mayer, M-A. Nicolet, T. M. Buck, G. Amsel and F. Eisen, Thin Solid Films 17, 1 (1973).

51. J. F. Ziegler, editor, New Uses of Ion Accelerators, Plenum Press, New York (1975).

52. M-A. Nicolet, J. W. Mayer and I. V. Mitchell, Science 177, 841 (1972).

53. E. J. Franzgrote, J. H. Patterson, A. L. Turkevich, T. E. Economou and K. P. Sowinski, Science 167, 376 (1970).

54. J. H. Patterson, A. L. Turkevich and E. J. Franzgrote, J. Geophys. Res. 70, 1311 (1965).

55. S. S. Lau, W. K. Chu, J. W. Mayer and K. N. Tu, Thin Solid Films 23, 205 (1974).

56. Robley D. Evans, The Atomic Nucleus, McGraw-Hill Co., Inc., New York (1955).

57. J. F. Ziegler and W. K. Chu, Thin Solid Films 19, 281 (1973).

58. J. S. Y. Feng, Thesis, California Institute of Technology (1974).

59. J. M. Harris, R. J. Blattner, I. D. Ward, C. A. Evans, Jr., H. L. Fraser, M-A. Nicolet and C. L. Ramiller, private communication.

60. S. S. Lau, private communication.

61. M. H. Read and D. H. Hanslwer, Thin Solid Films 10, 123 (1972).

62 M.H. Read, 27th Annual Pittsburgh Diffraction Conf., November, 1964.

63. C. Canali, S. U. Campisano, S. S. Lau, Z. L. Liau and J. W. Mayer, J. Appl. Phys. 7, 2831 (1975).

64. R. Pretorius, C. Ramiller, S. S. Lau and M-A. Nicolet, private communication.

65. J. K. Howard, R. F. Lever, P. J. Smith and P. S. Ho, J. Vac. Sci. Technol. 13, 68 (1976).